The Effect of Laser Assisting for Milling Process of Difficult-to-cut Materials

(難削材へのレーザ援用ミリング加工の効果)

学位取得年月 2019 年 9 月

Kamonpong JAMKAMON

Contents

List of Figures

ii

iii

List of Tables

Title (題目): The Effect of Laser Assisting for Milling Process of Difficult-to-cut Materials

(難削材へのレーザ援用ミリング加工の効果)

Kamonpong JAMKAMON

This dissertation presents the effect of laser assisting for milling process of difficult-to-cut materials. Milling is a generally accepted that a machining process has been widely used for manufactured part in various industries such as plastic mold, die forging, automobile and aerospace. The basically mechanic of milling process is the cutting tool directly interface with the workpiece, tool rotating to cut work material in the direction of cutting velocity leaded to initialed deformation in the primary shear zone, which the shearing region occurred in front of the cutting tool, the continuously movement of cutting tool also leaded to work material deformed in secondary shear zone and flow-off on the tool rake face as a chip. Therefore, the requirement of cutting forces is strongly depended on the cutting conditions such as cutting speed, depth of cut, feed rate and the machinability of materials is strongly depended on cutting tool and workpiece. Whereas, the high requirement of cutting forces which is caused that the low machinability cannot be avoided when machined difficult-to-cut materials such as nickel base super alloys as well as Inconel 718 and high hardness of surface hardening materials such as well as nitrided die steel.

Recently, lasers have been widely applied in various machining process to reduce refractory of difficult-to-cut materials. This is because the laser is a rapid heat source which has high energy concentration to heat materials locally in the machining zone. Although increase in initial temperature of workpiece leaded to softened work material and improved machinability, the effects of atmosphere in laser assisting on the machinability of difficult-to-cut materials has not investigated clearly. Therefore, the first objective of dissertation is an experiment to investigate the influence of cutting speed, preheating temperature and atmosphere on the improved machinability in the laser assisted for milling Inconel 718 with uncoated carbide inserts.

In addition, the pulsed laser surface treatment is well established to treat the surface of work materials as a report of laser surface hardening, polishing, cleaning and so on. On the other hand, the excessive thermal heat must be resulted in the damage on the work surface due to remelting process. This is potentially expected to reduce the hardness layer of nitrided die steel which is possible leading to improved machinability for reformed worn dies. However, a few of researcher was addressed on the pulsed laser surface treatment to reduce mechanical properties of nitrided die steel and the machinability of irradiated surface. Therefore, the second objective of dissertation is an experiment to fulfill knowledge on the application of pulsed laser surface treatment in order to improved machinability for milling process.

In this work, uncoated carbide tool (WC-Co) was used as a cutting tool. Therefore, the cutting temperature must be measured to avoid cutting conditions which leaded to temperature softening of carbide tool (1100ºC). Tool-work thermocouple method is powerful to measure

cutting temperature in the region of tool-chip/tool-workpiece interface. However, it is difficult to use for milling process because the cutting tool is rotating and thermal electromotive force (EMF) generates in the rubbing area (cold junction). Therefore, carbon brush was designed to use as a sliding contact to connect signal of EMF from the rotating part to oscilloscope. And, electromotive force generated in the rubbing area and the measuring circuit were investigated to compensate EMF in cutting test. The obtained results show that the EMF in the cutting test must be compensate before convert to cutting temperature because the difference ratio of calibration curves for the difference couple of material. For example, the ratio of EMF to temperature for carbon brush and tool holder was approximately 1 mV : 100°C. but EMF to temperature for carbide tool and Inconel 718 was approximately 1 mV : 54°C. Whereas, the compensate value increased with the rotating speed due to more heat generated at higher rubbing speed. The cutting temperature increased with the cutting speed due to more heat generated at higher cutting velocity.

The experimental results with various cutting speed and preheating temperature for milling Inconel 718 were found that the requirement of laser power for preheating workpiece proportionally increased with the particular heating temperature (300, 500, and 700°C) and table speed (30, 50, 75 and 100 mm/min). In addition, the highest temperature in the primary shear zone occurred at the highest preheating temperature which could maximally reduce in shear stress of workpiece approximately 20, 30, 35 and 34% to compare with conventional machining at the same cutting speed of 30, 50, 75 and 100 m/min, respectively. Tool wear in laser assisted machining was higher than conventional machining at the low cutting speed of 30 and 50 m/min, but the wear could be improved at relatively high cutting speed of 75 and 100 m/min.

The obtained results from laser assisted milling for Inconel 718 to investigate the influence of atmosphere on the performance of laser assisting showed that the higher laser power was required to particular heating temperatures in the argon gas, while the atmosphere containing oxygen (compressed air blow and dry machining) required lower laser power. This is because the oxygen in the air accelerated oxidation and burning on the irradiated surface which increase the optical absorptivity of laser. The experimental results from cutting tests showed that the specific cutting force decreased with the preheating temperature in any atmospheres, and the lowest specific cutting forces was obtained in the argon atmosphere due to the increase in friction coefficient leaded to higher cutting temperature and work material more softening.

An application of pulsed laser surface treatment improved machinability in the shape correction process by ball end-milling for forging dies. The die steel with high hardened layer by ion nitrided process was used as a workpiece that was irradiated by pulsed laser. Then, inclined milling experiments were performed on the irradiated workpieces which was simulated machining for walls of the dies with a draft. The machinability was evaluated from specific cutting force, actual depth of cut, tool deflection and uncut chip thickness. The result of improved machinability was found that the hardness of nitride layer can be reduced by the laser irradiated. Therefore, the laser irradiated surface responded to increase the actual depth of cut and uncut chip thickness, while the tool deflection and specific cutting force were small compared with those for non-irradiated surface.

Chapter 1

Introduction

1.1 Research background

For metal cutting, it is generally accepted that the machining process has been widely used for manufacturing part in the various industries such as plastic mold, die forming, automobile, aerospace and so on. Nowadays, the conventional machining processes (CM) are turning and milling which need cutting tool and consuming force to remove unwanted material from the workpiece in the form of chip in order to generated shape and dimension as a decision. The basically mechanics of cutting process is the cutting tool directly interface with the workpiece as shown in Fig. 1.1, the tool is going to cut the workpiece in the direction of cutting speed (V) leaded to work material initialed deformation and shearing region occurred in front of the cutting tool (primary shear zone), the continuously movement of tool/workpiece also leaded to work material deformed and flow-off on the tool face as a chip (secondary shear zone). Therefore, the requirement of cutting force in the machining process is strongly depended on the cutting conditions as well as tool and work materials.

| (a) Turning process | (b) Milling process |
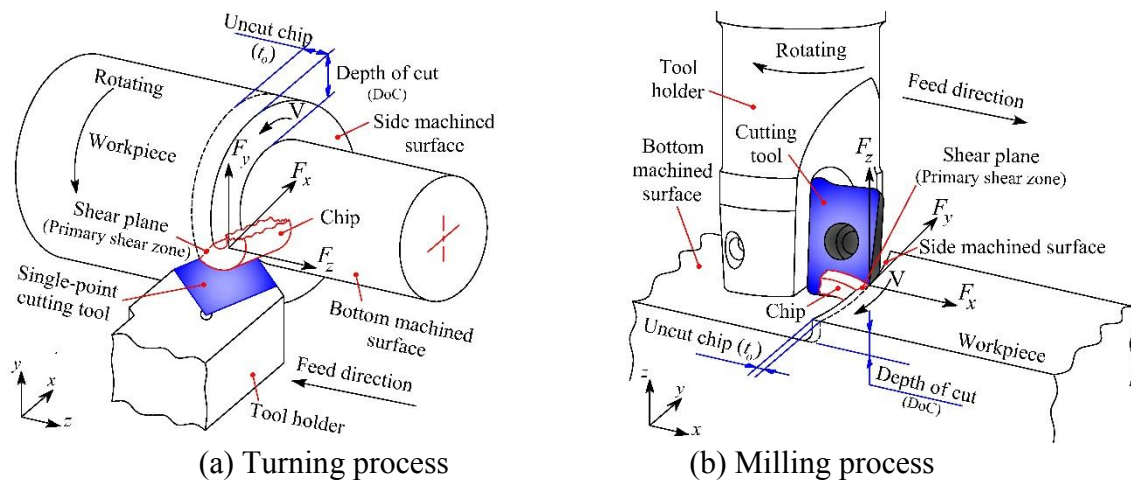
Fig. 1.1 Illustrate mechanics of conventional machining processes and cutting forces

With the reasons as a mention above, the metal cutting has a primordial objective of study on the factor which involved cutting operation such as cutting conditions (cutting speed, feed rate, depth of cut and etc.), cutting tool (material, mechanical properties, geometry and so forth) and workpiece (mechanical properties, thermal properties, work-hardening and so on) on the machinability. Although the machinability of workpiece can be improved by the optimal cutting conditions, the high requirement of cutting force which was caused low machinability cannot be avoided when machining difficult-to-cut material such as nickel based supper alloy as well as Inconel 718 and high hardness of surface hardening materials as well as nitrided die steel.

Recently, many studies have attempted to apply hot machining technique for reducing refractory of difficult-to-cut materials. This technique needs the external heat source such as induction, plasma, gas torch or laser in order to reduce the mechanical properties of work materials prior to the material removal by cutting tool [1, 2]. The laser has been widely applied in various machining process such as milling and turning because the laser assisted machining (LAM) is a rapid heat source which has high energy concentration to heat the material locally in the machining zone [3]. Although increase in the initial temperature of workpiece may be leaded to softening and improved machinability of work material, the effect of atmosphere on the machinability at elevated cutting temperature has not been investigated clearly [4-7]. Therefore, the researcher would like to investigate comprehensively influence of preheating temperature and atmosphere on the improved machinability with using low cost cutting tool as well as uncoated carbide insert.

In addition, the pulsed laser surface treatment is well established to treat the surface of work materials as a reports of laser surface hardening [8], laser ablation [8-10], laser polishing [11] and laser cleaning surface [12,13]. On the other hand, the excessive thermal heat must be leaded to damage on the work surface due to remelting process. The melting and recasting process are potentially expected to reduce amount of nitrogen and destroy the hardness of nitride layer [14] leading to improvement of machinability. Recently, a few of paper was focus on the pulsed laser surface treatment to reduce the mechanical properties high hardened die steel. And, the machinability of irradiated surface have never been report before. Therefore, the researcher would like to fulfill knowledge on the improvement of machinability of high hardness tool steel by using pulsed laser surface treatment.

1.2 Objective of and construction of research

Although the laser has been widely used to improve machinability of difficult-to-cut materials, the effect of preheating temperature and influence of atmosphere in the laser assisting for milling Inconel 718 on the improvement of machinability remain unclear. In addition, a few researches have addressed the advantage of pulsed laser surface treatment for improved machinability of high hardening surface of nitrided die steel (DH31S, Diado steel Co., Ltd.).

Therefore, the main objectives of this work intents to investigate the effect of laser assisted machining for milling Inconel 718 with uncoated carbide tool under the dry machining, compressed air blow and inert gas (argon) shielded cutting area. In addition, experiment to investigate the improved machinability of high hardness die steel by using pulsed laser surface treatment.

The flow chart for this work shows in Fig 1.2 and the construction for this study can be summarized as follow;

Chapter 1 discusses the background of the research as well as the objective and construction of the research.

Chapter 2 reviews the theoretical background of conventional machining and the present researches on the laser assisting for milling difficult-to-cut materials and related hot machining process.

In Chapter 3, The sliding contact is designed and manufactured for using to connect a signal of electromotive force (EMF) during cutting test from the rotating part (end-milling) to the oscilloscope (detected and recorded signal). The electromotive force generated at the cold junction is investigated to determine the compensated value of electromotive force generated in the measuring circuit. The calibration curves for converting electromotive force to cutting temperature are performed as a tool-work thermocouple. The cutting tests with various cutting speed are also performed and discussed.

In Chapter 4, a k-type thermocouple is embedded into the Inconel 718 to measure temperature in the workpiece. The various laser power is used to irradiate on the surface of workpiece in order to calibrating laser power to particular heating temperature at primary shear zone. The uncertain conditions in experimental setup for calibrating process is investigated and controlled. Then, the cutting tests with various cutting speed and preheating temperature are performed to investigate the effects of preheating temperature at primary shear zone in the laser assisted process for milling Inconel 718 with uncoated carbide tool.

In Chapter 5, chamber system is designed and manufactured to control the atmosphere surrounding of machining area in the cutting test. The calibration is conducted to decide the required laser power to retain the particular heating temperature at primary shear zone with in the workpiece under the atmosphere of dry machining, compressed air blow and argon gas. The influence of atmosphere on the requirement of laser power to retain particularly heating temperature is discussed. The work material (Inconel 718) is heated to the prescribed temperature by laser, and then the machined with uncoated carbide inserts to investigate the influence of atmosphere on the machinability.

In Chapter 6, pulsed laser surface treatment is applied to reduce the hardness of nitride layer on the die steel. After the treatment process, simulating the die walls with a draft and the inclined workpiece are machined with ball end-mills. The machinability of irradiated surface is investigated by mean of tool deflection, actual depth of cut, specific cutting force and calculated thickness of uncut chip, those results are compared with ones for non-treated workpiece.

Finally, the conclusions of this research are summarized in Chapter 7.

Chapter 1 Introduction

↓

Chapter 2 Theoretical Background and Literature Review

↓

Chapter 3

Precise Evaluation of Cutting Temperature in Milling Process by Tool-Work Thermocouple Method

➢ Design and manufacture sliding contact to connect the signal of electromotive force (EMF) from the rotating part (tool holder) to detected and recorded acquisition (oscilloscope)
➢ Experiment to evaluate EMF generated in measuring circuit to use for compensate EMF in cutting test
➢ Experiment to calibrate EMF with the temperature for Tool-work thermocouple (calibration curves)
➢ Cutting test to evaluate quality of detecting signal and cutting temperature

↓

Chapter 4

Effect of Preheating Temperature at Primary Shear Zone in Laser Assisted Milling process

➢ Introduce laser assisted milling process
➢ Experiment to evaluate and control error due to the uncontrolled conditions in calibrating process
➢ Experiment to calibrate laser power to hearting temperature at primary shear zone
➢ Cutting tests to evaluate influence of preheating temperature on the component of cutting forces, cutting temperature, chip thickness, shear stress, tool wear and integrity of machined surface

* It should be noted that the laser assisted machining is employed with varied preheating temperature of 300, 500 and 700°C for the cutting speed of 30, 50, 75 and 100 m/min.

↓

Chapter 5

Influence of Atmosphere on the Performance of Laser Assisted Milling for Inconel 718 with Carbide Tool

➢ Design and manufacture chamber for controlling atmosphere surrounding of machining area
➢ Experiment to calibrate laser power for retaining particularly heating temperature under the different atmosphere, and to investigate effect of atmosphere on the requirement of laser power
➢ Experiment to investigate influence of atmosphere on the machinability by means of cutting force, cutting temperature, specific cutting force, coefficient of friction, tool wear and integrity of machine surface (roughness and micro-hardness)

* It should be noted that the laser assisted machining is performed with varied atmosphere as well as dry machining, compressed air blow and argon gas shielded machining area.

↓

Chapter 6

Improved Machinability of High Hardened Die Steel Using Pulsed Laser surface Treatment

➢ Introduce high hardened die steel and expectation to reduce hardness of nitrided layer on die steel in order to improve the machinability in the reforming operation for forging die
➢ Pulsed laser surface treatment irradiate on nitrided die steel, and the damage on irradiated surface are investigated by means of surface profiles, SEM image and elemental mapping
➢ Cutting tests are performed to investigate tool deflection and actual depth of cut, specific cutting force and uncut chip thickness

↓

Chapter 7 General conclusion

Fig. 1.2 Construction of the research

Chapter 2

Theoretical Background and Literature Review

2.1 Introduction

This chapter discusses the theoretical background of machining process and the previous researches on the laser assisted for machining difficult-to-cut materials with related to the improvement of machinability. The difficult-to-cut materials are focus on the Inconel 718 and high hardened die steel.

2.2 Machining process

Machining is a term using to describe the method of material removal with a cutting tool to remove unwanted material from a workpiece to produce the desired shape. The categories of materials removed may be divided by size of individual removed as following; cutting process is generally involves single-point or multipoint cutting tool which is a clearly defined tool shape, abrasive processes such as a grinding, and advanced machining processes that utilize electrical, chemical and thermal as well as lasers [1].

(a) Mechanical chip formation

(b) Component of cutting force

(c) Resolution of resultant cutting force and tool face

(d) Resolution of resultant cutting force and shear plane

(e) Velocity diagram in the cutting zone
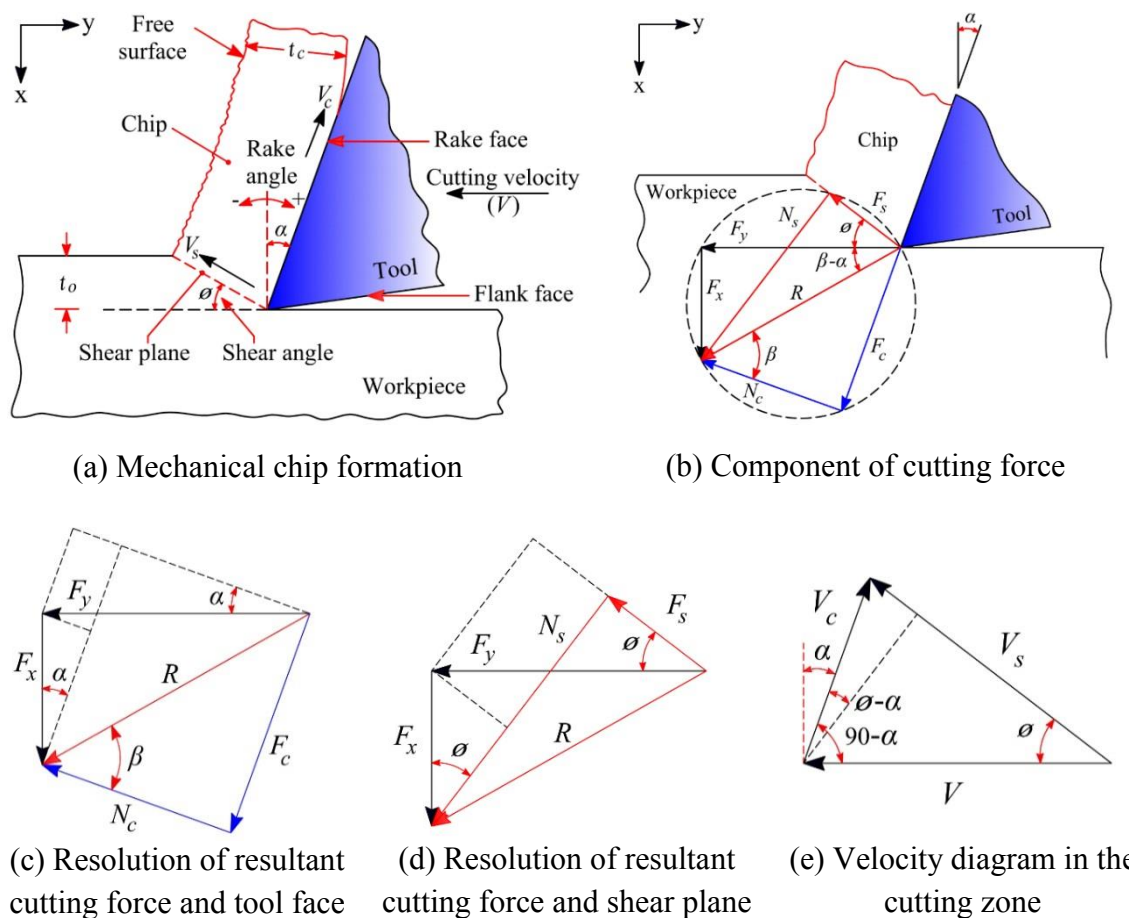
Fig. 2.1 Schematic illustration cutting process (orthogonal cutting) in metal cutting

Cutting processes remove material from the workpiece by producing chips. The commonly processes of material removal is well known as a turning and milling operation. The turning operation mean that the workpiece is rotated and cutting tool removes a layer of materials as a chip, and the milling operation mean that the rotating cutter travels along a certain depth in the workpiece and produces chips as shown in Fig. 1.1 (a) and (b), respectively. The mechanics of chip formation and component of cutting force in the cutting process can be simply presented as a two-dimensional cutting model (orthogonal cutting) as shown in Fig. 2.1.

The forces acting in the cutting process can be measured by dynamometer in the term of thrust force (F_x; force acts in a direction of uncut chip thickness (t_o)) and tangential force of cutting force (F_y; force acts in the direction of cutting velovity (V)). These two forces produce the resultant force (R) and relate to the forces acting on the tool face and shear plane. These relationship were suggested by Merchant circle diagram as shown in Fig. 2.1 (b) [16].

From the evident in Fig. 2.1 (c), a friction force (F_c; force acts along the tool-chip interface) and normal force (N_c; force acts perpendicular to F_c) act on tool face can be resolved as following equation 2.1 and 2.2, respectively.

$$F_c = F_y sin\emptyset + F_x cos\alpha \tag{2.1}$$

$$N_c = F_y cos\alpha - F_x sin\alpha \tag{2.2}$$

where, F_c is friction force (N), N_c is normal force (N), F_x is thrust force (N), F_y is tangential force (N), and α is the rake angle (deg.).

The ratio of F_c and N_c as shown in equation (2.3) is the coefficient of friction (μ) at the tool-chip interface. The coefficient of friction in metal cutting generally ranges from about 0.5 to 2, indicating that the chip encounters considerable frictional resistance while moving up the rake face of the tool [15]

$$\mu = F_c/N_c \tag{2.3}$$

According evident in Fig. 2.1 (d), a shear force (F_s; force acts along the shear plane) and normal force (N_s; force acts perpendicular to F_s) act on the workpiece can be resolved as following equation 2.4 and 2.5, respectively.

$$F_S = F_y cos\emptyset - F_x sin\emptyset \tag{2.4}$$

$$N_S = F_y sin\emptyset + F_x cos\emptyset \tag{2.5}$$

where, $\emptyset$ is shear angle (deg.) that can be derived from the measuring chip thickness and rake angle of cutting tool as following equation 2.6.

$$\emptyset = tan^{-1}\frac{(t_o/t_c)cos\alpha}{1-(t_o/t_c)sin\alpha} \tag{2.6}$$

where, t_o is the uncut chip thickness (mm), t_c is chip thickness, and α is rake angle (deg.).

The shear stress on shear plane (τ_s), which indicated strength of work materials during cut can be geometrically calculated from the experimental data as following equation (2.7).

$$\tau_S = F_s/A_s \qquad (2.7)$$

where, τ_s (N/mm^2) is shear stress on shear plane, F_s (N) is shearing force on the shear plane and A_s (mm^2) is area of shear plane, and

$$A_S = bt/sin\emptyset \qquad (2.8)$$

where, $\emptyset$ is shear angle (deg.), b is width of cut (in this test is 6 mm), and t_o is depth of cut (in this test is 0.75 mm).

Three velocities (chip velocity, V_c; shear velocity, V_s; cutting velocity, V) in the cutting process are interested. In accordance with the principles of kinetics, these three velocity vectors must form a closed velocity diagram as shown by the hodograph of Fig.2.1 (e) [15]. The vector sum of the cutting velocity and the chip velocity is equal to the shear velocity vector [16]. Hence, the chip velocity (V_c) and shear velocity (V_s) can be derived by following equation (2.9) and (2.10), respectively.

$$V_C = \frac{Vsin\emptyset}{cos(\emptyset-\alpha)} \qquad (2.9)$$

$$V_S = \frac{Vcos\alpha}{cos(\emptyset-\alpha)} \qquad (2.10)$$

where, V_c is chip velocity (the velocity of the chip relative to the tool and directed along the tool face, m/sec), Vs is shear velocity (the velocity of the chip relative to the workpiece and directed along the shear plane, m/sec), and V is cutting velocity (the velocity of the tool relative to workpiece and directed parallel to tangential force, m/sec).

These equations are potentially expected to use for estimated force acting on the tool face, friction coefficient, shear angle, shear tress, area of shear plane, chip velocity and shear velocity in order to explained influence of cutting conditions on the requirement of cutting force and chip formation as well as the temperature rise in the shear zone during cutting test. For the example, Ezugwu et al [17] explained relationship between cutting conditions and cutting phenomenon. They are referred that the yield strength of work materials generally decrease with increasing temperature. Therefore, the cutting forces decrease when cutting speed increased as the shearing forces are also lowed. This phenomena also explained by the fact that as the cutting speed decrease, the shear angle also decrease, a small shear angle results in a longer shear plane. For the shear strength is fix, the decrease in shear angle results to a longer shear plane, an increase in area of shear plane leads to an increase in requirement of cutting

forces for shearing work material. These are also leads to thicker chip formed. In addition, at the lower cutting speeds the friction coefficient increase, hence cutting forces are increased. However, in the process of laser assisted machining the influence of cutting conditions on the chip formation more complicate due to the initial temperature of workpiece changed by the laser irradiated during machining operation.

The operational characteristic of a cutting tool are generally describe by machinability in the term of tool life, finish machined surface and the power required to generate deformation of chip [16]. Machinability is also a term commonly used to explain how easy a work material can be cut under the given cutting conditions [18].

2.3 Difficult-to-cut materials

Difficult-to-cut materials are referred to the materials which during machining operations produce excessive tool wear, cutting temperature (heat) and/or cutting forces, difficulties in chip formation and/or poor surface quality [19]. These are leading to high manufacturing cast because of low materials removal rates and rapid tool wear [20]. In this literature review is focus on the nickel base-superalloys as well as Inconel 718 and high hardness layer of nitrided die steel.

Inconel 718 is a nickel based-superalloy widely employed in the aeronautical, aerospace, and energy industries for parts undergoing high mechanical loads and under high operation temperature due to its high temperature strength and high corrosion resistance [21]. This material is a solid solution hardened or precipitation hardened alloy with an austenitic face centred cubic (FCC) matrix phase (denote γ) with other many secondary phases in varying in size, distribution, and location. It receives much of it strength from small γ' (typically : $Ni_3[Al,Ti]$) and γ'' (typically: $Ni_3[Al,Ti,Nb]$,) precipitates [17,20]. The principal strengthening phase is the precipitate γ''. This consists of disc shaped particles which are coherent with the FCC present matrix. The intermetallic $\gamma''(Ni_3Nb)$ has a body center tetragonal (BCT) structure. This results in a microstructure of large grains containing the Ni_3Nb precipitated phase and a heavy concentration motion γ'/γ microstructure is responsible for high tensile and yield strength of Inconel 718 (approximately 1300 and 1100 Mpa, respectively, at temperature up to 600°C) [22,23].

Nickel base alloys have highly chemical reactive with tool material and low thermal properties leading to high cutting temperature in the cutting zone [21]. Therefore, the adhering materials as well as BUE/BUL are often formed leading to diffusion and attrition wear [19].
- Attrition and crater wear on the rake face and flank face are the dominant tool failure modes in machining nickel based alloys [19].
- Diffusion, adhesion and formation of BUE/BUL on the tool face cause attrition, alteration and crater wear while abrasion is dominant on the rake face [19].
- Adhesion wear means workpiece materials adhere to the tool that may not be stable and may be removed dragging along with tool particles. BUL and BUE is a form of adhesion locally

on the tool. The extension of BUL behind the cutting edge on the flank face is reasonable that the cutting edge location is high rubbing and pressure during milling [24]

- Abrasion wear is mainly attributed to the present of super alloy hard carbide particles such as TiC, CrC, MoC, NbC, FeC, WC, MC and etc. in the microstructure of the materials [19]. These carbide is sliding and scratching on tool face during chip formed leading to tool materials loss.

Shokrani et al. [19] concluded that strain hardening is an intrinsic property of nickel based alloys due to the present of molybdenum (Mo) and niobium (Nb) in the material. This is dominant in cutting operation as hardness of the chip is increased after being subjected to deformation at the first shear zone. While the strain hardened chips are very abrasive to the cutting tool, the strained hardened machined surface could notch the tool face. These leading to machining of Inconel 718 with uncoated carbide tool is limited to a low cutting speed of 30-60 m/min due to the high mechanical and thermal loads which adversely affect the tool life [25]. Yamamoto et al. [26] recommended that high-efficiency cutting for difficult-to-cut materials is necessary to improve tool materials and machining methods to reduce tool wear. Venkatesan et al. [25] suggested that preheating work material is an attractive alterative technique for machining of difficult-to-cut material using cheaper ceramic and coated tools because preheating temperature reduces the hardness, strain hardening and yield strength of the workpice.

2.4 Laser assisted machining

The conventional machining processes such as milling or turning are effective to improve for machining difficult-to-cut materials with various thermally-assisted methods such as plasma, induction, oxyfuel and laser. The laser assisted machining (LAM) is becoming increasingly popular with difficult-to-machine materials because it higher benefits, substantial growth in technology and the commercial viability [1].

High power laser locally heat the workpiece prior to materials removal with a traditional cutting tool, at elevated temperatures the yield strength of a brittle material decreases to below the fracture strength changing the materials deformation behavior from brittle to ductile. The main operating parameters associated with laser assisted machining are laser power, spot diameter of laser beam, cutting speed, feed rate and depth of cut [27]. In cutting processes, the direct cutting force is overcome the yield stress of the material for chip forming. Therefore, the performance of the machining process are high when material strength decreases. Hence, the application of external energy improves the machining process by using laser beam to heating and softening the workpiece thereby making it easier to cut [28, 29]. This process is based on the mechanical properties of the materials change with according to temperature.

Thermally assisted machining processes are gaining popularity among researchers and engineers as a method for improving the machinability [30]. The approximation for pre-heat Inconel 718 to a temperature of 400-500ºC. In addition, there is temperature rise due to shear and frictional heating produced by the cutting process. Hence, the total temperature rise is

expected to be closer to 750-880°C during laser assisted machining [31]. The ability of the tool to resist wear at these high temperatures will directly determine tool life because tungsten carbide begins oxidize at temperatures above 500°C [25]. The environmental cutting of laser assisted machining is under the dry cutting that process created a larger heat than conventional machining under cutting fluids and it have effected to tool wear. When decrease of oxygen content in the cutting area, under the good condition of nitrogen gas supply can be reduced the crater wear of the carbide tool P10 [32]. Gas such as carbon dioxide, argon, nitrogen and helium also provide an inert environment which could prevent the cutting tool and machined surface from oxidation at high cutting temperatures [19].

Thermally assisted machining are wide spread application to reduce the shear strength at the cutting zone of the workpiece [33]. The external temperature at the cutting zone could be generated from laser assisted and internal heating were generated from the friction at tool-chip interface and friction between the clearance face of the tool with work-piece [27]. The conventional cutting fluids cannot use in this process because the film boiling temperatures of is about 350 °C [28] that harmful to the operators and environment. Several researchers have used the laser energy to pre-heat the material during machining and observed that there is a reduction in cutting force/specific cutting energy, improvement in surface finish of work material and tool life under dry cutting. These experimental results are compared with conventional machining [24, 27, 29].

The cutting processes are generated heat from the friction between cutting tool and workpiece that have affected to the tool life. For the conventional cutting can reduce the tool wear by using cutting fluids, but it cannot use for laser assisted machining. Inert gas has been interest to use for prevent tool wear in the laser assisted machining because it could prevent the cutting tool and machined surface from oxidation and chip ignition at high cutting temperature [19,35] (the melting chip will be created the BUE/BUL). Currently, the literature very few focus on the inert gas shield cutting area for laser assisted machining because the inert gas such as argon in the conventional machining has some negative properties for lubrication and/or cooling, also it are poor heat capacity and thermal conductivity. Therefore, argon gas must have to increase cutting temperature and more tool wear [35, 37].

2.5 Improve machinability of high hardened die steel

Die steel is one of difficult-to-cut materials due to its strength and hardness. The hardness of surface layer of forging die is higher two times than substantial metal by nitriding process to improve wear resistance [38,39]. Hawryluk et al. [40] reported that wear and damage of forging tools causes a change in the geometry of the manufactured product, and any surface damage of defect are represent on the forging product. Buchmayr [41] suggested that the best practice repair technologies are filling material in worn region and machining with high speed cutting (HSC). Biermann [10] explained that the machining hardened materials with low stiffness of the milling tools result in an increased tool deflection which has a great influence on the geometry and dimension accuracy of the machined product. Vedani et al. [39] founded that welding nitrided steel results in the copious formation of gas pores due to nitrogen releases

during meld metal solidification (remelting). The remelting processes are possible to decrease the hardness and strength of nitrided layer. However, the melting process must be controlled in order to avoid damage on the substrate metal. Therefore, the pulsed laser surface treatment is an expected technology because the heat source can be controlled for the different surface treatment on the workpiece [13,14, 42-44].

Chapter 3

Precise Evaluation of Cutting Temperature in Milling Process by Tool-Work Thermocouple Method

3.1 Introduction

Machining of materials is one of the most used techniques for producing different shape of workpiece. In the machining processes the cutting tool removes some part of material from the workpiece. The removed materials slide on the tool face and leaves from the workpiece called chip. In this process, the cutting tool is interface with the workpiece and work material is deformed. The main regions of work material deformed and heat generated during the machining as an orthogonal cutting process are shown in Fig. 3.1. As shows in Fig. 3.1, the chip formation is categorized into two zones, namely primary and secondary deformation zones. In the primary deformation zone, the work material is being cut by elastro-plastic deformation and the majority of the energy used at the shear plane is transformed into heat. The local heating in this zone results in very high temperatures leading to the softening work material and allowing grater deformation. At the secondary deformation zone the produced chip slides on the rake face of cutting tool (chip-tool interface zone) resulting in high frictional force and heat. [19, 45]. The friction and heat generated on the rake face could result in the chipping and crater wear leading to the tool failure. In addition, the sliding of the tool flank face on the machined surface at the tertiary deformation zone generates friction and heat. This friction and heat could be caused flank wear on the flank face [19]
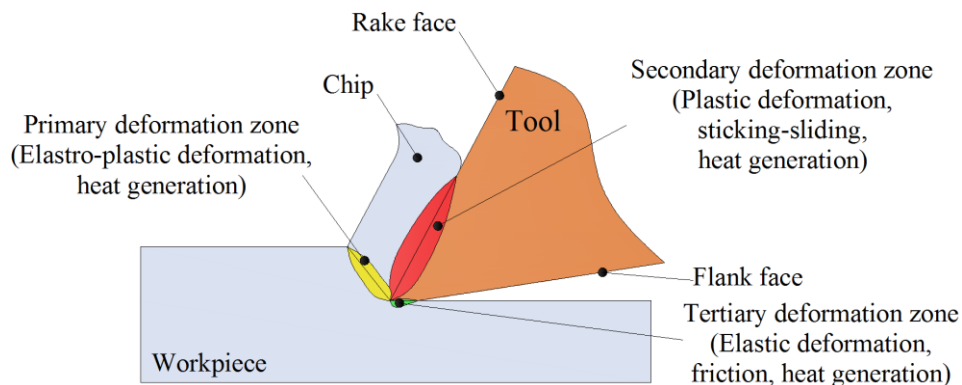
Fig. 3.1 Schematic view of the cutting zone and chip formation

The temperature in metal cutting is an important factor to control the tool life and the quality of machined surface. It is well known that high temperature is obtained in the rake face at the tool-chip contact area close to the cutting edge, when the difficult-to-cut materials are machined. Based on the researches of Abukhshim et al. [45] and Komanduri et ai. [46] recommended that the tool-work thermocouple method is based on the fact of the different two metals materials. The contact area between them forms a hot junction, which produces the

electromotive force (EMF) while the tool or workpiece themselves from the cold junction. Kitagawa et al. [47] was embedded a micro-thermocouple in the tool. The Hot junctions of thermocouple were created on the rake face within the tool to measure local temperatures. They were reported that the rake temperature reaches 1200°C at 150 m/min, which is close to the melting temperature of the Inconel 718. One of the concerns stated by tool-work thermocouple method is that the pair of materials requires accurate calibration and produces significant noise in the signal [45].
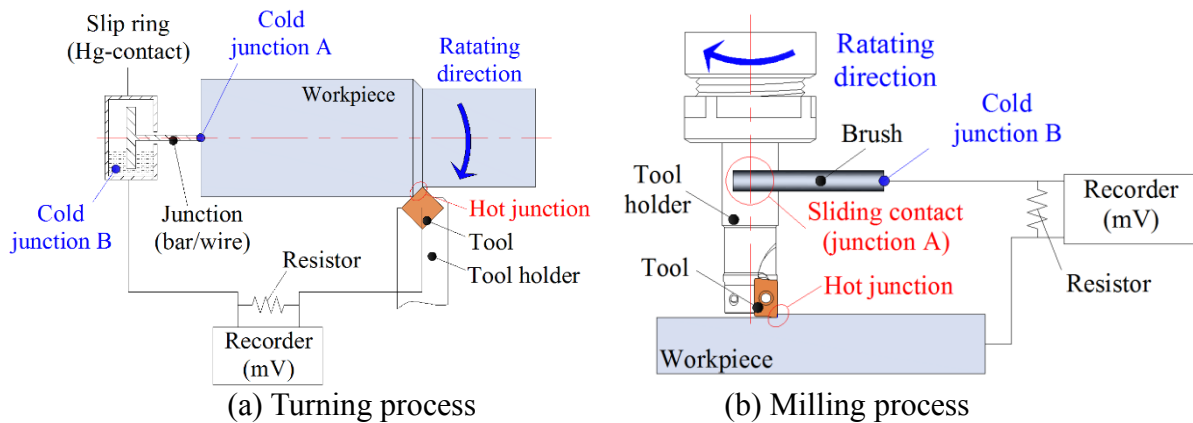
Fig. 3.2 Illustration diagram of the electromotive force (EMF) circuit for measuring cutting temperature in machining process

The tool-work thermocouple method can be used for measuring temperature at the region of tool-chip or tool-workpiece interfaces. In this measuring process, the EMF must be measured and converted to the temperature. The circuits for measuring EMF need a hot junction at the interface of tool-chip or tool-workpiece, while the another junctions must be controlled as same temperature (cold junction). Komanduri et al. [46] reported that the tool support system as well as the workholding device have to be electrically insulated. In addition, the slip ring (Hg-contact) as shown in Fig. 3.2 (a) is widely used in the measuring circuit of turning process in order to avoid the EMF generated in the cold junction. Moreover, Yashiro et al [48] avoided the EMF generated in the sliding contact area by using a cemented carbide rod which is made from same materials as the tool, and the sliding contact area is always kept in a conductive state by applying electro-conductive grease in the contact area of cemented carbide rod and tool. In addition, both cutting tool and workpiece are insulated from the structure of machine.

In the milling test to investigate the cutting temperature as shown in Fig. 3.2 (b), the circuit has at least one cold junction between the rotating part and sliding contact. However, it is very difficult to eliminate EMF generated at the cold junction in the test because the frictional heat is generated at the cold junction (rubbing area) and tool holder cannot completely insulate from the structure of machine. Therefore, the objectives of this study are to design the sliding contact to connect the EMF signal from tool holder to recorder (oscilloscope) and evaluate the EMF generated at the cold junction (EMF generated in the measuring circuit) to compensate the cutting temperature in end-milling process.

3.2 Experimental procedures

3.2.1 Design of sliding contact

Carbon brush was used to make a sliding contact in the electric circuit because carbon is an economical materials and has a property of solid lubricant. It can reduce the friction and the heat generation during rubbing with tool holder.

(a) Image of sliding contact and fixture design

(b) Sliding contact assembly on the spindle head

(c) Details of sliding contact design
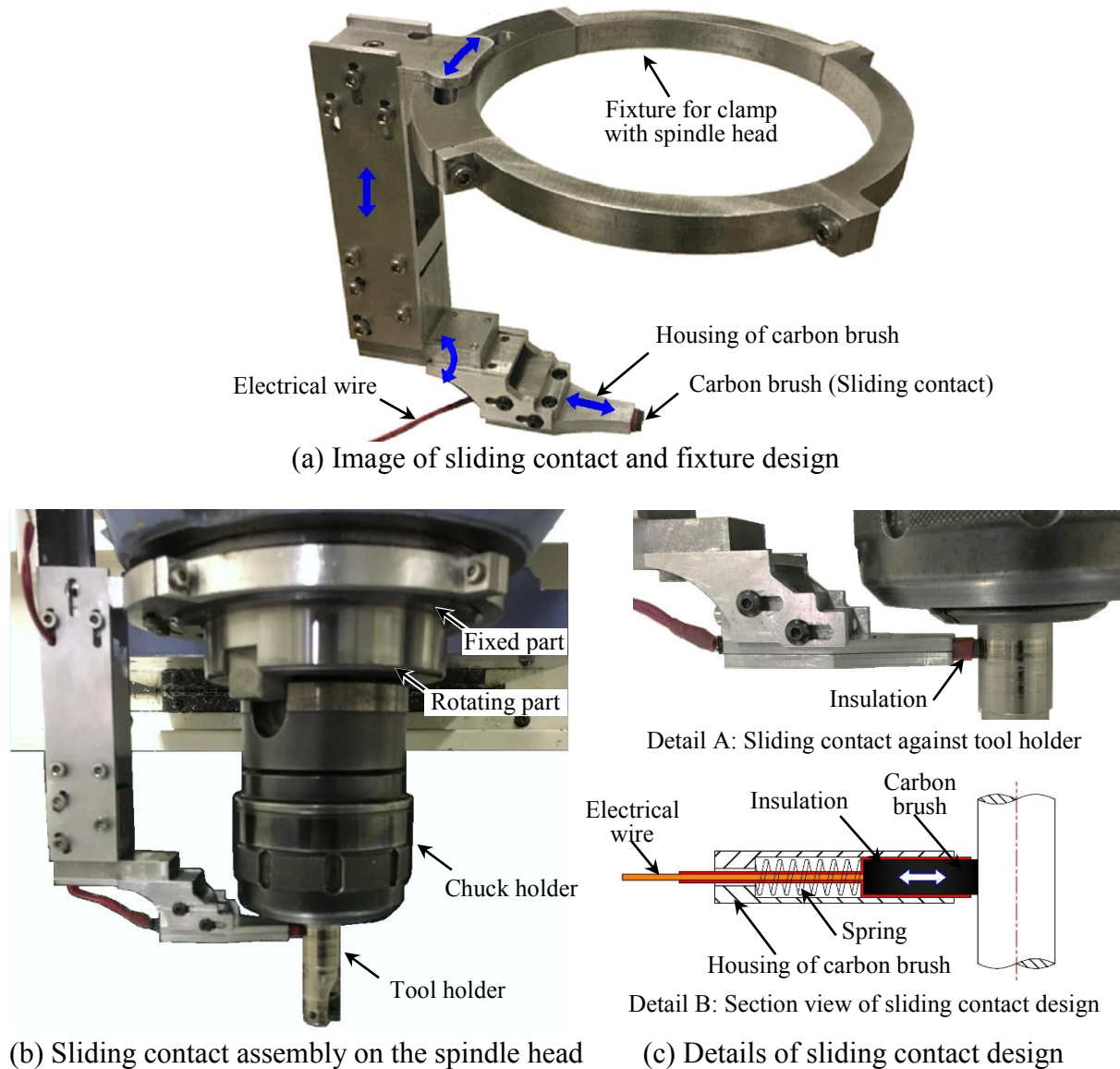
Fig. 3.3 Design sliding contact and fixture for assembly on the vertical milling machine

Figure 3.3 (a) the design of sliding contact and fixture shows that the carbon brush is covered by the aluminum housing. The position of carbon brush against tool holder can be adjusted along the x and z axis, and also can be rotated around the y and z axis. The housing of carbon brush is fixed on the spindle head of vertical milling machine by using fixture as shown in Fig 3.3 (b). The design of carbon brush is insulated from the structure of machine by using heat-shrink tub, the shape of contact area of carbon brush is same with the shape tool

holder, and carbon brush is always pressed onto the tool holder by spring as shown the details in Fig 3.3 (c). It should be noted that the sliding area is approximately 22 mm^2 (dimension of carbon brush; height is 3.6 mm; width is 6 mm; radius of sliding contactor is 8 mm) and the pressure of carbon brush against to tool holder is approximately 3.43 N (0.35g).

3.2.2 Evaluated electromotive force generates at cold junction

In the process of measuring EMF generated at the sliding contact, a mercury contact (Model No. 205H, MERCOTAC) with the maximum rotating speed of 3600 rev/min was used to replace the hot junction at the interface of tool-workpiece as shown in Fig. 3.4. In order to reduce noise, the mercury contact was insulated from the structure of machine and a resistance of 470 Ω was set in the parallel with the measuring position of voltage to prevent the circuit from opening.

The experiments were performed to evaluate generated EMF at the sliding contact with respects to the cutting conditions. The spindle speed was varied for 100, 300, 597, 995, 1492, 1990 and 2500 rev/min. The data of EMF was recorded after spindle was rotated for 10s and was continuously recorded every 30s (from 30 to 210s). The oscilloscope (DL750 ScopeCorder, YOKOGAWA) was used to detect and record the signal of EMF.

(a) Image of experimental setup   (b) Diagram of EMF circuits
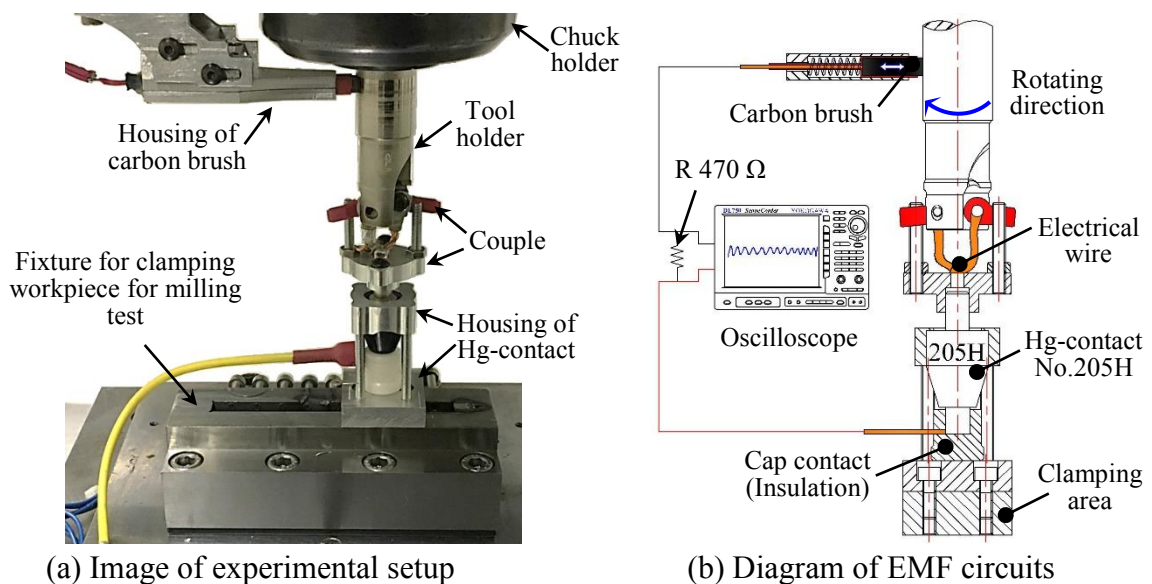
Fig. 3.4 Experimental setup for evaluated electromotive force (EMF) generated in the measuring circuit

3.2.3 Tool-work thermocouple calibration

The electromotive force (EMF) generated due to the heat in the different metal can be converted to the temperature. Generally, the EMF-temperature relation for thermocouple is non-linear and the relation of electromotive force to temperature depends on the pair of tool and work material [49]. Therefore, the electromotive force relation to temperature of Carbon brush-Tool holder and Inconel 718-Uncoated carbide inserts must be calibrated.

Precise Evaluation of Cutting Temperature in Milling Process by Tool-Work Thermocouple Method

(a) Illustration of ellipsoidal shape furnace   (b) Analogic plotter circuit
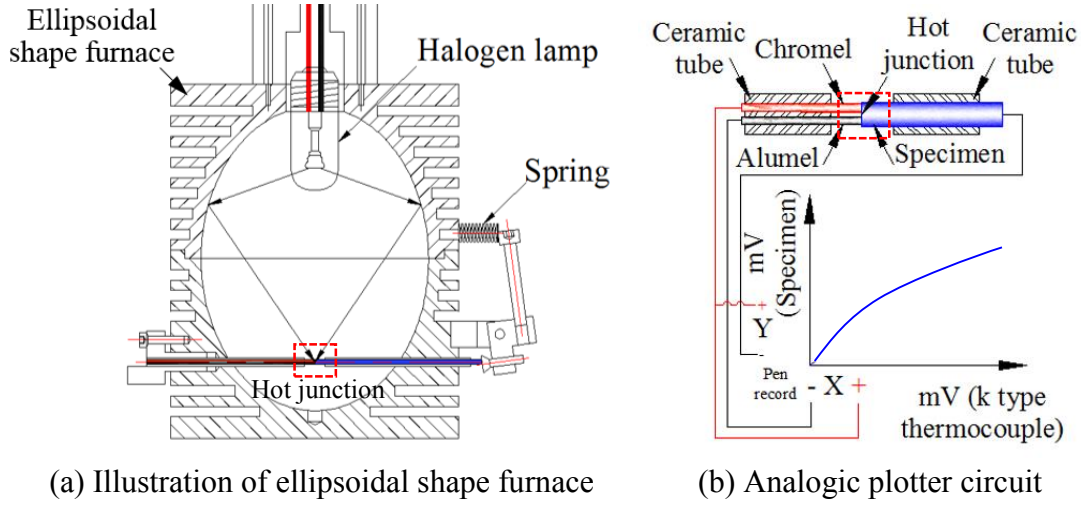
Fig. 3.5 Calibration setup and circuit for calibrating tool-work thermocouple

Figure 3.5 (a) shows an ellipsoidal furnace using for heating contact point between a K-type thermocouple (Chromel-Alumel thermocouple) and the work material or tool materials (specimen). It should be noted that the length of specimens should be long sufficiently to retain the temperature at the room temperature one side (cold junction) during heat is generated on another side (hot junction). In an ellipsoidal shape furnace was internally coated with gold and then polished in order to improve the surface reflection [18]. The halogen lamp of 1 kW is a heat source. Both the halogen lamp and the contact point (K-type thermocouple contact with specimen) are located on the focus of the ellipsoid, so that all rays of infrared heat are direct to the contact point and a hot junction occurs, in addition the hot junction can reach 1200ºC in a short time. The electromotive generated due to the different temperature the hot junction and cold junction was detected and recorded by the analogic plotter (GRAPHTEC-WX1200) with according to the circuit as shown in Fig. 3.5 (b). The electromotive force of a Chromel-Alumel (K-type thermocouple) was recorded in x-axis which relation in the electromotive force of Chromel-Speciment was recorded in y-axis. The finally calibration curve used in tool-work thermocouple method was calculated from the difference between the curves obtained for the tool and for the workpiece [50].

It should be noted that the electromotive force of K-type thermocouple is a standard to use for finding calibration curves of tool-work thermocouple. This is because the relation between electromotive force and temperature is available in the provided by manufacturers. The rational polynomial function provided as follows equation (3.1), gives an accurate approximation of the temperature according with voltage measured [51].

$$T = T_0 + \frac{(V - V_0)\Big(p_1 + (V - V_0)\big(p_2 + (V - V_0)(p_3 + p_4(V - V_0))\big)\Big)}{1 + (V - V_0)\Big(q_1 + (V - V_0)\big(q_2 + q_3(V - V_0)\big)\Big)} \tag{3.1}$$

where the coefficients can be evaluated according to the range of electromotive force measured (mV) as indicated in table 3.1.

Table 3.1. Coefficients for rational polynomial function used for a K-type thermocouple calibration [51]

Factor	Coefficients				
$Vmin$ (mV)	-6.404	-3.554	4.096	16.397	33.275
$Vmax$ (mV)	-3.554	4.096	16.397	33.273	48.838
$Tmin$ (°C)	-250	-100	100	400	800
$Tmax$ (°C)	-100	100	400	800	1200
T_0	-121.4716409	-8.793596224	310.18976	605.725621	1018.470523
V_0	-4.179085844	-0.344899142	12.63138642	25.14871778	41.99385085
p_1	36.06951328	25.67871906	24.06194895	23.53940069	25.78323885
p_2	30.72207573	-0.498879036	4.015862189	0.046547228	-1.836340284
p_3	7.791386025	-0.44705222	0.26853917	0.0134444	0.056176662
p_4	0.525939908	-0.044869203	-0.009718854	0.000592369	0.000185324
q_1	0.939395467	0.000238934	0.169985719	0.000834455	-0.074803355
q_2	0.277912853	-0.02039775	0.011413069	0.000461214	0.002384186
q_3	0.025163349	-0.001842411	-0.000392752	0.0000254881	0

The calibration curve from the experimental test for the carbon brush-tool holder is shown in Fig. 3.6 (a). In Figure 3.6 (a) can be observed curves for Chromel-Carbon brush, and one curve for Chromel-Tool holder, the final calibration curve resulted from the difference between curves of Chromel-Carbon brush and Chromel-Tool holder represents curve of Carbon brush-Tool holder. Therefore, the electromotive force (mV) generated at the sliding area of carbon brush and tool holder can be converted to the temperature which were derived by testing results of calibration as following equation (3.2).

Figure 3.6 (b) shows the obtained results of calibrating curves for Chromel-Uncoated carbide tool (IC28, ISCAR), and one curve for Chromel-Inconel 718 (AMS 5596K). The calibration curve resulted from the difference between curves of Chromel-Uncoatde carbide and Chromel-Inconel 718 represents curve of uncoated carbide tool-Inconel 718. Therefore, the electromotive force (mV) measured during milling test for milling Inconel 718 with uncoated carbide tool can be converted to the temperature which were derived by test results of calibration as following equation (3.3).

For the EMF between the sliding contact and the tool holder:

$$T = 3.1320x^3 - 20.640x^2 + 126.24x + T_R \tag{3.2}$$

For the EMF between the cutting tool and the work material:

$$T = 0.0358x^3 - 1.3681x^2 + 66.876x + T_R \tag{3.3}$$

where, T (°C) is the temperature measured, x (mV) is the EMF and T_R (°C) is the room temperature (≈ 20°C in this study).
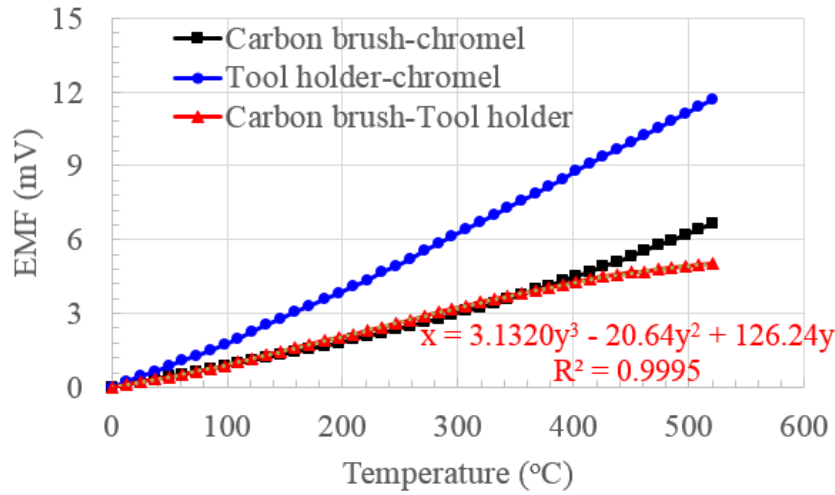
(a) Calibration curve for carbon brush-tool holder
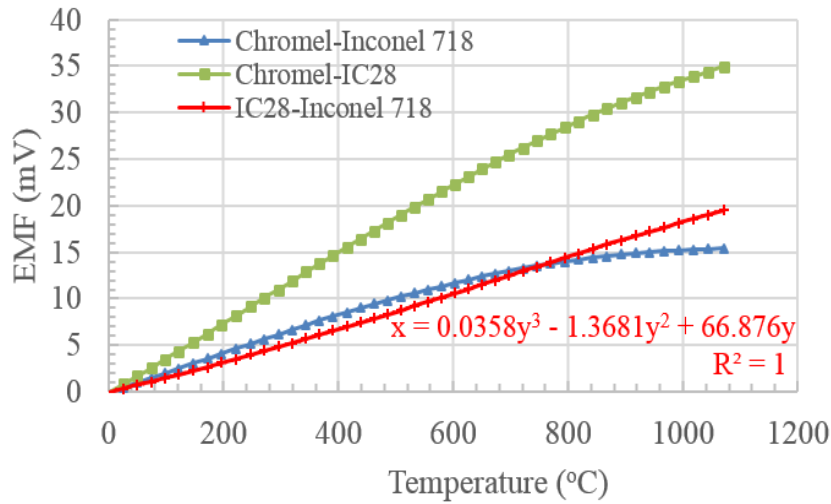
(b) Calibration curve for uncoated carbide tool (IC28)-Inconel 718

Fig. 3.6 Calibration curves for tool-work thermocouple

3.2.4 Cutting experiments

The cutting experiments are carried out on the vertical milling machine (Shizuoka ST-NR CNC). The uncoated carbide insert (APKR1003PDR-H IC28, ISCAR) is a cutting tool. Though two inserts can be mounted to the holder (HM90 E90A-D160-2-C16, ISCAR), single insert is mounted onto the holder. This is because to avoid the influence of difference in height of cutting edges between two teeth and to maintain constant cutting conditions. Inconel 718 is a work materials which is mounted on the table of machine by means of fixture and is insulated from the structure of machine as shown the experimental setup in Fig. 3.7 (a). In the cutting test for measuring cutting temperature the workpiece (Inconel 718) was replaced a Hg-contact (slip-ring) in the fixture as shown in Fig. 3.7 (b) and the details of cutting conditions for milling test is sumarized in Table 3.2.

(a) Image of experimental setup   (b) Diagram of EMF circuit
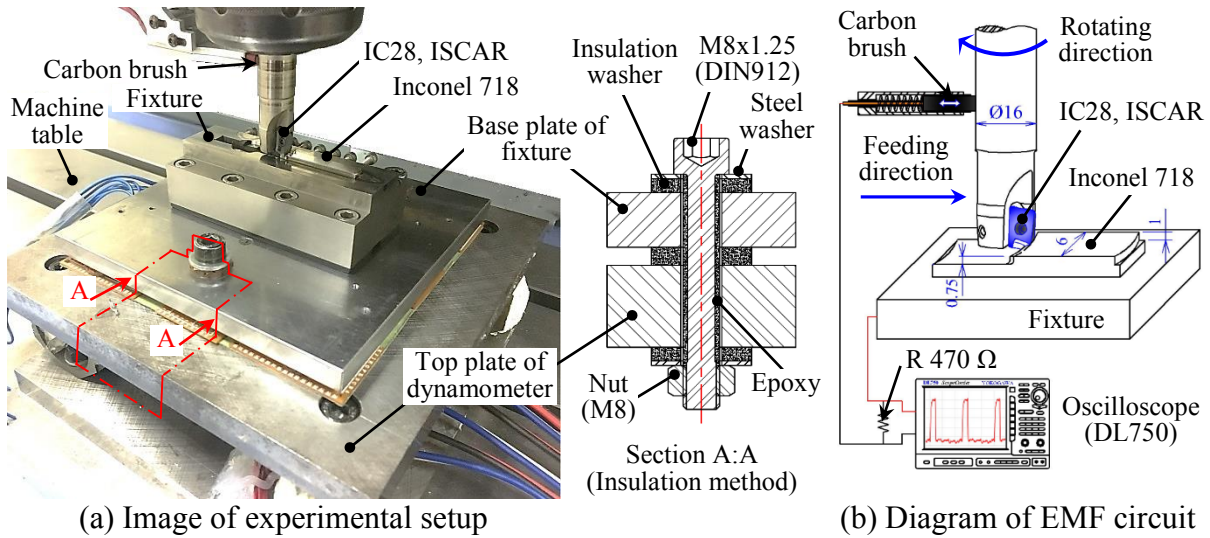
Fig. 3.7 Experimental setup for measured electromotive force (EMF) during cutting test

Table 3.2 Cutting conditions for cutting tests

Cutting conditions	Details
Cutting speed, V (m/min)	30, 50, 75, 100
Spindle speed, n (rev/min)	597, 995, 1492, 1990
Feed, f_z (mm/tooth)	0.05
Depth of cut, DoC (mm)	0.75
Width of cut, w (mm)	6.00 (symmetry face milling)
Tool holder (mm)	16.00
Cutting operation	Dry

3.3 Results and discussions

3.3.1 Electromotive force generated at the cold junction

Figure 3.8 shows the obtained results of electromotive force generated in the measuring circuits versus the rubbing time with difference of spindle speed. As shown in Fig. 3.8 (a) to 3.8 (f), the electromotive force generated in the measuring circuit repeat experimental test 6 times. It was found that the electromotive generated in measuring circuit was in the range of 0.103±0.10, 0.106±0.10, 0.142±0.12, 0.303±0.14, 0.524±0.22, 0.566±0.20 and 0.474±0.36 mV for the spindle speed of 100, 300, 597, 995, 1492 and 1990 rev/min, respectively. It can be also observed that the electromotive force increased with the spindle speed due to the more heat generation at the high rubbing speed.

In addition, the influence of measuring time could be ignored for the spindle speed in the range of 100 to 1990 rev/min because the average electromotive force was almost constant when rubbing time varied. However, the increased spindle speed of 2500 rev/min resulted in the highest fluctuation of electromotive force in the measured circuit with varied rubbing time as shown in Fig. 3.8 (g). This is because the increase of spindle speed resulted in the unstable connect of sliding contact. This fact can be observed from the obtained results of

the increase in electromotive force distributed (tolerance of EMF from the average value) as the spindle speed increased when experiment repeated. However, the researcher believed that the increased force for pressing carbon brush against tool holder could be decreased in the unstable contact in the measuring circuit.
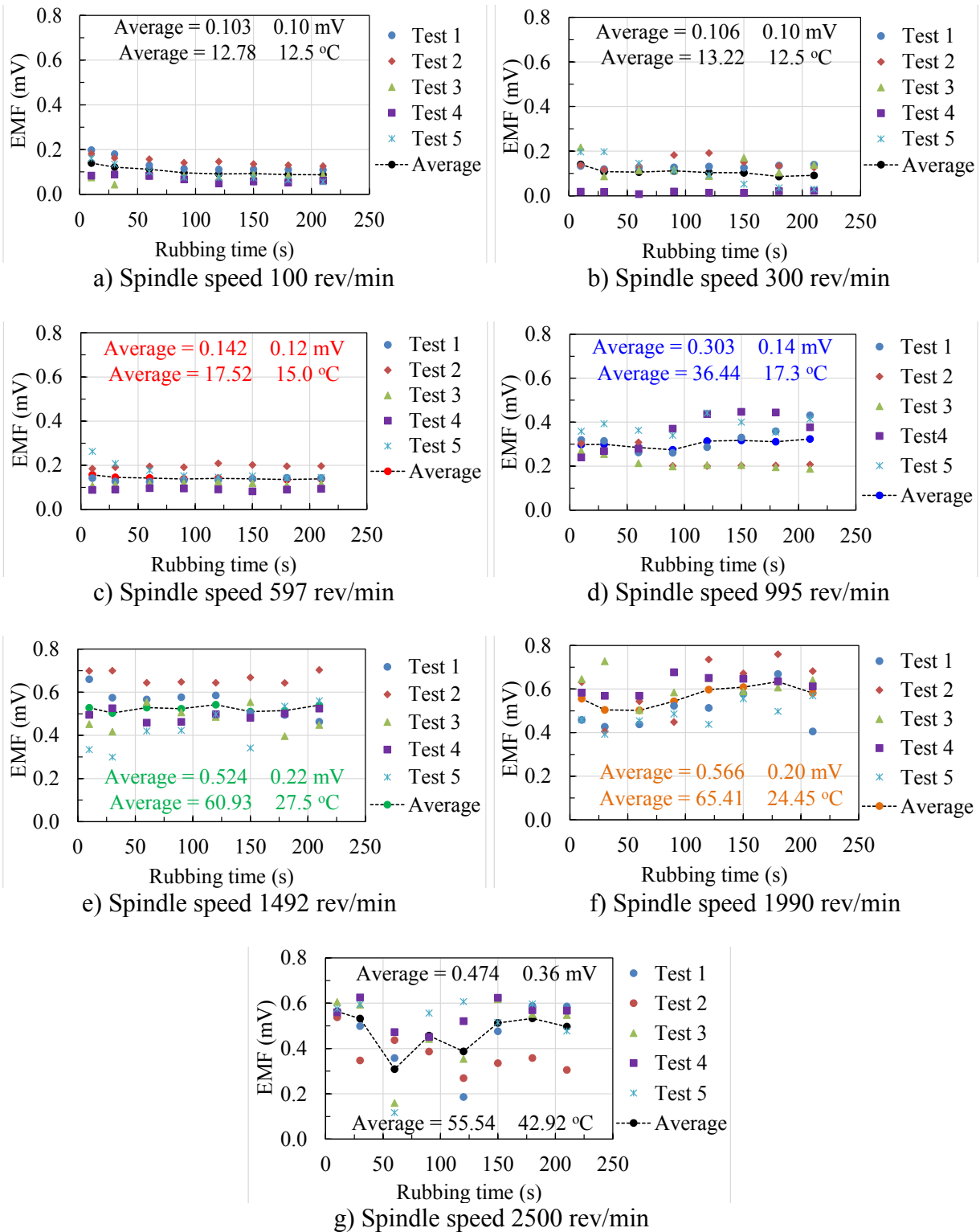
Fig. 3.8 Results of electromotive force (EMF) generated in the measuring circuit with various rubbing time and spindle speed
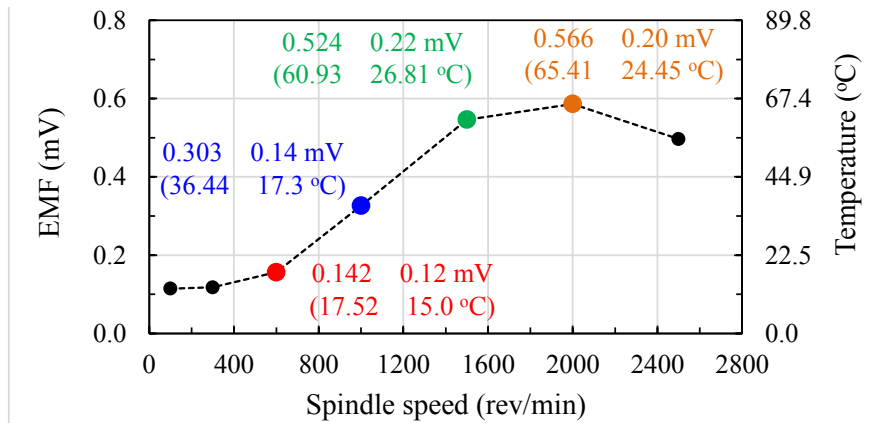
Fig. 3.9 Results of electromotive force (EMF) generated in the measuring circuit

Figure 3.9 shows the results of electromotive force (EMF) generated in the measuring circuit. From this results, it is possible to measure the cutting temperature distinctively from EMF generated at the sliding contact. The electromotive force generated in the cutting test must be compensated before convert to the cutting temperature because the response of electromotive force to the temperature are depended on the pair metal for the tool-work thermocouple.

It should be note that the electromotive force in the measuring circuit as presented in this chapter was included the noise generated in the machining operation because the tool holder cannot completely insulate from the structure of machine.

3.3.2 Cutting temperature

Figure 3.10 shows a single wave form of cutting temperature when the uncoated carbide insert was used for milling Inconel 718 with variable cutting speeds. This signal in Fig. 3.10 (a) was obtained when carbon brush and tool holder were unstable contact. Figs. 3.10 (b), (c), (d) and (e) were obtained for the cutting speed of 30, 50, 75 and 100 m/min, respectively. Results show that the cutting temperature increased rapidly when the cutting edge engaged with the work material. Then, it slightly increased and became the maximum, and the signal finally drastically dropped because of the cutting tool breakaway from the work material. The maximum cutting temperatures obtained were approximately 571, 629, 700 and 764°C for the cutting speed of 30, 50, 75 and 100 m/min, respectively.

The duration time of tool-work interface during face milling for a single cutting cycle in calculation was approximately 12.30, 7.38, 4.92 and 3.67 ms for the spindle speed of 597, 995, 1492 and 1990 rev/min, respectively. However, the duration time of tool-work interface in experimental cutting as presented in Figs. 3.10 (b), (c), (d) and (e) was approximately 14, 9, 6.5 and 5.5 ms for the spindle speed of 597, 995, 1492 and 1990 rev/min, respectively. The duration time in cutting experiment was slightly higher than calculation. This is because the Inconel 718 was sticky in nature of materials. Therefore, the work materials was easily to deform as a burr in the direction of cutting speed and the chip (work material) was easily to

adhere on the rake face of cutting tool. These are leading to increasing time of tool-workpiece interface. This fact can be confirmed by the photograph during cutting test as shown in Fig. 3.11.

(a) Unstable EMF at V 30 m/min

(b) EMF at V 30 m/min

(c) EMF at V 50 m/min

(d) EMF at V 75 m/min

(e) EMF at V 100 m/min
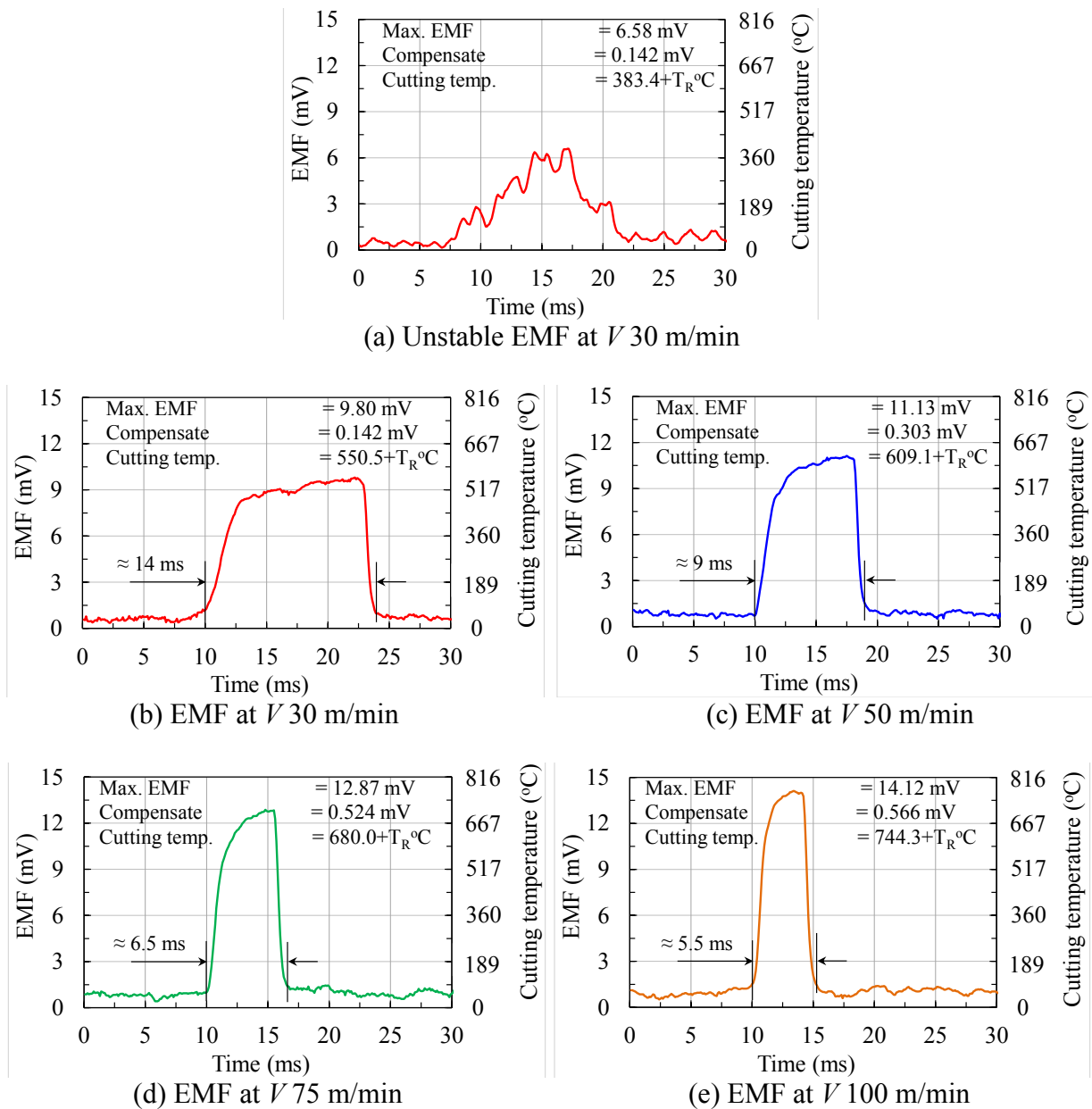
Fig. 3.10 Signal of electromotive force (EMF) and cutting temperature with various cutting speed (V).

(a) Photograph of tool-work interface   (b) Burr generated on the workpiece
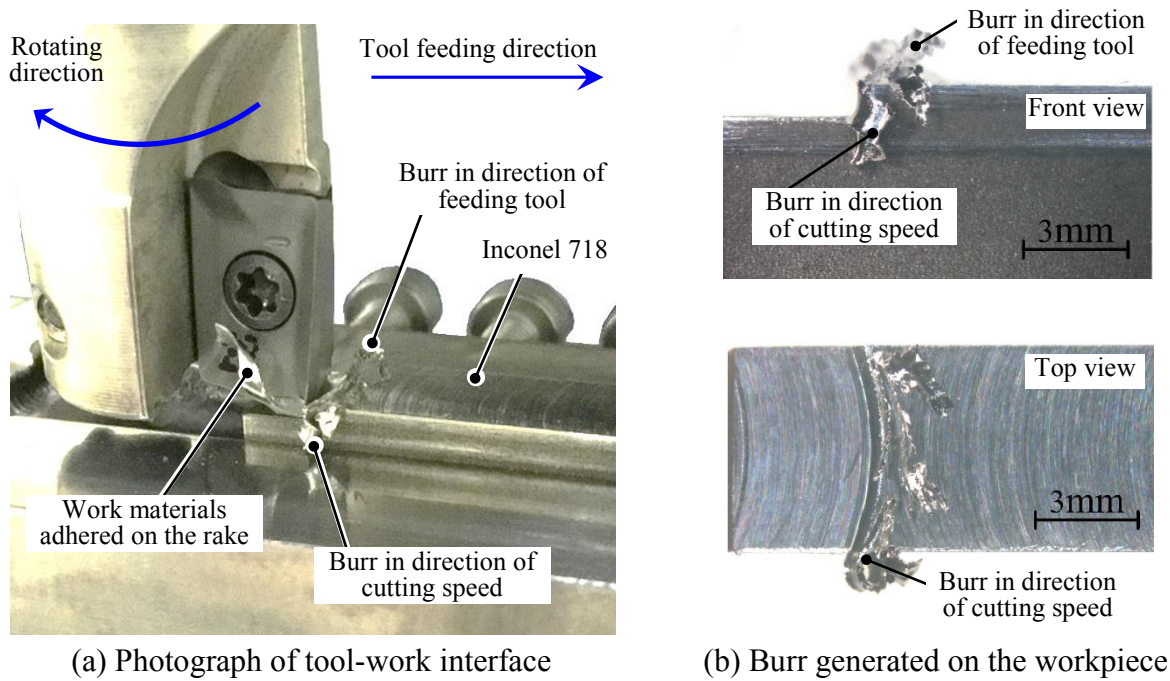
Fig. 3.11 Burr in the direction of cutting speed and chip adhered on the rake face of cutting tool during face milling test with the cutting speed (V) of 30 m/min.

3.4 Conclusions

In this chapter, carbon brush was designed to use as a sliding contact for connect electromotive force (EMF) signal from tool holder to the data acquisition system. The rubbing area of carbon brush was approximately 22 mm^2 and always pressed to the tool holder by spring with the pressure approximately 3.43 N (0.35g). The electromotive force generated in the measuring circuit, and the electromotive force relation to the temperature for the tool-work thermocouple were investigated in this study. In addition, the cutting test were performed to investigate cutting temperature in face milling for Inconel 718 with uncoated carbide tool. The conclusions can be summarized as follows:

1. The electromotive force (EMF) of carbon brush-tool holder and uncoated tungsten carbide (IC28, ISCAR)-Inconel 718 can be converted to the temperature by test results of calibration curves. The response of EMF generated to the temperature was approximately 1 mV : 100ºC for the carbon bush-tool holder and was approximately 1 mV : 54ºC for uncoated carbide tool-Inconel 718 thermocouple.

2. The electromotive force (EMF) generated in the measuring circuit was increased with the spindle speed due to more heat generated at the higher rubbing speed. The average of electromotive force generate was 0.142±0.12 mV (18±15ºC), 0.303±0.14 mV (36±18ºC), 0.524±0.0.22 mV (61±27ºC) and 0.566±0.20 mV (65±24ºC) for the spindle speed of 597, 995, 1492 and 1990 rev/min, respectively. Therefore, the cutting temperature can be distinctively evaluated from electromotive force generated at the sliding contact by compensation of measured electromotive force in the machining process.

3. The cutting temperature was increased with the cutting speed. The highest cutting temperature in the process of face milling for Inconel 718 was approximately 571, 629, 700 and 764ºC for the cutting speed of 30, 50, 75 and 100 m/min, respectively.

4. It should be noted that the time duration of tool-work interface in the cutting test was larger than the geometrical calculation due to the chip adhered on the rake face of cutting tool and burr occurred in the direction of cutting velocity leading to an increase in tool-work contact length. In addition, the electromotive force generated in the measuring circuit decreased with the increased cutting speed of 2500 rev/min due to the unstable contact at the sliding area. However, the researcher believed that the unstable contact at the high speed can be improved by increased force for pressing carbon brush to the tool holder.

Chapter 4

Effects of Preheating Temperature at Primary Shear Zone in Laser Assisted Milling Process

4.1 Introduction

It is well-known that the hot machining technique can improve the machinability of difficult-to-cut materials. This technique needs the external heat source such as induction, plasma, gas torch or laser in order to reduce the refractory of work materials prior to the material removal by cutting tool [1, 2]. Laser has been widely applied in various machining process such as turning, grinding and milling as shown in Fig. 4.1 because the laser is a rapid heat source which has high energy concentration to heat the material locally in the machining zone [3].

(a) Laser assisted turning [52]   (b) Laser assisted grinding [54]

(c) Laser assisted milling [53]   (d) Schematic of laser heating
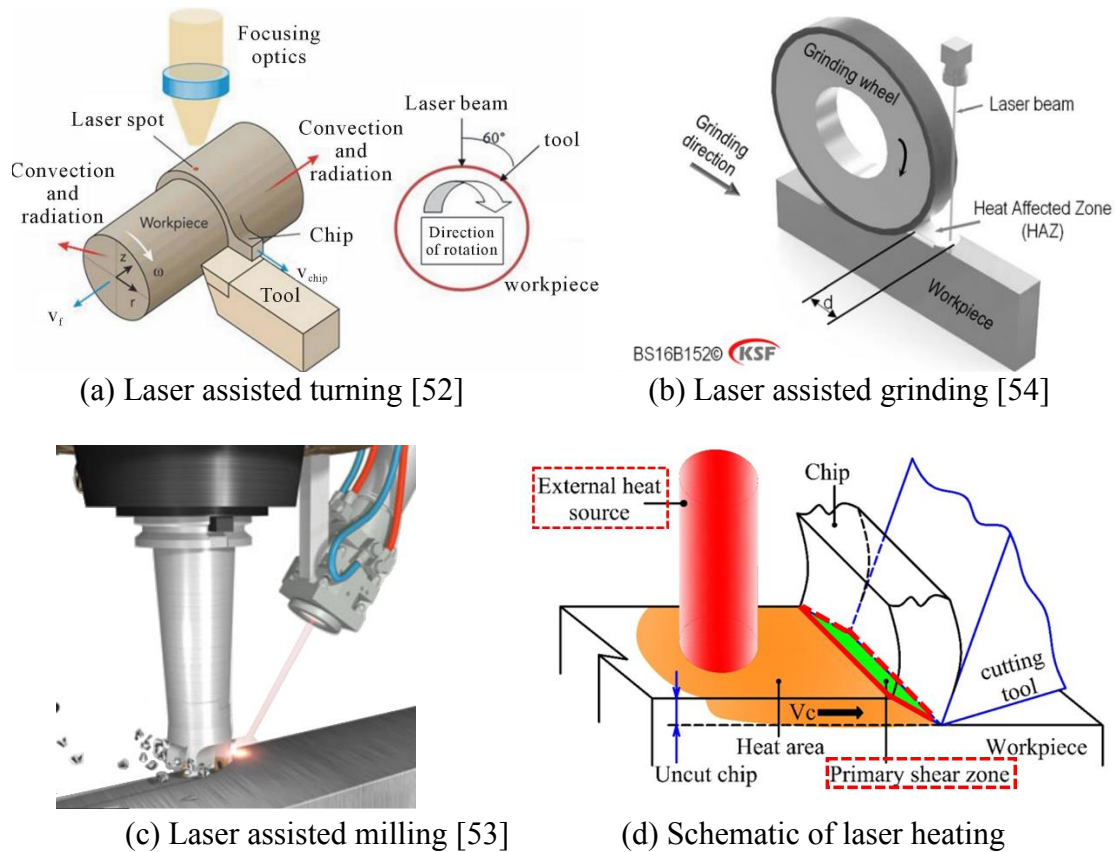
Fig. 4.1 Application of laser in machining processes

Based on the literature reviews, it is found that the heat energy to sufficiently soften workpiece depended on the materials as shown in Fig. 4.2 (a). The heating temperature within the machining zone requires sufficient laser power to significantly reduce the mechanical strength and hardness of work materials. In addition, the cutting conditions such as shown in

25

Fig. 4.2 (b) also affect to the requiring laser power. It is well known that the hardness of Inconel 718 increases as the temperature increased below 650°C [19] and significantly reduces tensile strength when the temperature is above 750°C [19,55]. Whereas, the peak temperature higher than 950°C (recrystallization) would damage the machined surface because the mechanical properties and microstructure of material are changed [1]. Thus, in order to soften the work materials and avoid the damage from laser heating, the peak heating temperature and preheating temperature at the primary shear zone must be evaluated and controlled.

(a) Mechanical strength of difficult-to-cut   (b) Cutting condition on the heating
materials with elevated temperature   temperature in machining process
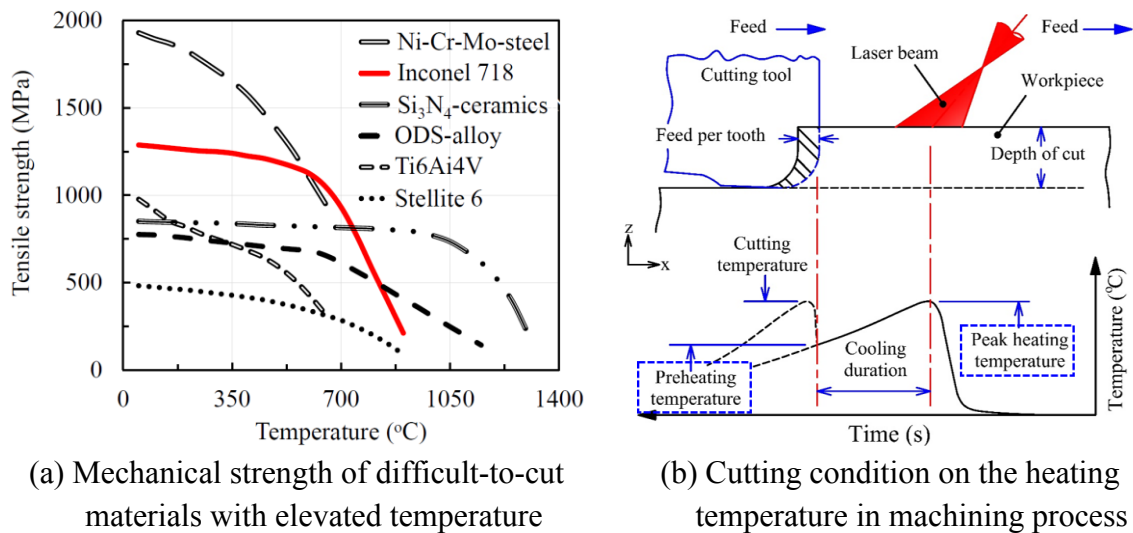
Fig. 4.2 Mechanical strength of materials and conditions on the heating temperature

The goals of this study are to evaluate and control the laser power from the viewpoint of the peak and preheating temperature at the primary shear zone of work material in the milling experiment. Furthermore, the influence of cutting conditions and preheating temperature on the components of cutting force, cutting temperature in the region of tool-chip interface, tool wear and integrity on machined surface (roughness and hardness) are evaluated to compare with the conventional machining.

4.2 Experimental procedures

Two stages of experiment were performed in this study. The first stage, a K-type thermocouple was embedded to measure temperature in the Inconel 718 with the varied laser power irradiated on the surface of workpiece in order to calibrating laser power to particular heating temperature at primary shear zone. The uncertain conditions (error) in the experimental setup was also investigated. In addition, the peak heating temperature was limited below 950°C. In the second stage, uncoated carbide insert was used in the process of LAM for face milling Inconel 718 to compare the cutting performance with conventional machining.

4.2.1 Calibrating laser power

A diode laser (Laserline LDF 6000-40) with the maximum power of 6 kW was used as a heat source. The focusing head was mounted on the spindle head of a vertical milling machine, and the laser beam axis was set at 50° to x-y plane and 45° to y-z plane as show in

the Fig. 4.3 (a). The beam spot of 3.5-4 mm was positioned 4 mm ahead of the cutting point (the center of beam spot to the edge of cutting tool).

A K-type thermocouple with the diameter of 1.0 mm was inserted into a drilled hole (Ø ≈ 1.2 mm). The hot junction contacted with the hole bottom at the depth 0.75 mm and the thermal electromotive force (EMF) was detected and recorded by an oscilloscope as shown details in Fig. 4.3 (b). In order to evaluate the relationship between the laser power and temperature, the experiments were conducted under the conditions shown in Table 4.1 and Table 4.2. It should be noted that prior to each experimental trials, the work surface was polished by sand paper in order to avoid the different absorption on the surface of workpiece. Moreover, the concurrent experiments were performed to reduce and evaluate the error in the calibration process.
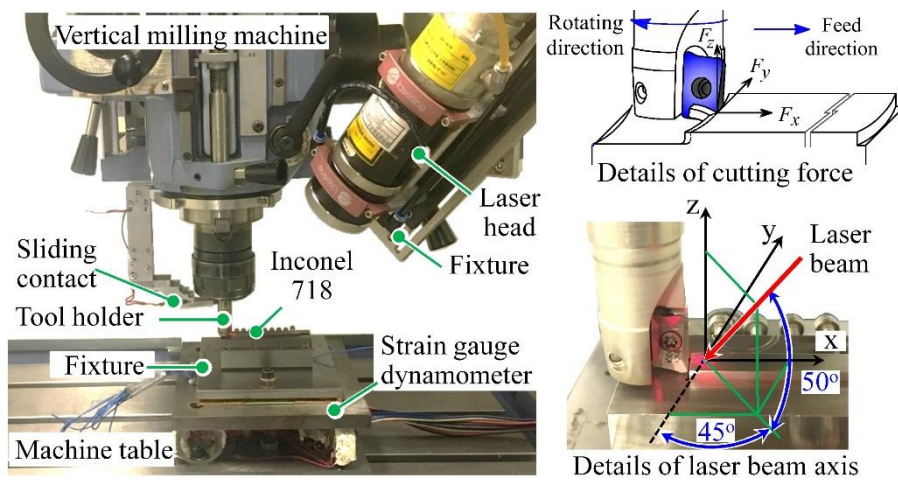
(a) Position of laser fixed head on milling machine
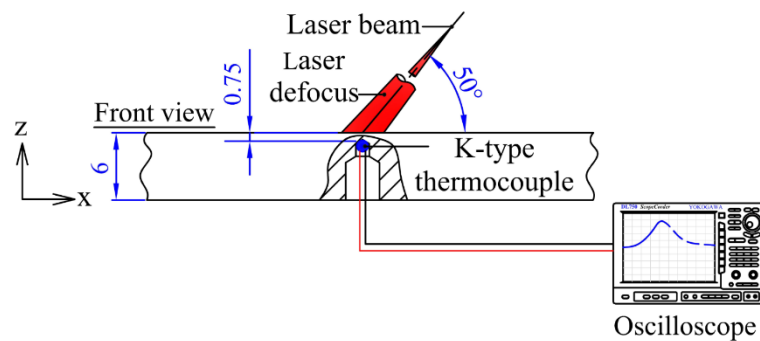
(b) Details of laser assisted machining setup

Fig. 4.3 Schematic illustration of experimental setup for calibrating laser power

Table 4.1 Cutting conditions in experiment with various cutting speed

Conditions	V (m/ min)	Feed (mm/ tooth)	Tool diameter (mm)	Axial depth of cut (mm)	Spindle speed (rpm)
1	30				597
2	50	0.05	16	0.75	995
3	75				1492
4	100				1990

Table 4.2 Laser power used for calibrating temperature

Table speed (mm/min)	Laser power (W)			
	Level 1	Level 2	Level 3	Level 4
30	119	165	223	313
50	150	190	253	332
75	190	232	310	388
100	220	275	340	430

4.2.2 Laser assisted machining experiments

Symmetrical face milling tests were performed to evaluate the cutting performance with various preheating temperatures of approximately 20, 300, 500, and 700ºC for the cutting speed of 30, 50, 75 and 100 m/min. The used cutting tool was an uncoated cemented carbide inserts (APKR1003PDR-H IC28, ISCAR). A single insert was mounted onto the tool holder (HM90A-D16-2-C16, ISCAR) in order to avoid the influence of difference in height of cutting edges between teeth and maintain the constant depth of cut (DoC). Inconel 718 was a work material, which was mounted onto the dynamometer by means of fixture as shown in Fig. 4.4 The components of strain in the gauge changed in three directions (εx, εy and εz) during the experimental cutting were detected and recorded by a digital oscilloscope (Yokogawa DL750 ScopeCorder). Then, the changed strain in the gauges was converted to the components of cutting force (Fx, Fy and Fz) by test results of calibration [56] as follows;

For the test results of changed strain in the gauges with varied forces following equation (4.1).

$$\begin{Bmatrix} \varepsilon x \\ \varepsilon y \\ \varepsilon z \end{Bmatrix} = \begin{bmatrix} 0.2118 & 0.0057 & -0.0256 \\ 0.0572 & 0.2212 & 0.0053 \\ -0.055 & 0.0017 & -0.2221 \end{bmatrix} \begin{Bmatrix} Fx \\ Fy \\ Fz \end{Bmatrix} \qquad (4.1)$$

where, εx (μSTR) is changed strain in the gauges in the direction of feeding tool (x-axis), εy (μSTR) is strain in the gauges changed in the direction of cutting speed (y-axis) and εz (μSTR) is changed strain in the gauges in the direction of axil of cutting tool (z-axis).

The changed strain in the cutting process can be converted to the component of cutting forces as following equation (4.2).

$$\begin{Bmatrix} Fx \\ Fy \\ Fz \end{Bmatrix} = \begin{bmatrix} 4.6136 & -0.1147 & -0.5345 \\ -1.1654 & 4.5489 & 0.2429 \\ -1.1514 & 0.0632 & -4.3683 \end{bmatrix} \begin{Bmatrix} \varepsilon x \\ \varepsilon y \\ \varepsilon z \end{Bmatrix} \qquad (4.2)$$

where, F_x (N) is a thrust force (force in the direction of feeding), F_y (N) is a tangential force (force in the direction of cutting speed) and F_z (N) is a axial force (force in the direction to tool perpendicular with machined surface).

In the cutting test, work material was insulated from the structure of the machine for measuring electromotive force (EMF) during cutting process by tool-work thermocouple. The electromotive force generated in the cutting tests must be compensated the electromotive force generated in the measuring circuit before convert to the cutting temperature (refer chapter 3 section 3.3.1). The electromotive force of uncoated carbide tool-Inconel 718 can be converted to the cutting temperature by test results of calibrated curves (refer chapter 3 section 3.2.3) as following equation (3.3).

$$T = 0.0358x^3 - 1.3681x^2 + 66.876x + T_R \qquad (3.3)$$

where, T (^{o}C) is the measured temperature, x (mV) is the EMF from tool-work thermocouple and T_R (^{o}C) is the room temperature (in this test is approximately 20°C).
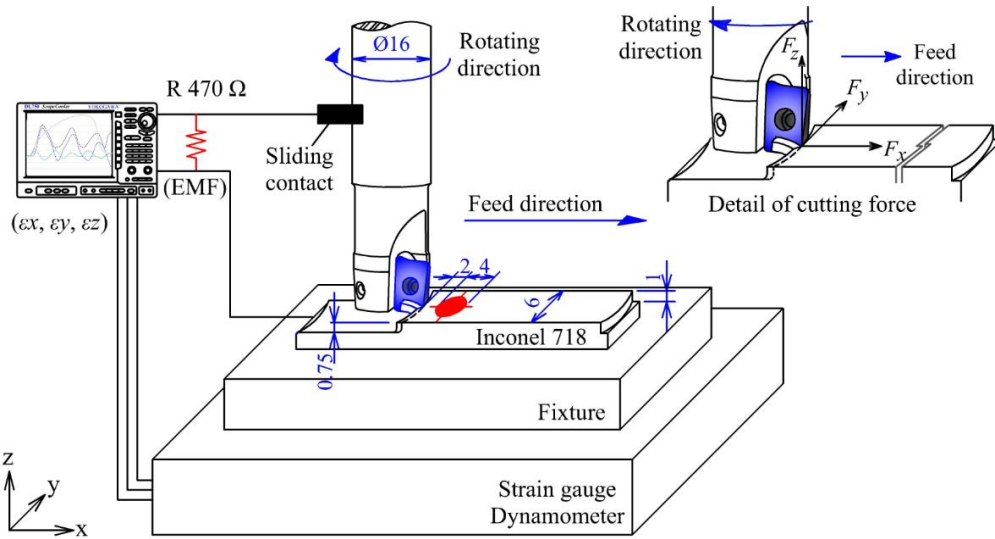
Fig. 4.4 Illustrate diagram of experimental setup for cutting test

The maximum flank wear was measured with a toolmaker's microscope (Mitutoyo). The roughness of machined surface (Ra) was measured by Surfcorder SE-30D (Kosaka Lab, Ltd). The hardness of machined surface was evaluated by Vickers hardness tester (MMT-X7-LCD, MATSUZAWA). The load in tests was 200g (1.96 N) and the average hardness value was calculated from the fifteen points testing.

It should be noted that prior to the cutting experiment, a skin cut of 0.2 mm thickness was done in order to remove any deformities on the work surface, and it was polished with the

sandpaper to keep the surface absorption constant during the process of calibrating laser power. In addition, edge of workpiece at the start and end of cutting test were pre-machined to limit cutting distance of 4.5 m (machining length 36.60 mm) for any cutting conditions.

4.3 Results and discussion

In this study, conditions in experimental setup (error) was investigated and controlled before calibrating power of laser to the heating temperature. Then, the relationship of laser power and heating temperature was used to estimate the laser power for particular preheating temperature. Finally, the influences of preheating temperature on the cutting temperature, shear stress, tool wear and integrity of machined surface were analyzed and discussed.

4.3.1 Calibrating laser power to preheating temperature

The uncertain conditions in experimental setup was investigated and controlled prior calibration laser power to preheating temperature. According to higher thermal expansion and heating temperature generally occur under the conditions of large duration time of laser irradiated with the high laser power. Therefore, the lowest table speed of 30 mm/min with laser power of 223 W (laser power higher than approximately 250 W could damage surface of workpiece) was performed to evaluate the approximately distance from the starting position of laser irradiated to a K-type thermocouple, and to investigate the error in calibrating process. The examples of heating temperature in test are shown in Fig. 4.5

(a) Heating temperature versus time and moving distance

(b) Heating temperature with offset lay of laser moving

(c) Heating temperature with repeated experiments
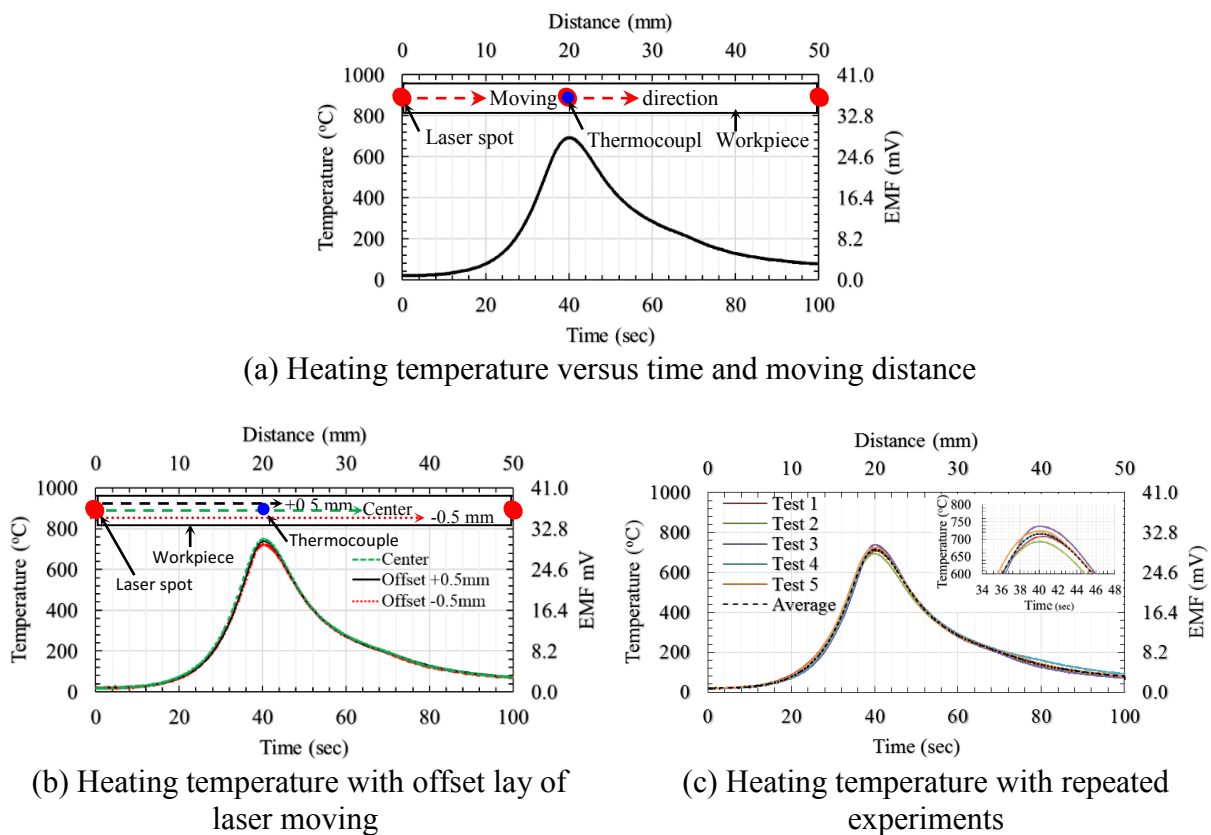
Fig. 4.5 Profile of heating temperature were obtained when the laser power of 223 W was used for the table speed of 30 mm/min

Figure 4.5 (a) shows the experimental results for the approximately distance of laser starting to irradiate to the position of a K-type thermocouple. It was found that the minimum sufficient distance to detect EMF was larger than 15 mm. This is because the temperature slightly increased when laser spot moved close on thermocouple of approximately 15 mm. Then, the temperature was drastically increased and became maximum when laser spot travelled through the thermocouple, after that the temperature was gently reduced because of the laser heat source moved far away from the thermocouple (this mean cooling period). It should be note that the sufficient distance between laser starting to irradiate and thermocouple could be decreased when the table speed increased due to the decrease in the time of laser irradiated and thermal diffusion.

Figure 4.5 (b) shows the profile of heating temperature when the positions of laser spot were offset $\pm$ 0.5 mm from the center of workpiece along the y-axis. The peak temperature was obtained approximately 735, 724 and 710°C for the laser moving along the center of workpiece, offset of +0.5 mm, and offset of -0.5 mm from the center of workpiece, respectively. These results can be referred that the error of laser setup positions in the range of $\pm$ 0.5 mm insignificant to change the heating temperature. The average of peak temperature and error were approximately 723$\pm$13°C (error approximately 2 % of the average heating temperature).

Figure 4.5 (c) shows the profiles of heating temperature when the experimental irradiations were repeated. The obtained results shows that the peak heating temperature was approximately 709, 693, 737, 718 and 725°C for repetition of 5 times. From these results, it can be concluded that the average of peak heating temperature was approximately 716°C, while the error of heating temperature due to the uncertain of testing conditions (experimental arrangements, polishing surface of workpiece and so on) was in the range of $\pm$ 23°C (approximately 3 % of the average heating temperature).

Figures 4.6, 4.8, 4.10, and 4.12 provide temperature profiles measured for the table speed of 30, 50, 75, and 100 mm/min, respectively. And, Figures 4.7, 4.9, 4.11, and 4.13 are the relationships between the laser power and the temperature measured for the table speed of 30, 50, 75, and 100 mm/min, respectively.

Figure 4.6 shows the temperature profiles measured for the table speed of 30 mm/min. It was found that the peak heating temperature (T_p) was 268, 424, 694 and 943°C when the laser power varied at 119, 165, 223 and 313W, respectively. The obtained results showed that the temperature proportionally increased with the laser power as shown in Fig. 4.7. However, the region of primary shear zone is 4 mm behind the center of laser spot. Therefore, the preheating temperature at shear zone (T_s) is slightly lower than the peak temperature (T_p) for each laser power, because of the cooling time of 8 s. For example, it can be observed that the highest laser power of 313 W yielded the preheating temperature of 708°C, and peak temperature of 943°C.

31

Effects of Preheating Temperature at Primary Shear Zone in Laser Assisted Milling Process
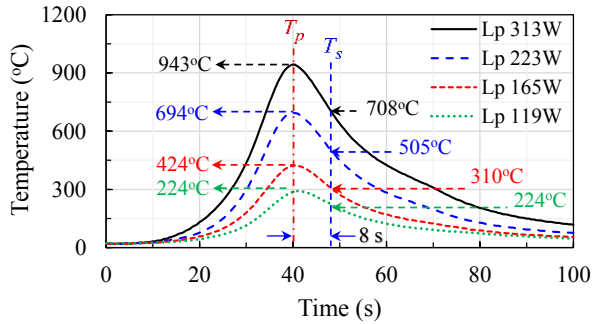
Fig. 4.6 Profile of heating temperature with the table speed of 30 mm/min
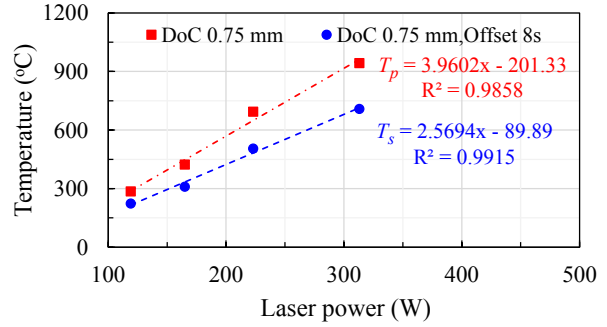
Fig. 4.7 Relationship between laser power and heating temperature of table speed 30 mm/min
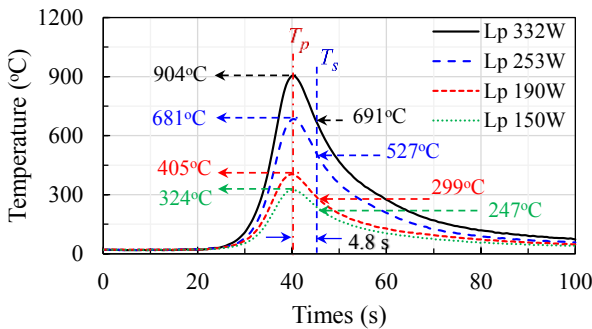
Fig. 4.8 Profile of heating temperature with the table speed of 50 mm/min
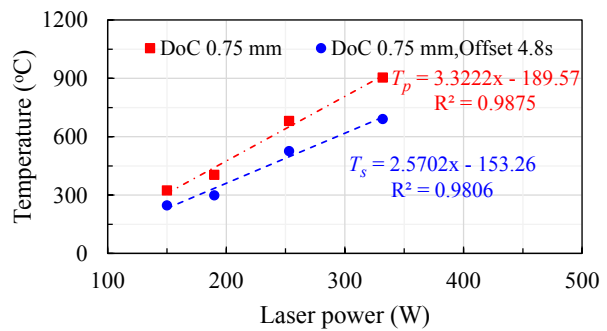
Fig. 4.9 Relationship between laser power and heating temperature of table speed 50 mm/min
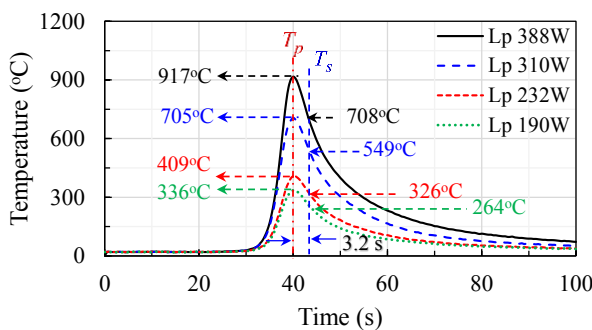
Fig. 4.10 Profile of heating temperature with the table speed of 75 mm/min
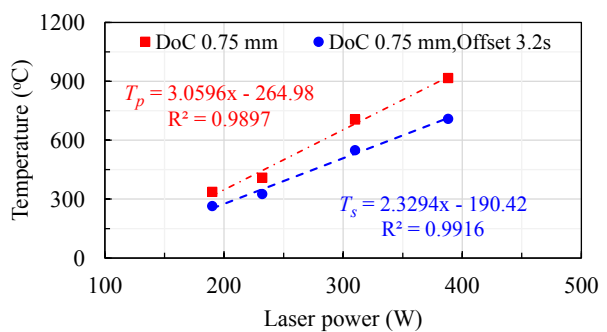
Fig. 4.11 Relationship between laser power and heating temperature of table speed 75 mm/min
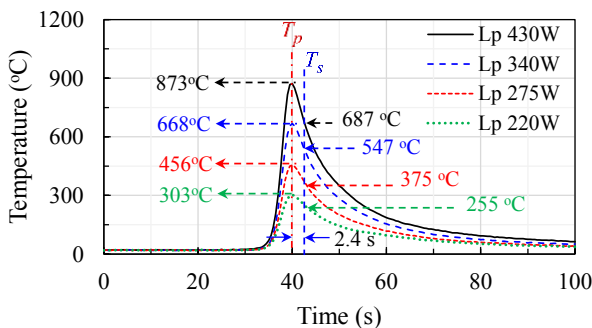
Fig. 4.12 Profile of heating temperature with the table speed of 100 mm/min
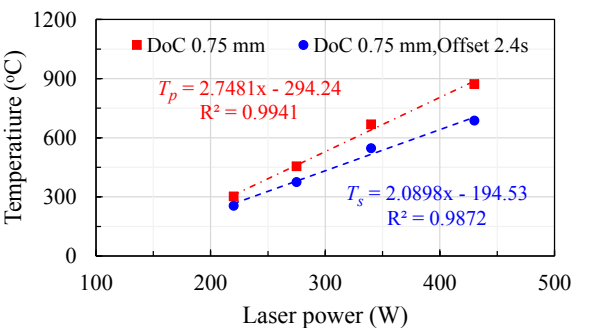
Fig. 4.13 Relationship between laser power and heating temperature of table speed 100 mm/min

The peaks heating temperature (T_p) of 324, 405, 681 and 904 were obtained when the laser power varied at 150, 190, 253 and 332W, respectively. These results show that the temperature was proportionally increased as a function of laser power as shown in Fig. 4.9. The offset in feed direction caused 4.8s cooling time for the cutting speed of 50 m/min. Thus, the highest preheating temperature at primary shear zone (T_s) can be approximated 691°C and the peak heating temperature can be approximated 904°C for the laser power 332W.

Figure 4.10 shows the temperature profiles measured for the table speed of 75 mm/min, and Fig. 4.11 shows the relationship between the laser power and temperature. These results show that the peak heating temperature (T_p) of 336, 409, 705 and 917 °C were obtained when the laser power varied 190, 232, 310 and 388W, respectively. Here, the preheating temperature in the primary shear zone (T_s) can be estimated with the cooling time of 3.2 s. So, the highest preheating temperature (T_s) of 708°C and the highest peak heating temperature (T_p) of 917 °C were obtained when the laser power was 388 W in experiment.

Figure 4.12 shows the temperature profiles measured for the table speed of 100 mm/min, and Fig. 4.13 shows the relationship between the laser power and heating temperature. These results show that the varied laser power of 220, 275, 340 and 430 W generated peak heating temperature (T_p) of 303, 456, 668 and 873°C, respectively. The offset in feed direction caused 2.4 s cooling time for the table speed of 100 mm/min. Therefore, the preheating temperature at primary shear zone (T_s) can be approximated 255, 375, 547 and 687 °C for the laser power of 220, 275, 340 and 430 W, respectively.

Comparing results in Figs. 4.6, 4.8, 4.10 and 4.12, it can be confirmed that the profiles of heating temperature changed with the table speed. This is because the period time for thermal diffusion decreased. The error of estimated preheating temperature as following equation as shown in Figs. 4.7, 4.9, 4,11 and 4.13 was less than 35°C to compared with the test results (refer Figs. 6, 8, 10 and 12). And, the error of preheating temperature was in the range of ± 3.57% under the position of irradiating point in experimental setup was error ± 0.25 mm.

From the obtained results in Figs. 4.7, 4.9, 4.11, and 4.13, it can be concluded that the heating temperature increased with the laser power for any table speed, and the requirement of laser power was increased for retaining as the same heating temperature when the table speed was increased. This is because the heating time was reduced when the table speed was increased. However, the heating temperature has a trend to increase as a linear function of the laser power for any table speed (30, 50, 75 and 100 mm/min). Therefore, these relationships can be used to estimate the laser power for each preheating temperature (300, 500 and 700°C) and peak heating temperature in this study.

4.3.2 Cutting force and cutting temperature

Figure 4.14 shows the signal of changed strain in the gauges and electromotive force generated during cutting test for a cycle of cutting tool interface with the workpiece. The changed strain in the gauges can be converted to the cutting force by test results of calibrating

Effects of Preheating Temperature at Primary Shear Zone in Laser Assisted Milling Process

force as derived in equation (6.2) and electromotive force can be converted to the cutting temperature by test results of calibrated curves as derived in equation (3.3), respectively.

(a) CM 20°C with *V* 30 m/min   (b) LAM 700°C with *V* 30 m/min

(c) CM 20°C with *V* 50 m/min   (d) LAM 700°C with *V* 50 m/min

(e) CM 20°C with *V* 75 m/min   (f) LAM 700°C with *V* 75 m/min

(g) CM 20°C with *V* 100 m/min   (h) LAM 700°C with *V* 100 m/min
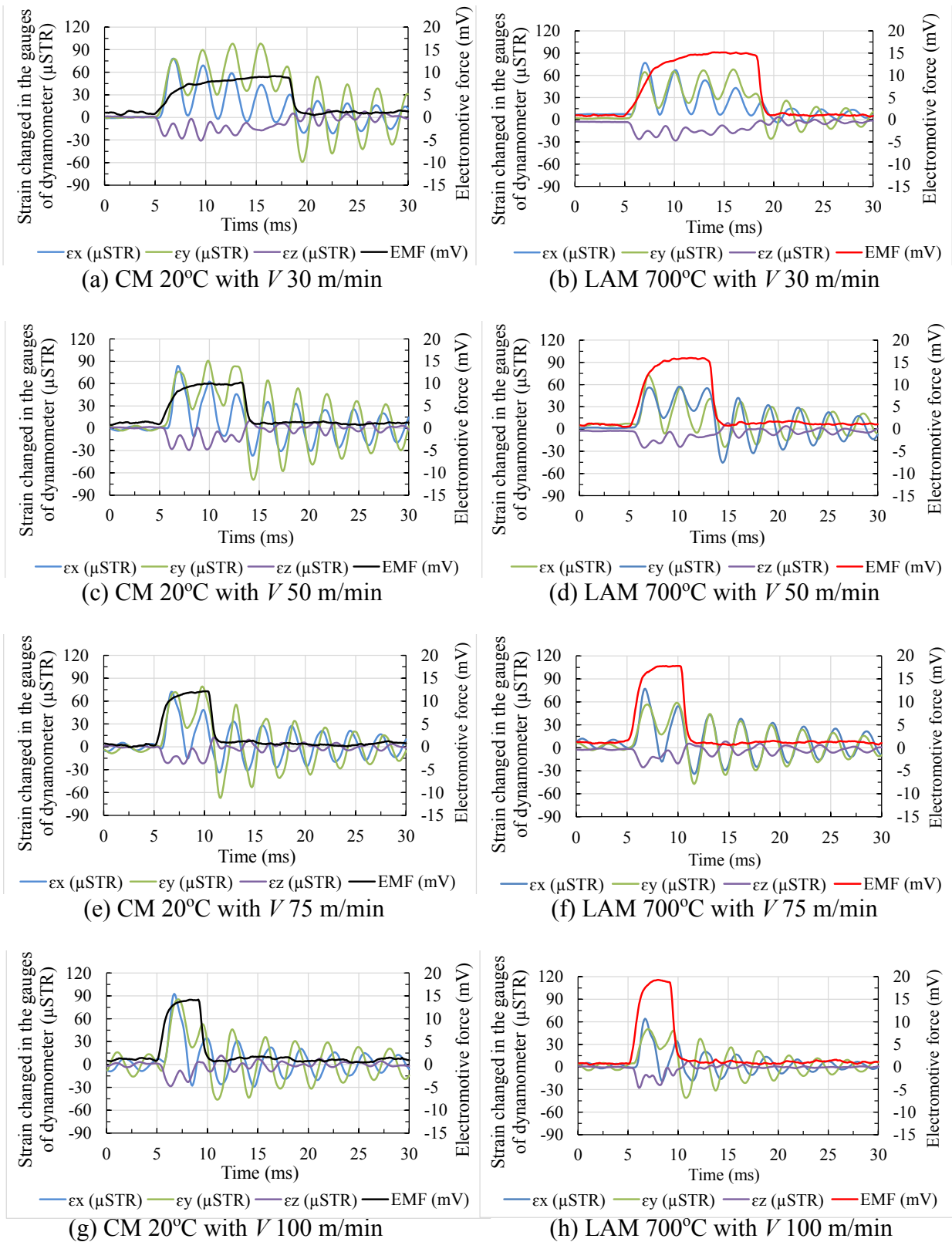
Fig. 4.14 Signal of changed strain in the gauges of dynamometer and electromotive force generated during cutting test with various cutting speed for CM and LAM

Effects of Preheating Temperature at Primary Shear Zone in Laser Assisted Milling Process
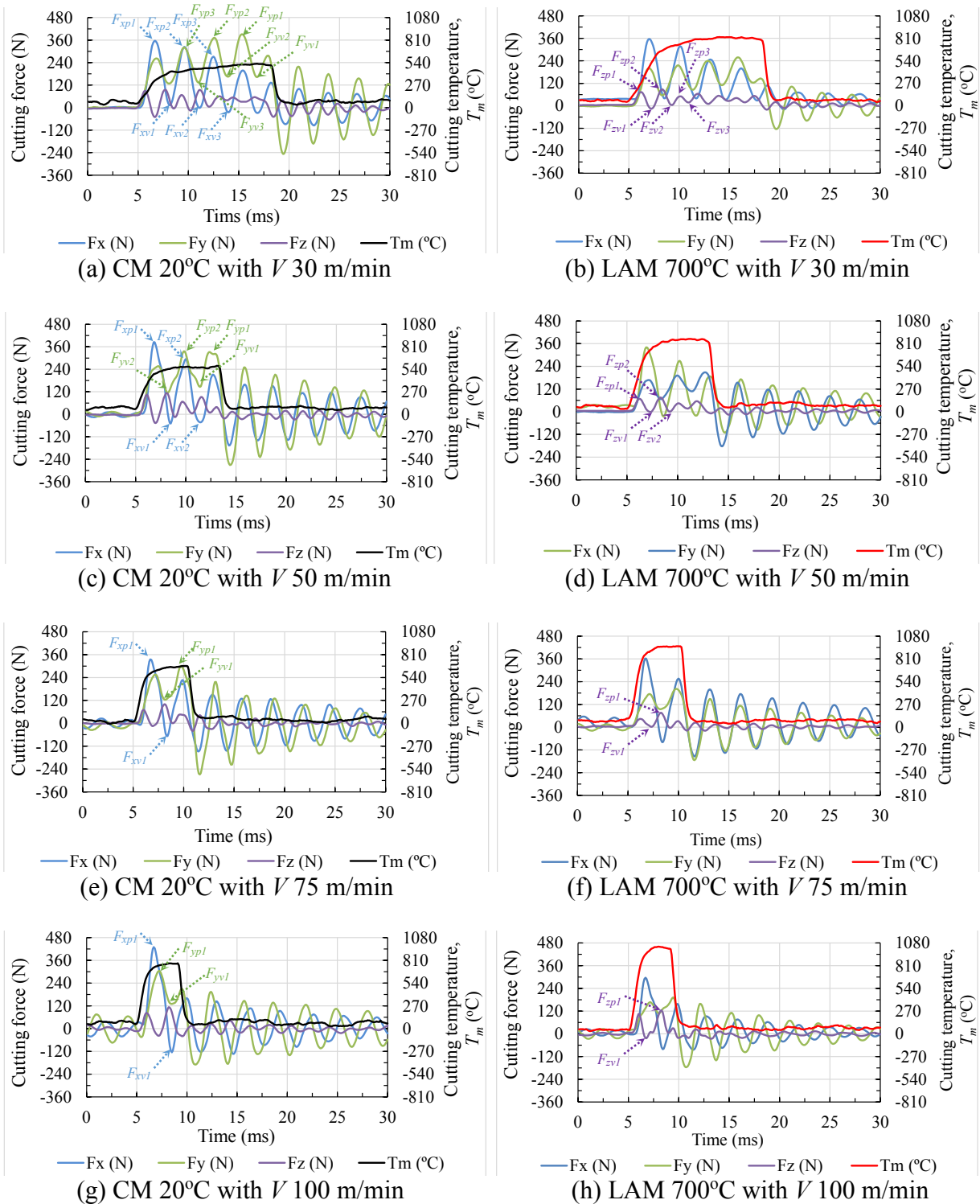
Fig. 4.15 Cutting forces and cutting temperature converted from the changed strain and electromotive force generated in cutting test with various cutting speed for CM and LAM

Figure 4.15 shows the cutting force and cutting temperature which was converted from the changed strain in the gauges and electromotive force generated in the cutting test, respectively. As can be seen in figure, the wave form of cutting forces presented the peak and valley during the cutting edge of tool interfered with the workpiece. This is because natural

frequency of dynamometer was contained in components of cutting force (F_x, F_y and F_z) for both conventional machining (CM) and laser assisted machining (LAM). In addition, the number of peak and valley in a cutting cycle decreased when the cutting speed increased. This is because the duration of cutting tool interference with the workpiece decreased when the cutting speed increased. Therefore, the cutting forces in a cutting cycle could be calculated from the summation of peak and valley, then divided by the number of couple of peak and valley. For example (refer Fig. 4.15 (a)), the thrust force (F_x) in a cutting cycle for the cutting speed of 30 m/min can be calculated as follows; $F_x = (F_{xp1}+F_{xp2}+F_{xp3}+F_{xv1}+F_{xv2}+F_{xv3})/3$. In the case of cutting temperature can be directly convert from the electromotive generated (refer to equation (3)).

Figure 4.16 shows the component of cutting forces (F_x, F_y and F_z) and Fig. 4.17 shows the measured cutting temperature (T_m). The cutting forces represented the mean of average cutting force and the measured cutting temperature represented the mean of peak cutting temperature in the area of chip-tool interface (measured by tool-work thermocouple method). The cutting test for both of cutting forces and cutting temperature were repeated at least 3 times for any cutting conditions with the new cutting inserts.

Thrust force, F_x (N)	20°C	300°C	500°C	700°C
V 30 m/min	184.17	161.97	150.68	142.89
V 50 m/min	164.67	140.04	137.52	127.18
V 75 m/min	158.10	135.25	130.91	121.71
V 100 m/min	140.85	115.44	110.39	96.18

(a) Thrust force (F_x)

Tangential force, F_y (N)	20°C	300°C	500°C	700°C
V 30 m/min	232.20	218.86	194.16	166.96
V 50 m/min	222.31	199.30	192.75	165.83
V 75 m/min	217.20	187.40	173.38	159.42
V 100 m/min	192.51	165.56	156.30	139.88

(b) Tangential force (F_y)

Axial force, F_z (N)	20°C	300°C	500°C	700°C
V 30 m/min	35.64	40.51	40.86	30.20
V 50 m/min	40.55	40.83	41.60	35.99
V 75 m/min	41.82	47.34	44.32	39.01
V 100 m/min	49.13	50.22	50.22	39.54

(c) Axial force (F_z)

Fig. 4.16 Cutting force with varied cutting speed (V) and preheating temperature (T_w)

Figure 4.16 (a) shows the result of thrust force (F_x) with varied cutting speed (V) and preheating temperature (T_w). The decrease in the thrust force was substantial with the cutting speed increasing from 30 to 100 m/min for any preheating temperature. The maximum decrease

of thrust force at the cutting speed of 100 m/min was approximately 24, 27, 29, and 33% for the preheating temperature of 20, 300, 500, and 700 °C, respectively. And, the thrust force was slightly decreased with the increase of preheating temperature. Compared with the conventional machining (T_w 20°C), the maximum decrease of thrust force with the preheating temperature of 700°C was approximately 22, 23, 23 and 32 % for the cutting speed of 30, 50, 75, and 100 m/min, respectively.

The change of tangential force (F_y) with the various cutting speed and preheating temperature (T_w) are shown in Fig. 4.16 (b). It can be seen that the tangential force drastically decreased at relatively high cutting speed of 100 m/min for any cutting conditions, the maximum decrease of tangential force at the cutting speed of 100 m/min was approximately 17, 24, 19 and 16 % for the preheating temperature of 20, 300, 500, and 700 °C, respectively. In addition, the tangential force decreased with increase of preheating temperature, the maximum decrease of the tangential force was approximately 28, 25, 27 and 27 % when compared to the conventional machining (T_w 20°C) for the cutting speed of 30, 50, 75, and 100 m/min, respectively.

Figure 4.16 (c) shows the results of axial force (F_z) with various cutting speed and preheating temperature (T_w). It can be seen that the axial force slightly increased with the increase of cutting speed and insignificantly changed with the increase of preheating temperature. In addition, the axial force was very low when compare to the thrust and tangential force. Therefore, in the section of calculation of shear angle, the researcher assumed the cutting test in here as an orthogonal cutting.

In the case of conventional machining (refer Figs. 4.16 (a) and (b), T_w = 20°C), the highest thrust and tangential force occurred at cutting speed of 30 m/min, while it was slightly decreased for the cutting speed of 50 and 75 m/min. This is believed that the heat generated in cutting process affected to increase the strain hardening [57], therefore the cutting force was increased for efficient shearing of the workpiece. However, the thrust and tangential forces drastically decreased at the cutting speed of 100 m/min. This is believed that the sufficiently heat was generated in the cutting process leaded to a decrease in strength of work material and results in lower requirement of cutting force [58].

From these results can be concluded that the increased cutting speed (V) of 100 m/min and preheating temperature (T_w) of 700°C were affected to the highest decrease in the tangential force of 32% and thrust force 27% to compare with the conventional machining. The reason is that the increasing of cutting speed results in an increase of shear angle due to the increase of strain rate [59]. This is also resulted in a decrease of chip thickness. A large shear angle giving a small shear plane, for a fixed shear strength, a decrease in shear plane area decreasing the shear forces requirement to produce the stress required for deformation [23]. In addition, the increasing of preheating temperature via the laser irradiated in the primary shear zone lead to a decrease in the strength of Inconel 718.

	20ºC	300ºC	500ºC	700ºC
V 30 m/min	587	675	756	828
V 50 m/min	656	752	810	887
V 75 m/min	735	836	889	986
V 100 m/min	825	917	951	1060
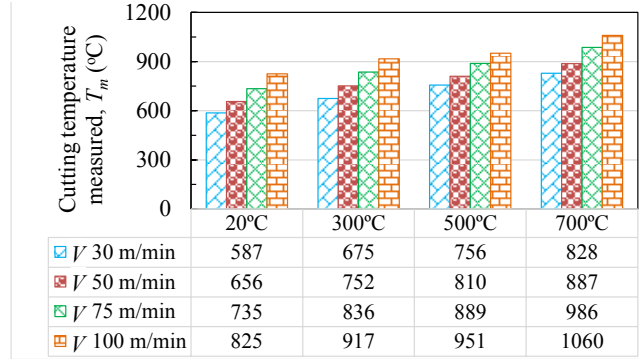
Fig. 4.17 Cutting temperature (T_m) with varied cutting speed (V) and
preheating Temperature (T_w)

Figure 4.17 shows the results of cutting speed (V) and preheating temperature (T_w) on the measured cutting temperature (T_m) in the region of tool-chip interface by tool-work thermocouple method. It can be seen that the measured cutting temperature increased with the cutting speed due to more heat generation at the high strain rate in deformation zones [60] and the high sliding velocity of tool-chip interface. In addition, the measured cutting temperature increased with the preheating temperature of workpiece.

4.3.3 Estimated temperature in the deformation zone

In the metal cutting process, the mechanical work (energy) consumption in machining process is converted into the heat and the heat generation or temperature in the deformation zones are highly dependent on the cutting conditions [45]. Therefore, the total energy consumption in cutting process can be assumed as a combination of the shear energy in the primary deformation zone and the friction energy in the secondary deformation zone. In other words, the temperature rise in primary zone (ΔT_p) and secondary zone (ΔT_s) can be estimated from the measured cutting temperature (T_m) and the obtained results of cutting forces as following question (4.4) and (4.4), respectively.

$$\Delta T_p = \frac{\Delta T}{F_y V}(F_S V_S)$$
(4.3)

where, ΔT_p is temperature rise in primary shear zone (ºC), ΔT is difference of measured cutting temperature (T_m) and preheating temperature (T_w), F_y is tangential force (N), V is cutting speed (m/s), F_S is cutting force on the shear plain (N), and V_S is shear velocity (m/s)

$$\Delta T_s = \frac{\Delta T}{F_y V}(F_C V_C)$$
(4.4)

where, ΔT_s is temperature rise in secondary shear zone (ºC), F_C is friction fore (N), and V_C is chip velocity (m/s)

The change of temperature in the deformation zones caused in machining of different cutting speed (V) and preheating temperature (T_w) is summarized in Fig. 4.18. Figure 4.18 (a)

shows the estimation of temperature rise (ΔT_p) and temperature in the primary zone (T_p). It can be seen that the temperature rise (ΔT_p) increased with the cutting speed due to more heat (energy) generated at the height of cutting speed. On the other hand, the temperature rise in primary zone decreased with the increase of preheating temperature (T_w) because the reduced strength of work materials lead to low energy consumed for shearing work materials. However, the temperature in primary shear zone (T_p) increased with the preheating temperature (T_w) due to the increase of temperature in the workpiece.
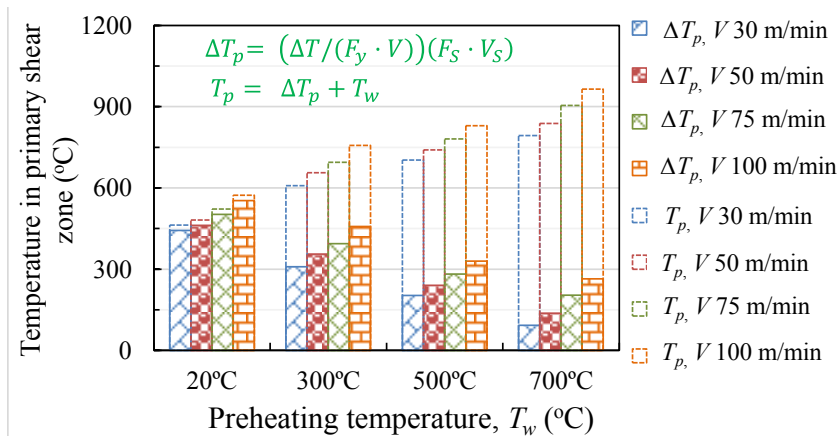
(a) Temperature in the primary deformation zone (T_p)
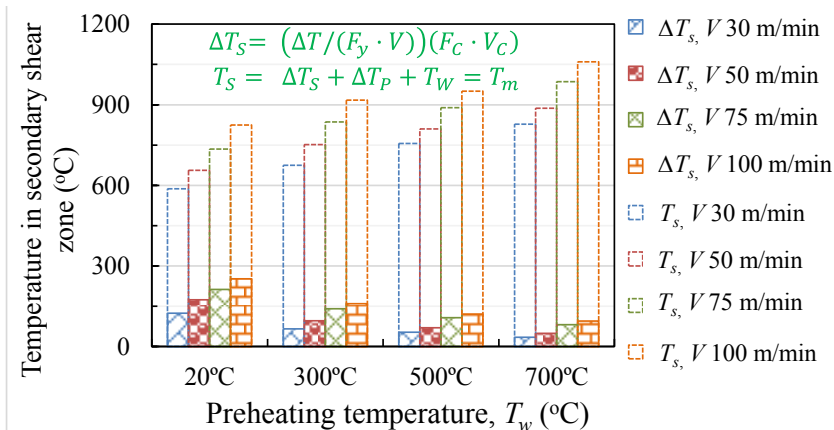
(b) Temperature in the secondary deformation zone (T_s)

Fig. 4.18 The influence of cutting speed (V) and preheating temperature (T_w) on the temperature in deformation zones (T_s)

Figure 4.18 (b) shows the estimation of temperature rise (ΔT_s) and temperature in the secondary zone (T_s). It can be observed that the temperature rise in secondary zone has a similar trend with the temperature rise in the primary shear zone (refer Fig 4.18 (a)). The degree of temperature rise in the secondary zone was lower than in the primary zone, approximately 75% of temperature rise was generated in the primary shear zone. Howeve, the temperature in the secondary zone (T_s) was higher than the temperature in primary shear zone (T_p) . This is because the heat generated in the primary shear zone was distributed into chip and heat energy is successively generated in the secondary shear zone.

It should be noted that the estimated temperatures in primary shear zone covered the range which the mechanical properties of work material (Inconel 718) changed over. For example, the hardness increases with the temperature below 650°C [57] and the yield strength significantly reduces with the temperature above 750°C [61, 62]. In addition, the measured cutting temperatures in secondary shear zone of approximately 1060°C was higher than the temperature at which the carbide tool (WC-Co) starts to decrease the strength (above 500°C) [63], but it was lower than the softening temperature of carbide tool (above 1100°C) [57]. Therefore, the estimated temperature in the deformation zones was considered to explain the influence of laser assisted milling on the characteristically deformation of Inconel 718 in next section.

4.3.4 Chip thickness and shear stress in deformation zone

The basic mechanism of metal cutting for milling is plastic deformation and shearing in chip generation process by edges of the end-mill, it involves localized shear deformation of work material ahead of the tool cutting edge (primary shear zone). Then, the machined material (chip) is further subjected to extensive plastic deformation and slides over the rake face of cutting tool (secondary shear zone). Therefore, the characteristics of chip deformation highly depend on the cutting conditions such as cutting speed, cutting tool, work materials and so on. Consequently, the thickness of chip deformed could be used to explain the influence of cutting speed and preheating temperature on the requirement of cutting force in laser assisted machining for milling Inconel 718.

(a) New carbide insert   (b) Chip deformed on the tool
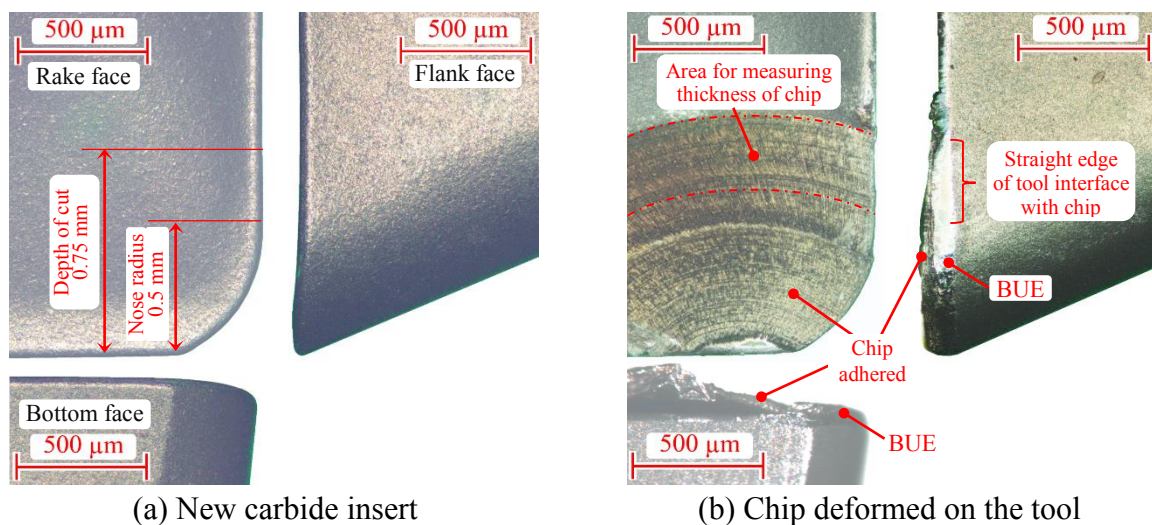
Fig. 4.19 New carbide insert and deformation of chip on the surface of cutting tool

In order to avoid influence of tool wear, the new carbide inserts as shown in Fig. 4.19 (a) were used to generate 20 chips by limited machining length of 1 mm for any cutting conditions (refer Table 4.1). In Figure 4.19 (b) can be seen that the color and shape of chip deformed was varied with the cutting temperature and tool shape. Therefore, the positions measured of thickness on chip were specific in the area of straight edge of cutting tool interface

with the work materials, and the example of chip with preheating temperature show in Figs. 4.20, 4.21, 4.22 and 4.23 for the cutting speed of 30, 50, 75 and 100 m/min, respectively.

(a) Preheating temperature 20°C, CM

(b) Preheating temperature 300°C, LAM

(c) Preheating temperature 500°C, LAM

(d) Preheating temperature 700°C, LAM
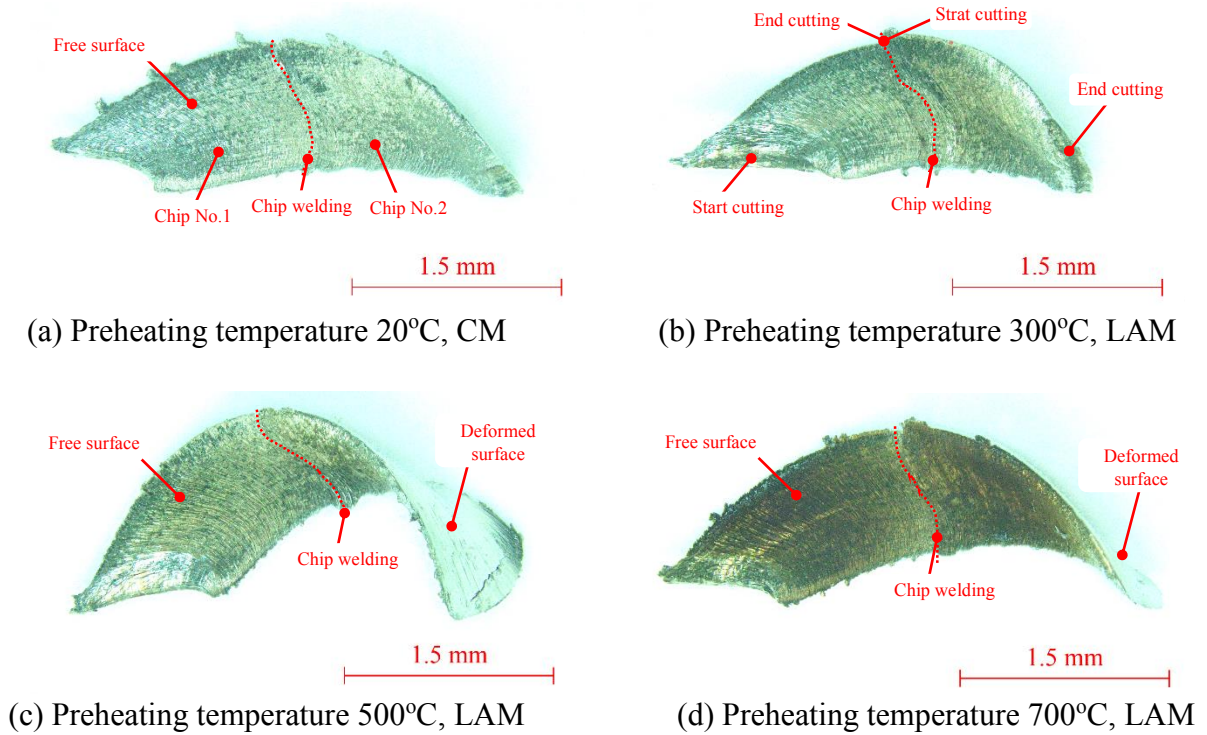
Fig. 4.20 Photograph of chip generated with cutting speed of 30 m/min (chip welded)

(a) Preheating temperature 20°C, CM

(b) Preheating temperature 300°C, LAM

(c) Preheating temperature 500°C, LAM

(d) Preheating temperature 700°C, LAM
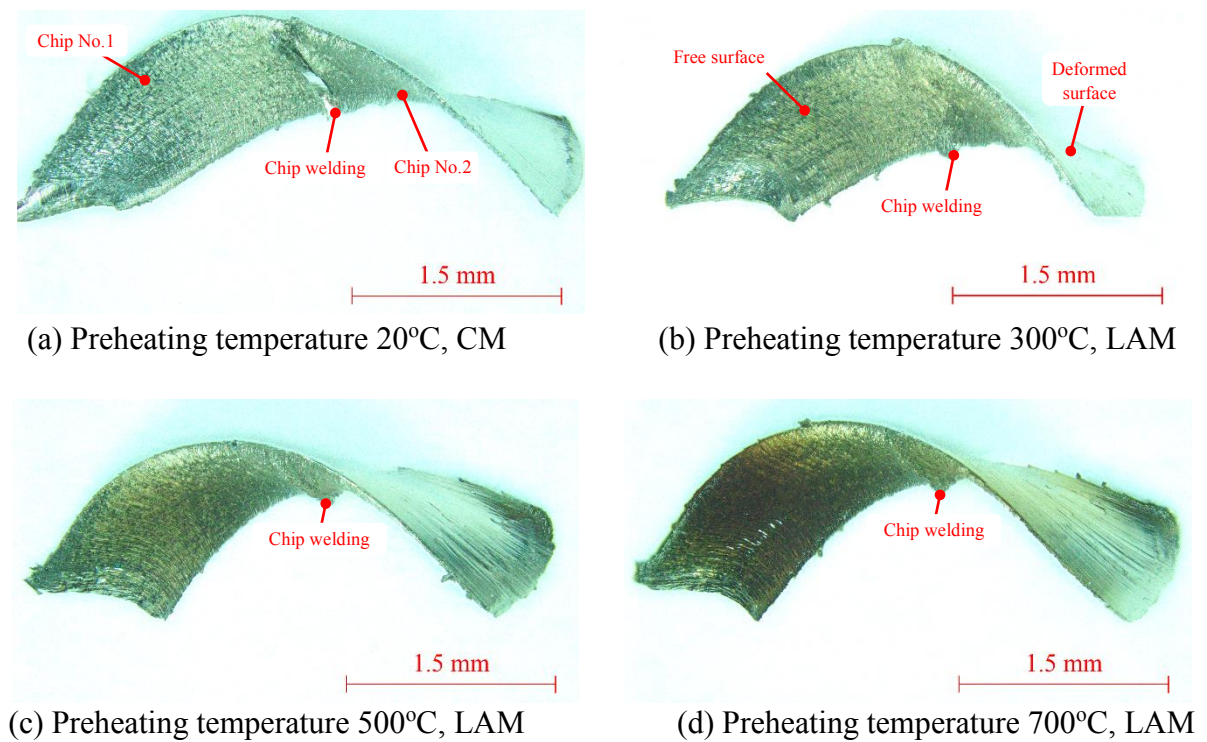
Fig. 4.21 Photograph of chip generated with cutting speed of 50 m/min (chip welded)

41

(a) Preheating temperature 20°C, CM

(b) Preheating temperature 300°C, LAM

(c) Preheating temperature 500°C, LAM

(d) Preheating temperature 700°C, LAM
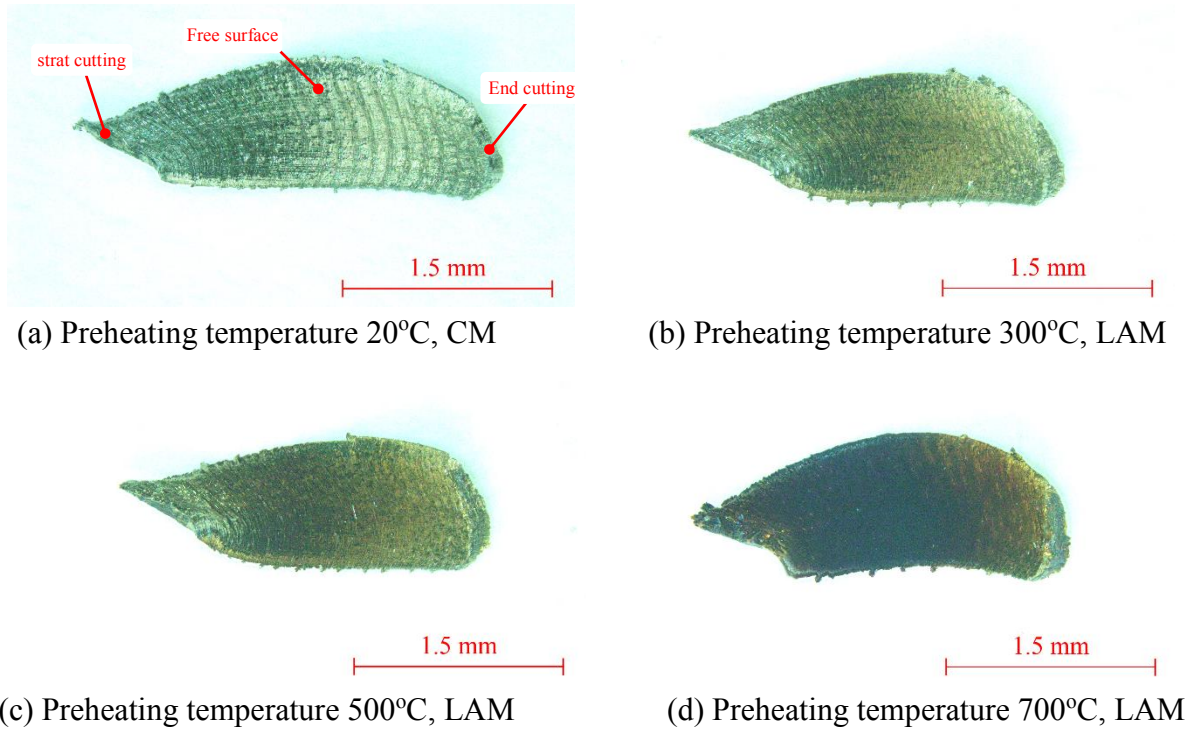
Fig. 4.22 Photograph of chip generated with cutting speed of 75 m/min (single chip)

(a) Preheating temperature 20°C, CM

(b) Preheating temperature 300°C, LAM

(c) Preheating temperature 500°C, LAM

(d) Preheating temperature 700°C, LAM
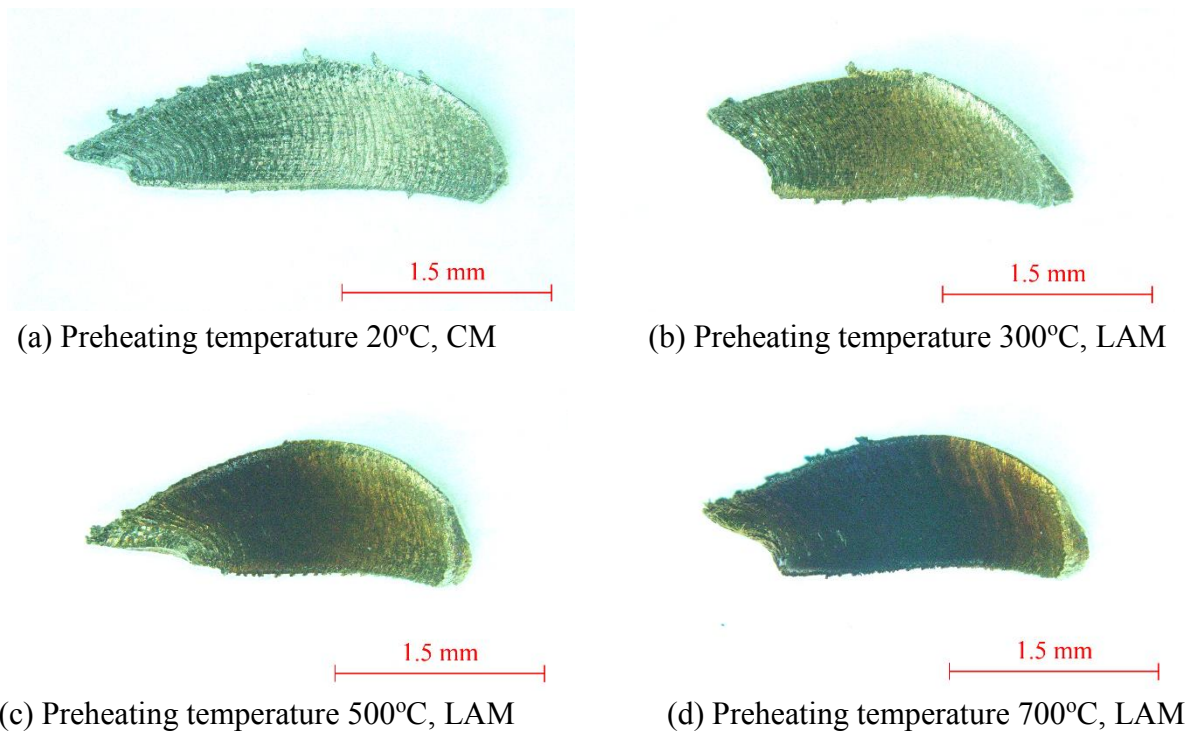
Fig. 4.23 Photograph of chip generated with cutting speed of 100 m/min (single chip)

In this work, twist chip was generated in the cutting test. In addition, the secondary chip deformed (chip no.2) consequently weld on the prior chip deformed (chip no.1) and continuous chip formed due to the high pressure welding at the low cutting speed of 30 and 50

m/min. Moreover, the color of chip changed to dark with the increase in cutting speed, and the preheating temperature due to higher cutting temperature accelerated oxidation.

The thickness of chips (t_c) were measured by micrometer (point contact) for 15 chips to obtain the averaged thickness. The averaged thickness of chip and shear angle with variation of cutting temperature in primary shear zone (T_p) for the cutting speed of 30, 50, 75 and 100 m/min is showed in Fig. 4.24.

As can be seen in Fig. 4.24 (a), the thickness of chip for the conventional machining drastically decreased with the increase in the cutting speed, while the different of chip thickness gradually reduced with the increase in cutting temperature in primary shear zone (T_p). In Figure 19 (a), it can be also observed that the thickness of chip at the cutting speed of 30 m/min drastically increased with the cutting temperature of approximately 600ºC, then the thickness of chip drastically decreased with the cutting temperature. While, the thickness of chip for the high cutting speed of 100 m/min slightly increased with the cutting temperature. Therefore, it could be concluded that the thickness of chip in laser assisted machining is probably thicker than that in conventional machining for almost cutting speed (except for the cutting speed of 30 m/min with the preheating temperature of 700ºC).
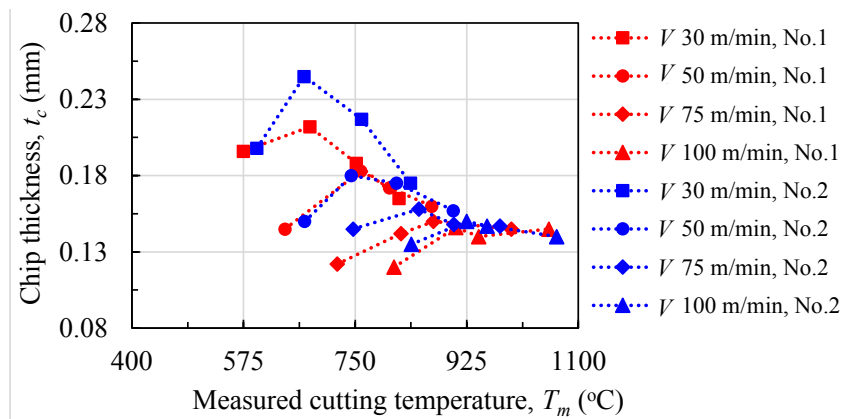
(a) Chip thickness versus cutting temperature in the primary shear zone
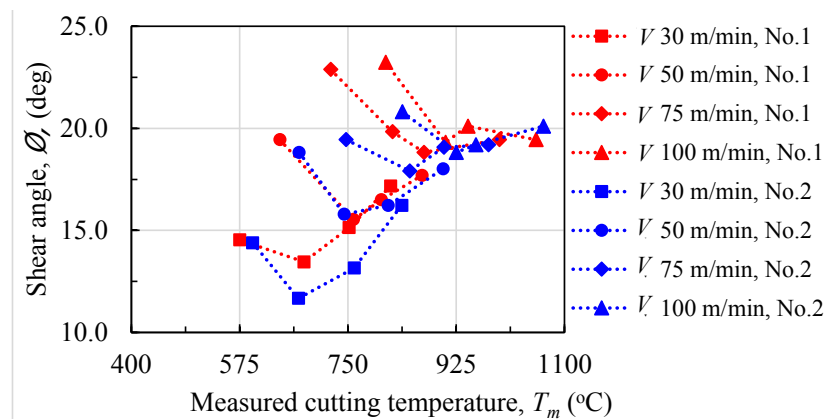
(b) Shear angle versus cutting temperature in primary shear zone

Fig. 4.24 Chip thickness (t_c) and shear angle (Ø) with varied cutting speed (V) and cutting temperature (T_m)

Figure 4.24 (b) shows the results of shear angle ($\emptyset$) calculated using the cutting geometry (equation (6)). It can be observed that the behavior of shear angle with the cutting temperature was inverted with the chip thickness. Venkatesan et al. [64] explained that the increase in chip thickness and decrease in shear angle during laser assisted machining as compared to conventional machining are due to the chip division frequency (segmentation) increased during laser assisted machining of Inconel 718, which was caused by the reduced strength of work materials due to the increase in preheating temperature.

Based on literature reviews, Ginta et al. [65] reported that high temperature increases chemical reactivity between work material (chip) and tool materials which leads to the formation of built-up-edge (BUE). Martinaz et al. [18] reported that amount of adhesion decreased with the increased cutting speed and strength of work material. Therefore, the increase in cutting speed and preheating temperature possibly change the contact areas of tool-chip interface and deformation of chip. On the other hand, the change of contact area or amount of adhesion is also possible to use for confirmed tendency of chip thickness changed.

Figures 4.25, 4.26, 4.27 and 4.28 show the rake face and flank face of cutting tool after cutting test with limited machining length of 1 mm (20 cutting cycles) for the cutting speed of 30, 50, 75 and 100 m/min, respectively. The adhesion of chip can be observed on tool face for some cutting conditions, and the example of chip adhered on tool face can be seen in Fig 4.25 (d). The chip adhered on the tool could be fell out during milling test due to the increase in mass of materials adhered (refer Fig. 3.11 (a) in chapter 3) or the dynamic force since the edge of cutting tool rotating and interruptedly interferes the workpiece. The areas of built-up-layer (BUL) and tool-chip interface could be observed when the work materials (chip) adhered was removed as shown in Fig. 4.25 (a), (b) and (c). Unfortunately, the built-up-edge (BUE) is difficult to identify neither chip adhered on the tool face nor the chip adhered fall-out from the tool face.

Song et al. [66, 67] classified three main parts of the tool-chip contact zone as following. First one, close to the cutting edge where the sliding velocity is very low but the contact pressure is very high, the thick of built-up-layer is difficult to form at this zone. Second one, adhesion zone where adhesion is formed quickly and adhesion wear tends to be more intensive. The last one, sliding zone where the relative sliding velocity tends to equal the chip velocity and flowing grooves can be easily formed. Therefore, the contacts length of tool-chip is able to measure from the edge of cutting tool to the end of flowing grooves. The built-up-layer is able to measure in the unit of area where the work materials adhered on the rake face of cutting tool. The measured positions for the contacts length of tool-chip and the areas of built-up-layer can be showed in Fig. 4.29, 4.30, 4.31 and 4.32 for the cutting speed of 30, 50, 75 and 100 m/min, respectively.

Effects of Preheating Temperature at Primary Shear Zone in Laser Assisted Milling Process

(a) preheating temperature 20°C, CM

(b) preheating temperature 300°C, LAM

(c) preheating temperature 500°C, LAM

(d) preheating temperature 700°C, LAM
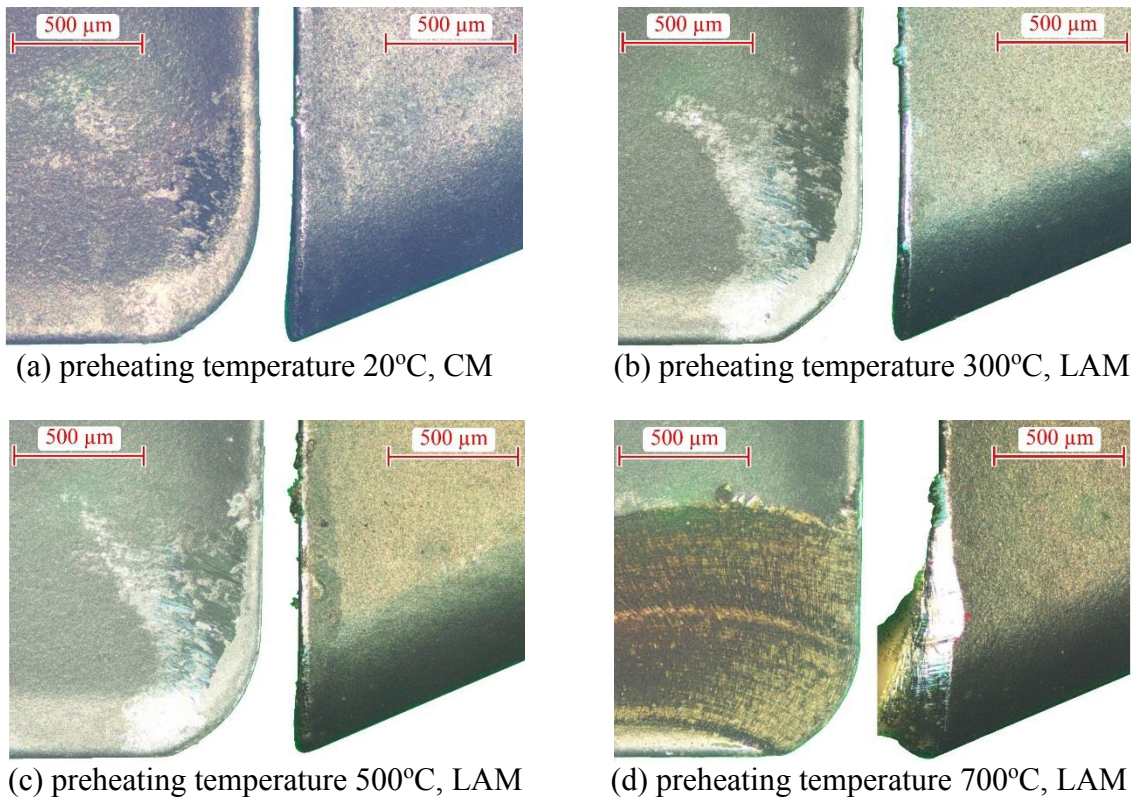
Fig. 4.25 Rake and flank face of cutting tool at finish machining length of 1 mm with cutting speed of 30 m/min

(a) preheating temperature 20°C, CM

(b) preheating temperature 300°C, LAM

(c) preheating temperature 500°C, LAM

(d) preheating temperature 700°C, LAM
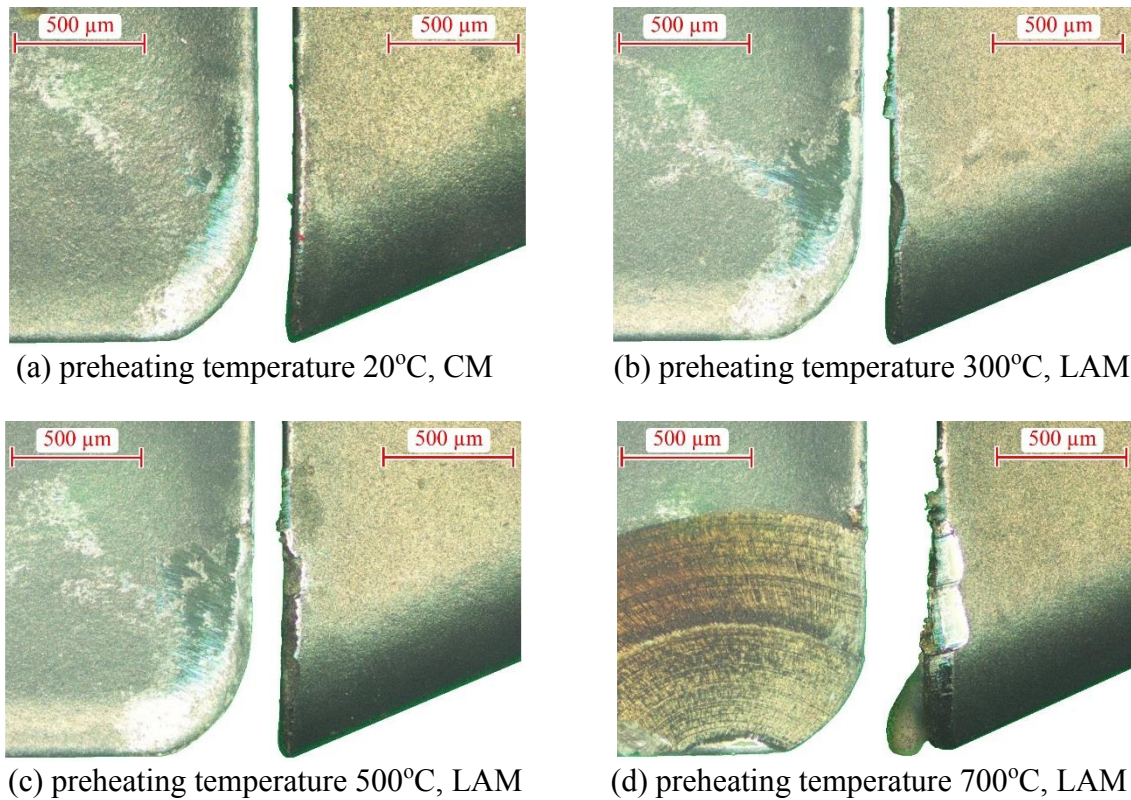
Fig. 4.26 Rake and flank face of cutting tool at finish machining length of 1 mm with cutting speed of 50 m/min

(a) preheating temperature 20°C, CM

(b) preheating temperature 300°C, LAM

(c) preheating temperature 500°C, LAM

(d) preheating temperature 700°C, LAM
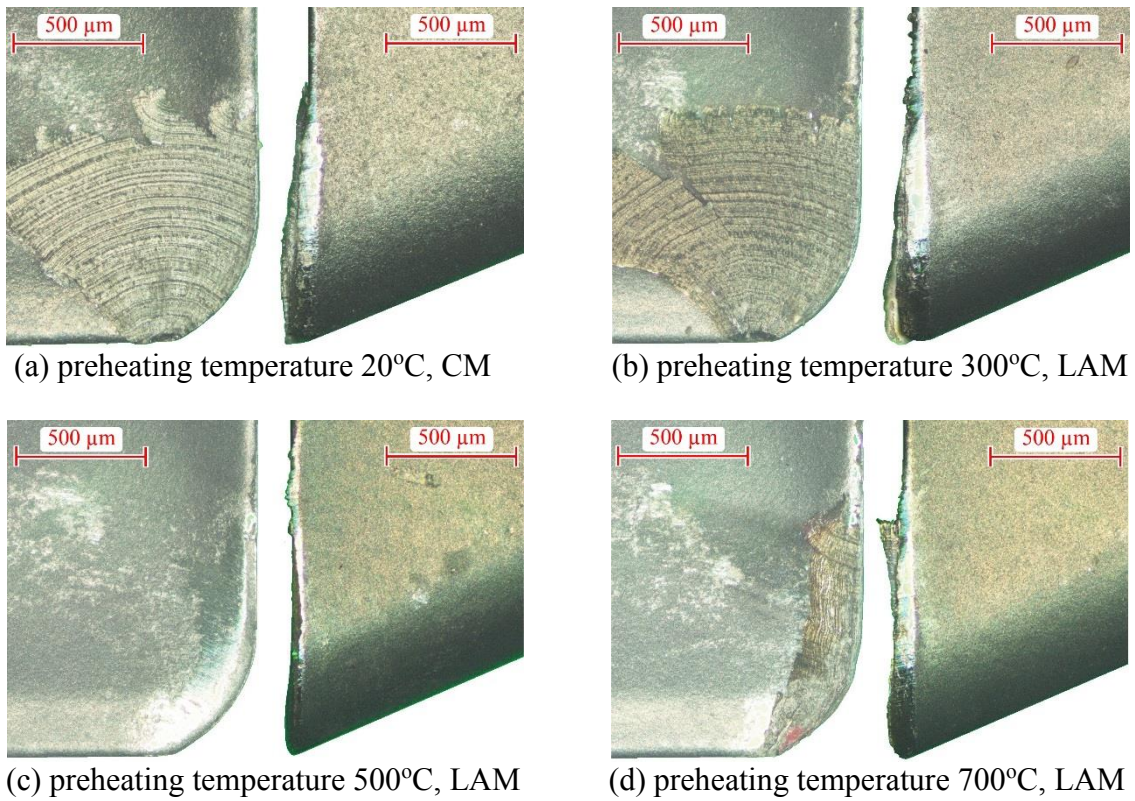
Fig. 4.27 Rake and flank face of cutting tool at finish machining length of 1 mm with cutting speed of 75 m/min

(a) preheating temperature 20°C, CM

(b) preheating temperature 300°C, LAM

(a) preheating temperature 500°C, LAM

(b) preheating temperature 700°C, LAM
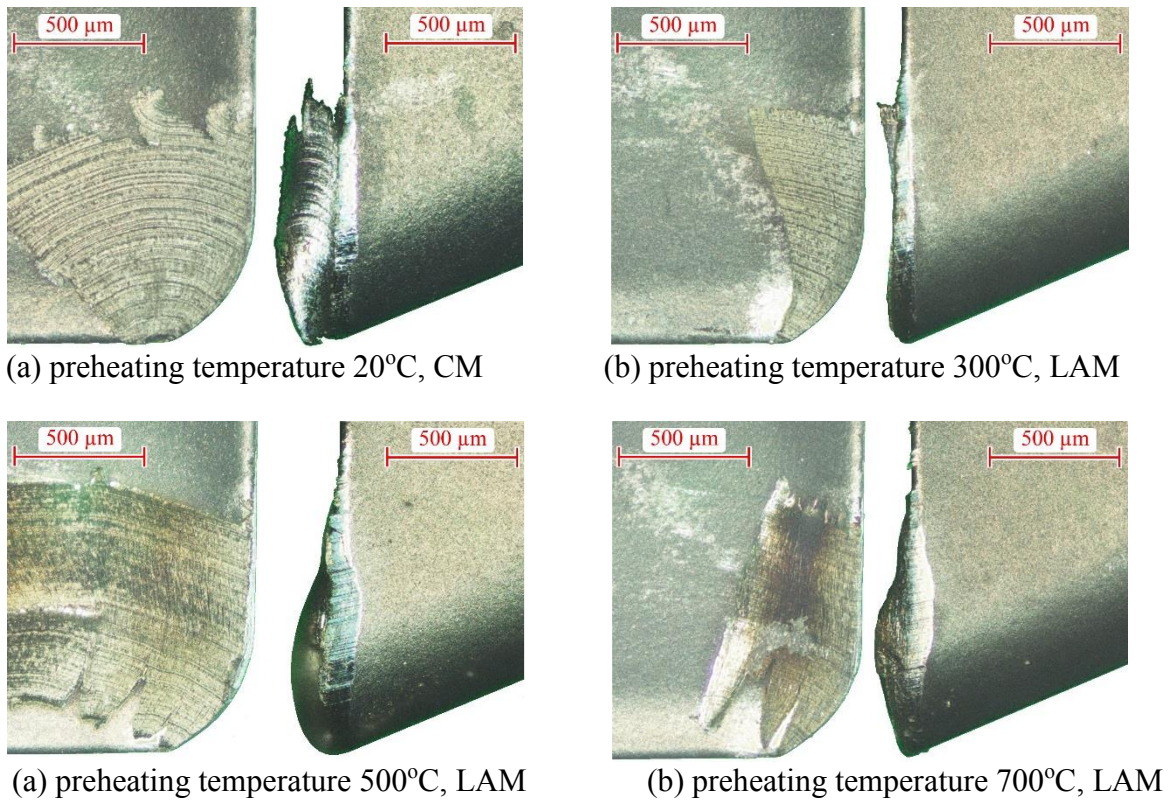
Fig. 4.28 Rake and flank face of cutting tool at finish machining length of 1 mm with cutting speed of 100 m/min

Effects of Preheating Temperature at Primary Shear Zone in Laser Assisted Milling Process

(a) preheating temperature 20°C, CM

(b) preheating temperature 300°C, LAM

(c) preheating temperature 500°C, LAM

(d) preheating temperature 700°C, LAM
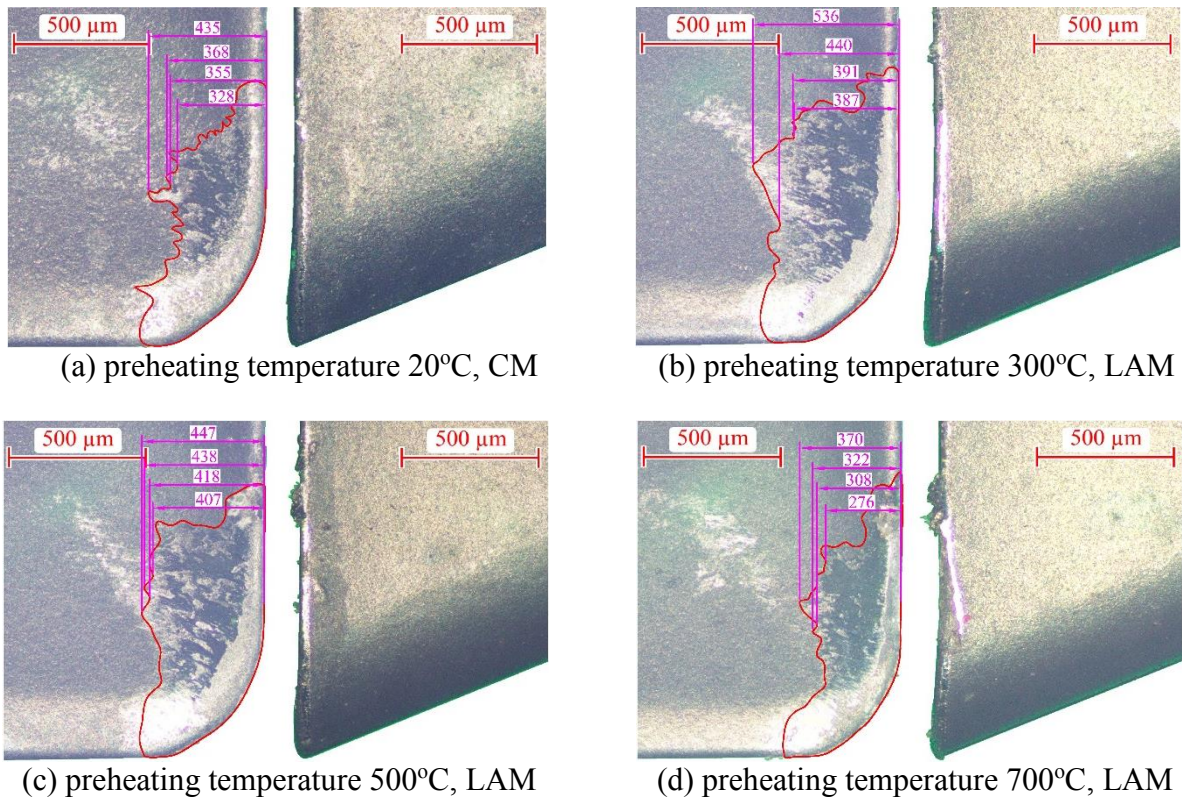
Fig. 4.29 Built-up-layer on the tool with varied preheating temperature for the cutting speed of 30 m/min (relative Fig. 4.25)

(a) preheating temperature 20°C, CM

(b) preheating temperature 300°C, LAM

(c) preheating temperature 500°C, LAM

(d) preheating temperature 700°C, LAM
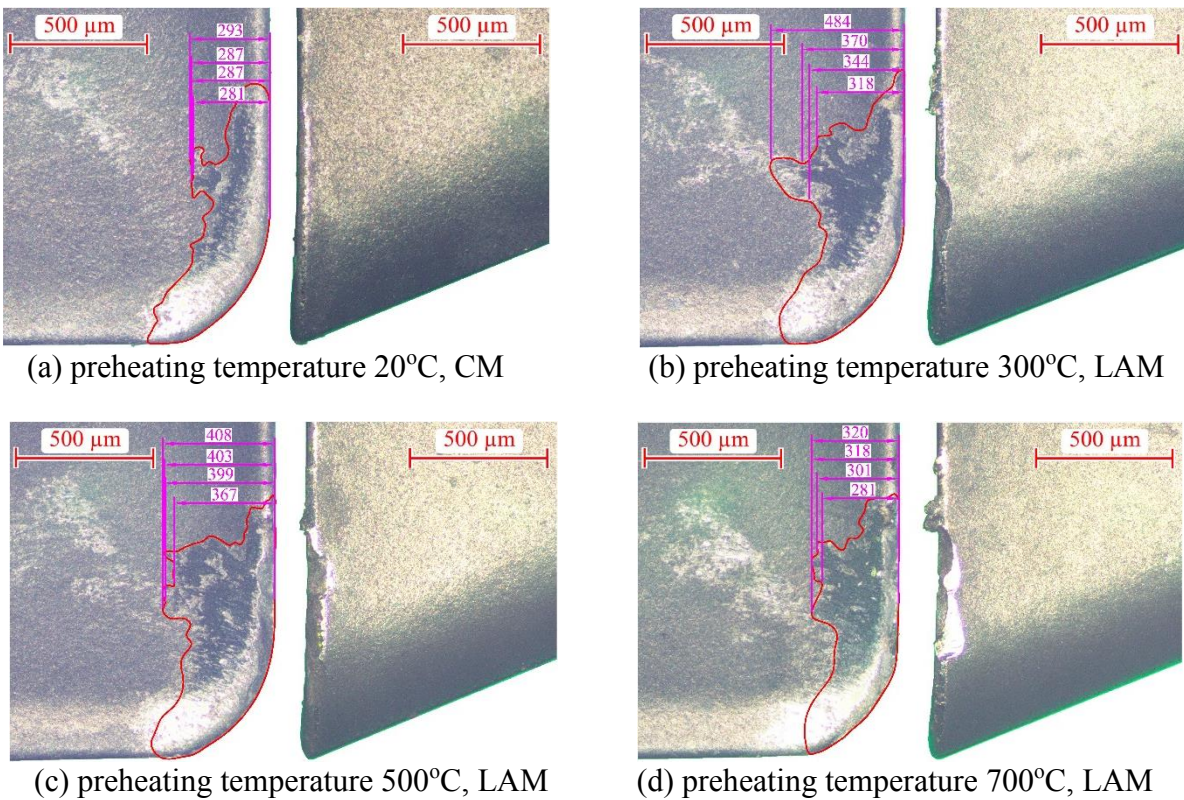
Fig. 4.30 Built-up-layer on the tool with varied preheating temperature for the cutting speed of 50 m/min (relative Fig. 4.26)

Effects of Preheating Temperature at Primary Shear Zone in Laser Assisted Milling Process

(a) preheating temperature 20ºC, CM

(b) preheating temperature 300ºC, LAM

(c) preheating temperature 500ºC, LAM

(d) preheating temperature 700ºC, LAM
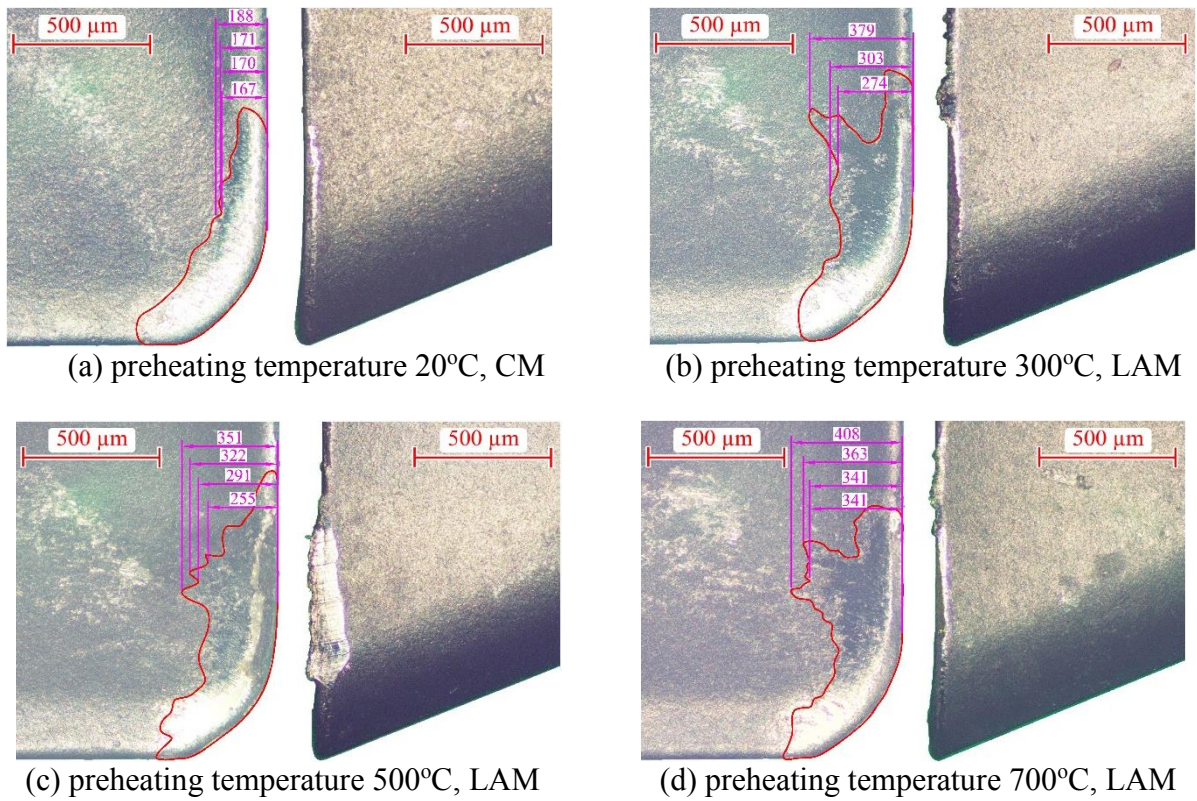
Fig. 4.31 Built-up-layer on the tool with varied preheating temperature for the cutting speed of 75 m/min (relative Fig. 4.27)

(a) preheating temperature 20ºC, CM

(b) preheating temperature 300ºC, LAM

(c) preheating temperature 500ºC, LAM

(d) preheating temperature 700ºC, LAM
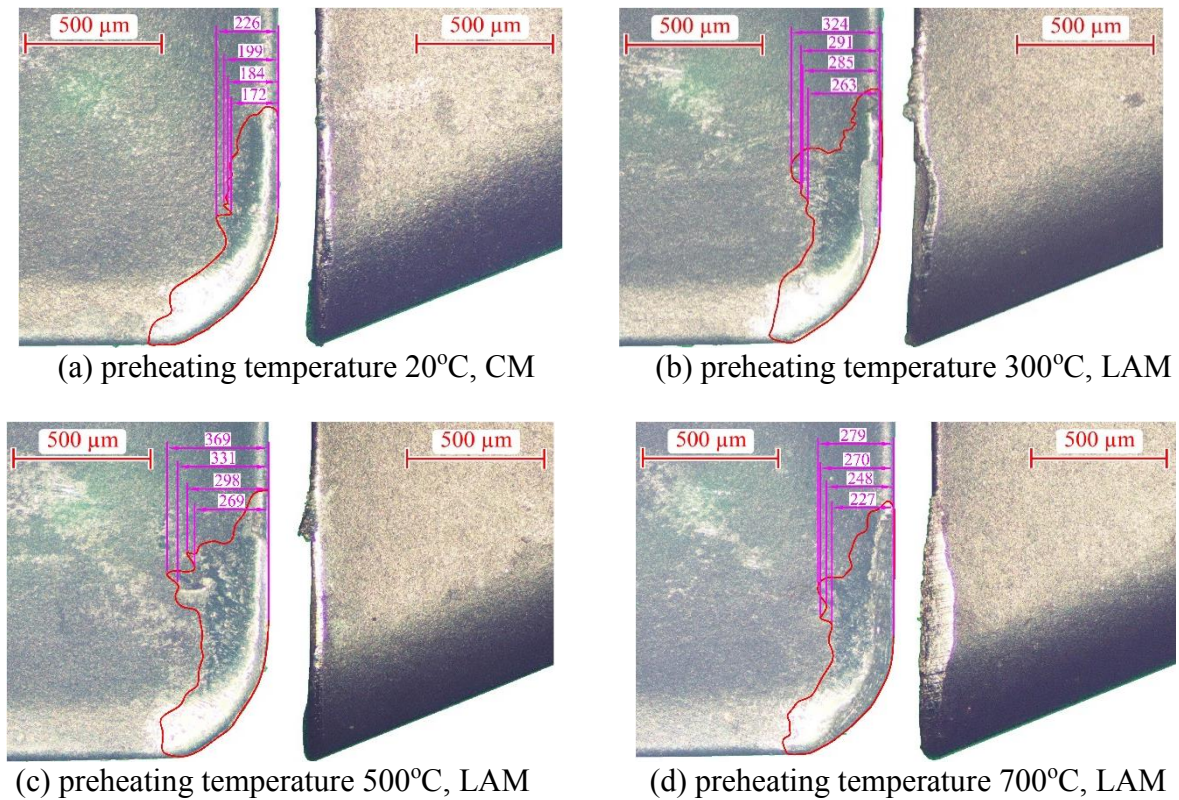
Fig. 4.32 Built-up-layer on the tool with varied preheating temperature for the cutting speed of 100 m/min (relative Fig. 4.28)

(a) Areas of built-up-layer versus measured cutting temperature

(b) Contact length of tool-chip versus measured cutting temperature
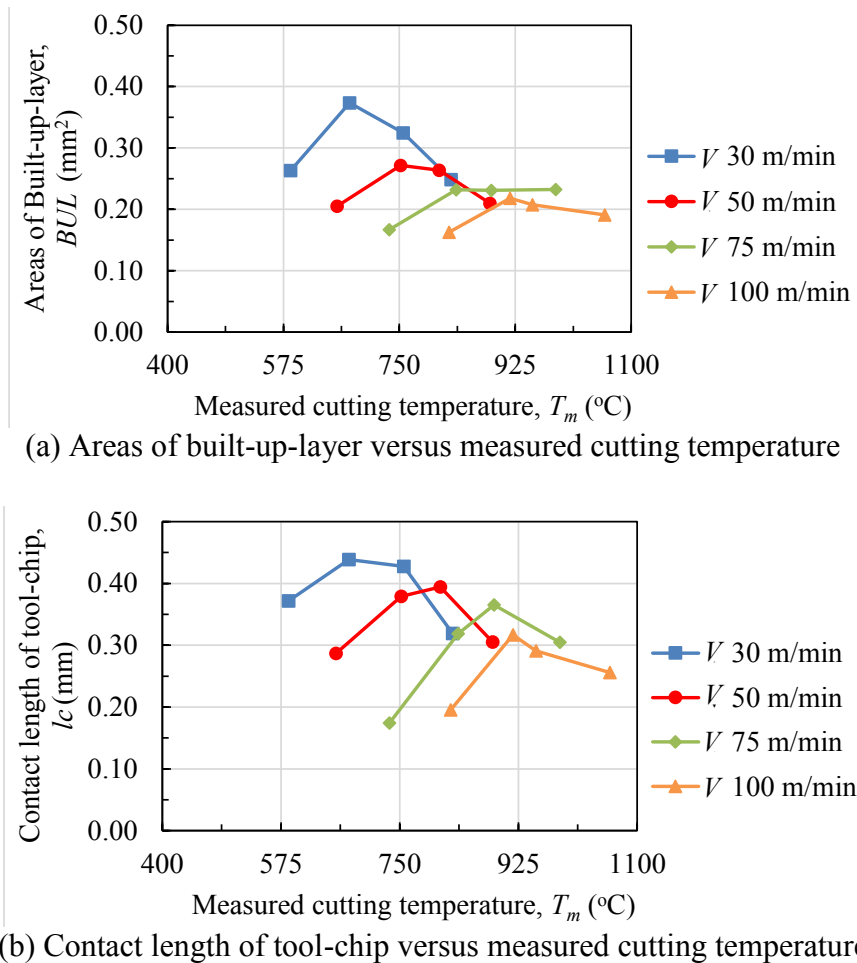
Fig. 4.33 Area of built-up-layer (*BUL*) and tool-chip (*l*$_c$) contact length with varied cutting speed (*V*) and cutting temperature (*T*$_m$)

Figure 4.33 shows the relation between the area of built-up-layer (*BUL*) or the contact length of tool-chip interface (*l*$_c$) with the measured cutting temperature for different cutting speed. It can be seen that the increase in cutting speed leading to decreased area of built-up-layer (*BUL*) and the contact length of tool-chip interface (*l*$_c$) both. The area of built-up-layer (*BUL*) and the contact length of tool-chip interface (*l*$_c$) also increased with the measuring cutting temperature. The tendency changed of the areas of built-up-layer and contact length of tool-chip interface were similar with the tendency of thickness of chip when the cutting speed and cutting temperatures changed. Therefore, it could be concluded that the increase in cutting speed leading to the increase in shear angle, which decreases the thickness of chip, and the increase in cutting temperature increases the thickness of chip especially at the high cutting speed. This fact can be confirmed by the results of built-up-layer and the contact length of tool-chip interface.

Figure 4.34 shows the results of friction coefficient (μ), which can be geometrically calculated from the experimentally measured forces *F*$_x$ and *F*$_y$ as following equation (2.3). It should be noted that the rake angle is approximately 4 deg. in this cutting tests.
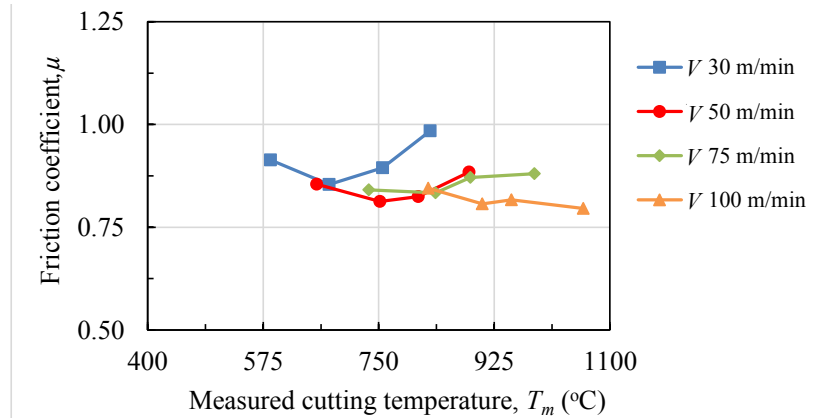
Fig. 4.34 Friction coefficient (μ) with varied cutting speed (V) and preheating temperature (T_w)

From figure 4.34, it can be observed that the friction coefficient for the conventional machining slightly decreased when the cutting increased. This is because the increase of cutting speed leaded to an increase in cutting temperature and shear angle, it also leaded to decreasing of chip thickness and tool-chip contact, which was caused to reduce friction force (F_c) more than normal force (N_c).

At the low cutting speed of 30 and 50 m/min, it was found that the friction coefficient (μ) with laser assisted machining was lower than conventional machining due to heating causing less friction at the tool-chip interface and causing a significant decrease in friction coefficient. However, the excessive preheating temperature leading to increased friction coefficient. This is possible to explain that the softening at the higher preheating temperature leading to increase in the work materials adhered on the tool tip. The formation of adhering layer on the tool must be changed tool geometry and contact condition at tool-chip interface [66]. Therefore, it is possible that the thrust force (F_x) could be reduced less than tangential force (F_y) due to an increase in tool edge radius. The another reason might be that due to the tool wear and built-up-layer formed on the flank face. This is leading to rubbed/smeared work materials struck on the wear cutting edge. Therefore, the built-up-layer on the flank face is possible to shearing/rubbing with the workpiece in the tertiary shear zone (side face of machined surface) [68], which was also leading to thrust force (F_x) reduced less than tangential force (F_y). However, at the increased cutting of 100 m/min the preheating temperature was less influence on the friction coefficient.

Figure 4.35 shows the results of shear stress on shear plane (τ_s), which can be geometrically calculated from the experimental data as following equation (2.7). It should be noted that the width of cut (b) in the cutting test is 6 mm and the depth of cut (t_o) in the cutting test is 0.75 mm.

Effects of Preheating Temperature at Primary Shear Zone in Laser Assisted Milling Process
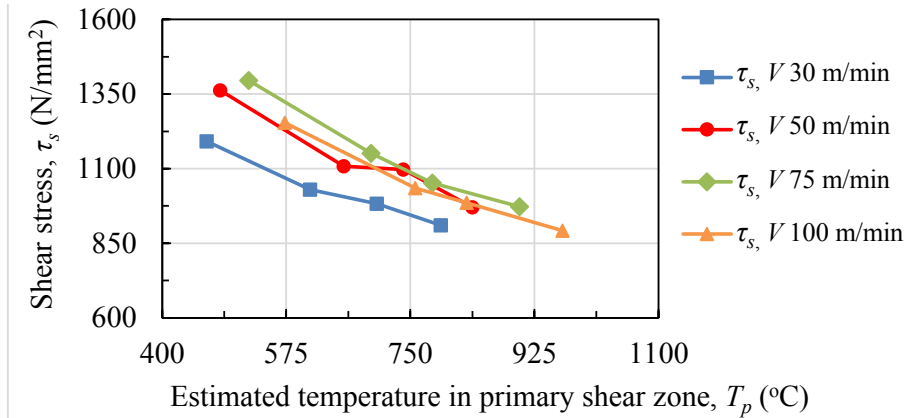
Fig. 4.35 Shear stress (τ_s) with varied cutting speed and preheating temperature (T_w)

In this experiment, the shear stress under the conventional machining with varied cutting speed revealed that the shear stress absolutely increased approximately 1191, 1362 and 1395 N/mm^2 for cutting speed of 30, 50 and 75 m/min, respectively. The increase in shear stress with the cutting speed could be explained by that the insufficient of heating temperature in primary shear zone increase the work hardening effect, thus the shear deformation of Inconel 718 becomes difficult during the chip formations. The other reason might be that strain hardening in machined surface increased due to the high plastic deformation in the region of tertiary shear zone. Furthermore, the increase in cutting speed of 100 m/min leaded to shear stress slightly decreased of approximately 1254 N/mm^2. This is believed that the strength of materials decreased at elevated cutting temperature.

In Figure 4.35, it can be observed that the shear stress drastically decreased but the estimated temperature in primary shear zone drastically increased when the laser assisted machining was performed. The shear stress also absolutely decreased but the estimated temperature in primary shear zone also absolutely increased with the increase in preheating temperature for any cutting speed.

According to Ren et al. [69] Inconel 718 is higher strengthening the grain boundary with the formation of complex metallic carbides, which impedes the movement of dislocation and including higher plastic deformation. Kear et al. [70] pointed out that Inconel 718 is large amount of γ' (Ni$_3$(Ai,Ti)) and γ'' (Ni$_3$Nb) precipitates when this alloy is deformed. This leads to difficult movement of dislocations, and it is the main reason of work hardening. Liao et al [10] reported that the Inconel 718 becomes harder and harder with the increase of cutting temperature below 650ºC. And Shokrani et al. [19] suggested the instance cutting forces in machining Inconels 718 reduce significantly at cutting temperatures above 750ºC due to significant reduction in its strength and hardness.

Therefore, the highest estimated temperature in primary shear zone could maximally reduce the shear stress of approximately 20, 30, 35 and 34% to compare with conventional machining for the cutting speed of 30, 50, 75 and 100 m/min, respectively. These can be explained by the fact that the higher temperature initially in the workpiece accompanying with the higher cutting temperature could be heavily reduced ultimate stress of the work material.

4.3.5 Tool wear

In this work, the flank wear on the cutting tool was measured after cutting test with machining length limited of 36.60 mm (cutting distance is 4.5 m). The cutting tests were performed with the new cutting tool for any cutting conditions. The flank wear (VB_{max}) on the tool versus measured cutting temperature (temperature in secondary shear zone) with varied cutting speed can be showed in Fig. 4.36.
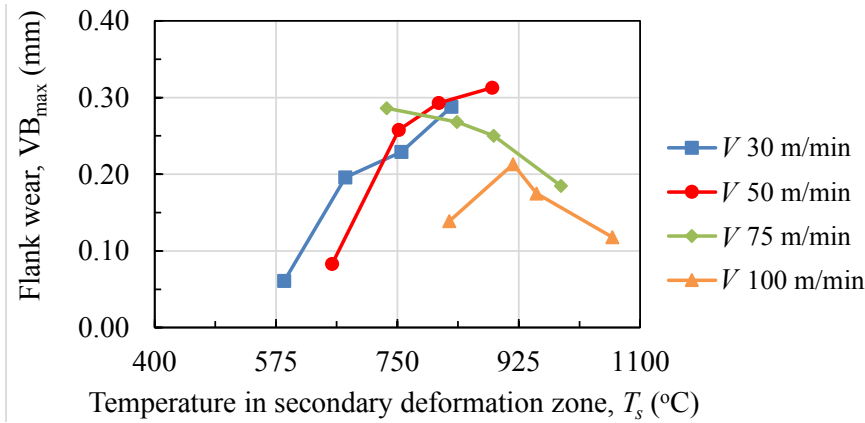
Fig. 4.36 Flank wear land of cutting tool (VB_{max}) versus measured cutting temperature (T_s) with varied cutting speed (V)

For the conventional machining can be observed that the flank wear increased with the cutting speed and the highest flank wear of 0.286 mm occurred at the cutting speed of 75 m/min. This could be explained that the increase in cutting speed resulted in decreasing of contact area of tool-chip interface (refer Fig. 4.33 (b)) accompany with the higher shear stress required for plastic deformed in machining process (refer Fig. 4.35) leading to higher stress on the cutting tool. However, the flank wear decreased to 0.139 mm with the increased cutting speed of 100 m/min. This could be due to the reducing of shear stress, which was caused by cutting heat is sufficient to soften work materials.

From Figure 4.36 can be seen that at low cutting speed of 30 and 50 m/min the tool flank wear increased with the cutting temperature measured. According to the increase in temperature leads to an increase in chemical reactivity which lead to work materials adhered on the tool face [65], and amount of adhesion increased with the decreased cutting speed and strength of workpiece [18]. Therefore, the large tool wear at the low cutting speed and height of cutting temperature is possible to explain that the large adhering layers on the tool rake/flank face easily to formed and fall-off in the cutting process. The BUE or BUL formed by the adhered workpiece material was not stable in interrupted cutting. In another word, the adhered layers was continuously removed by the moving material under high pressure also carrying aggregates of tool material with it and hence, accelerating tool wear at the increased of heating temperature by laser assisted machining. On the other hand, the tool wear at the high cutting speed of 75 and 100 m/min had a trend to decrease with the increase in cutting temperature. This effect could be due to the preheating of the workpiece causing reduction of shear strength at the shear zone leading to reduction of cutting force and tool wear [71].

From this work, it can be deduced that adhesion wear mechanism is a major cause of tool were in the machining of Inconel 718 for both conventional and laser assisted machining. It will not be wrong to say that in most of the cutting conditions, the tool wear is actually initiated by the adhesion mechanism as referred initial wear in Fig. 4.25- 4.32, and the tool wear consequently increases with the cutting distance, more tool wear mechanism such as chipping and fracture can be observed for some cutting conditions after cutting test of 4.5 m as shown in Figs. 4.37-4.40 (Photograph of tool wear after removed chip adhered).

(a) preheating temperature 20ºC

(b) preheating temperature 300ºC

(c) preheating temperature 500ºC

(d) preheating temperature 700ºC
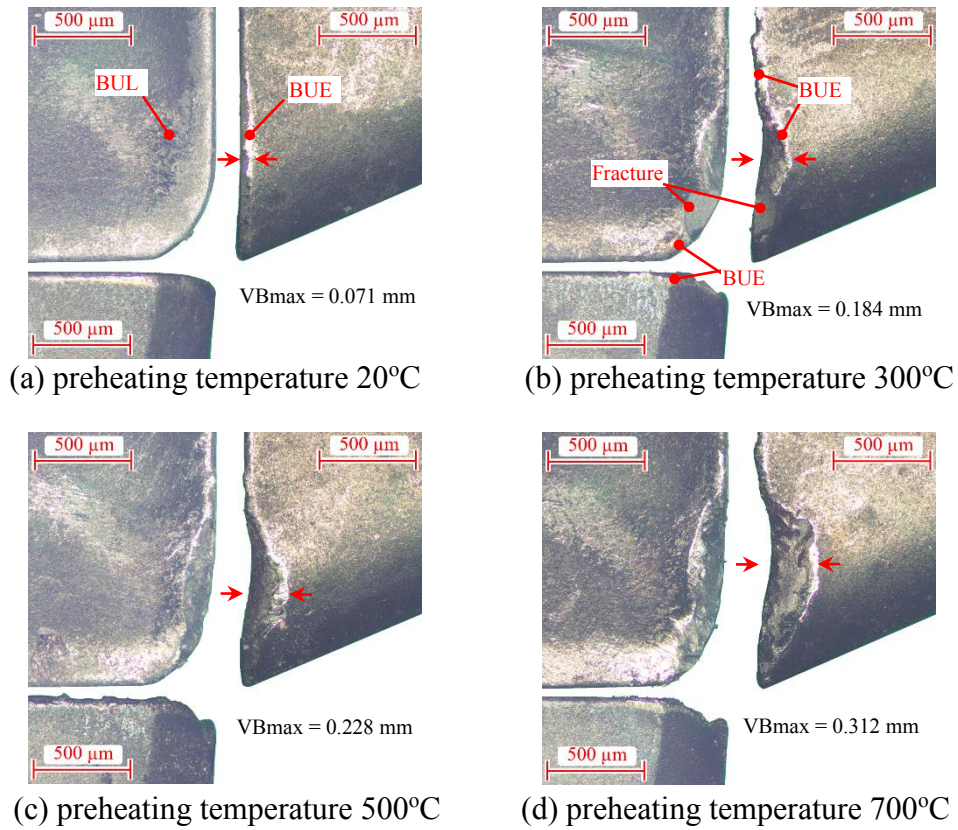
Fig. 4.37 Tool wear after cutting distance of 4.5 m for the cutting speed of 30 m/min

(a) preheating temperature 20ºC

(b) preheating temperature 300ºC

(c) preheating temperature 500ºC

(d) preheating temperature 700ºC
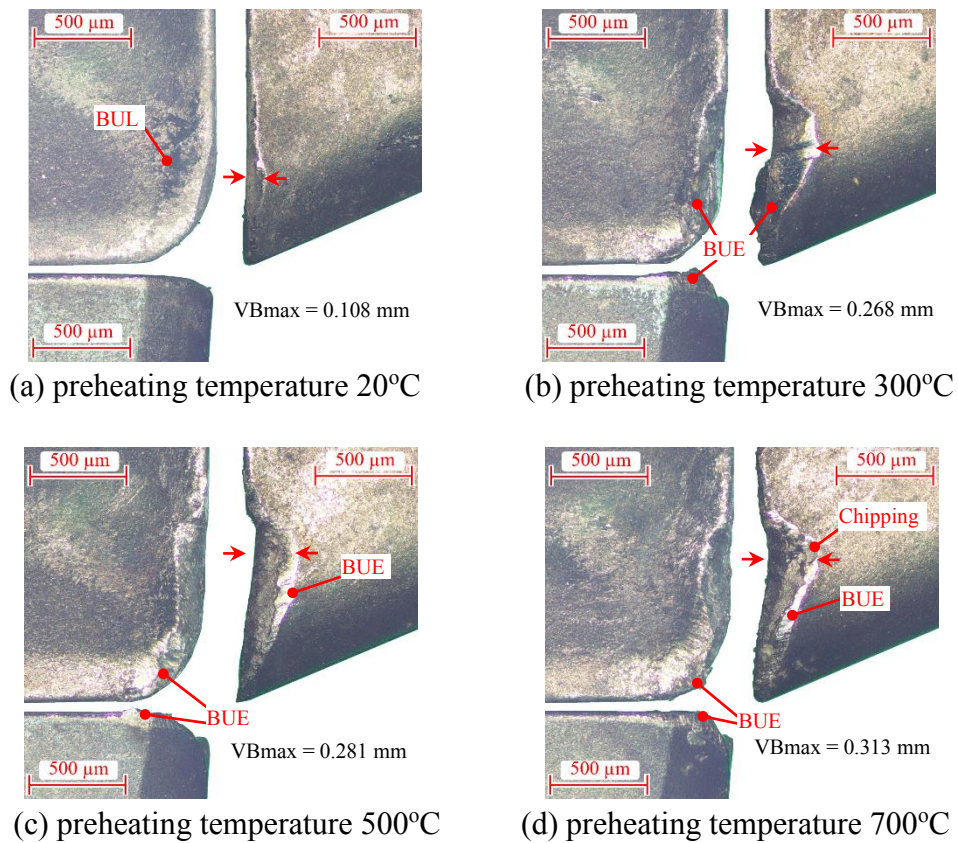
Fig. 4.38 Tool wear after cutting distance of 4.5 m for the cutting speed of 50 m/min

(a) preheating temperature 20°C

(b) preheating temperature 300°C

(c) preheating temperature 500°C

(d) preheating temperature 700°C
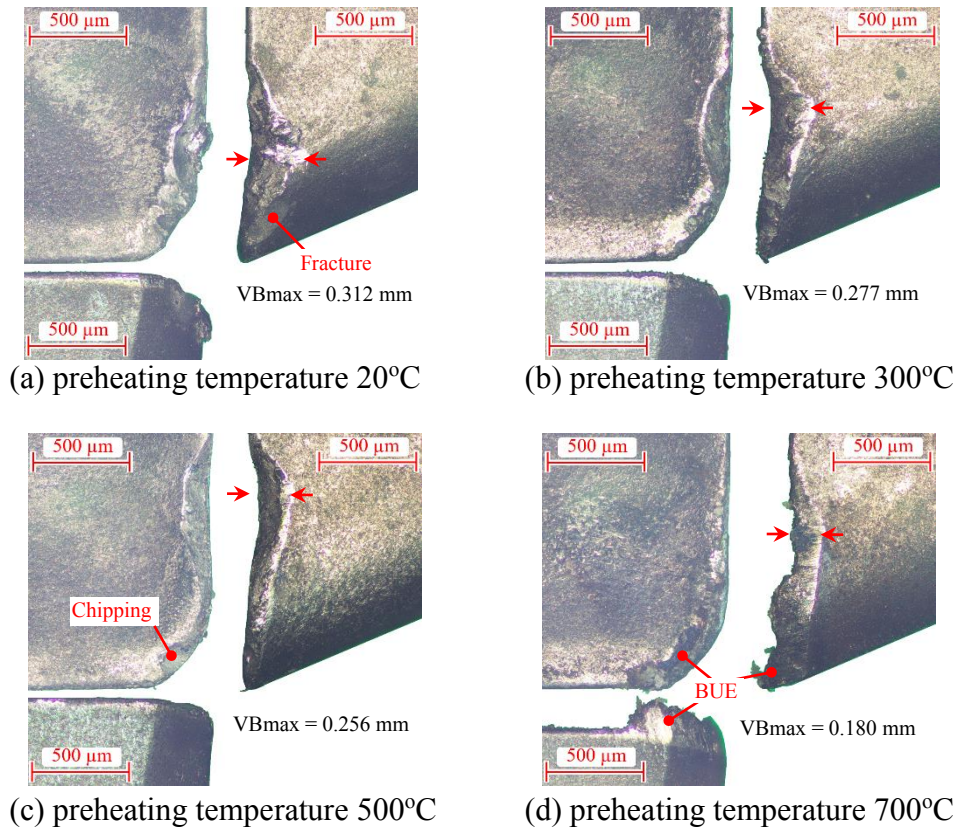
Fig. 4.39 Tool wear after cutting distance of 4.5 m for the cutting speed of 75 m/min

(a) preheating temperature 20°C

(b) preheating temperature 300°C

(c) preheating temperature 500°C

(d) preheating temperature 700°C
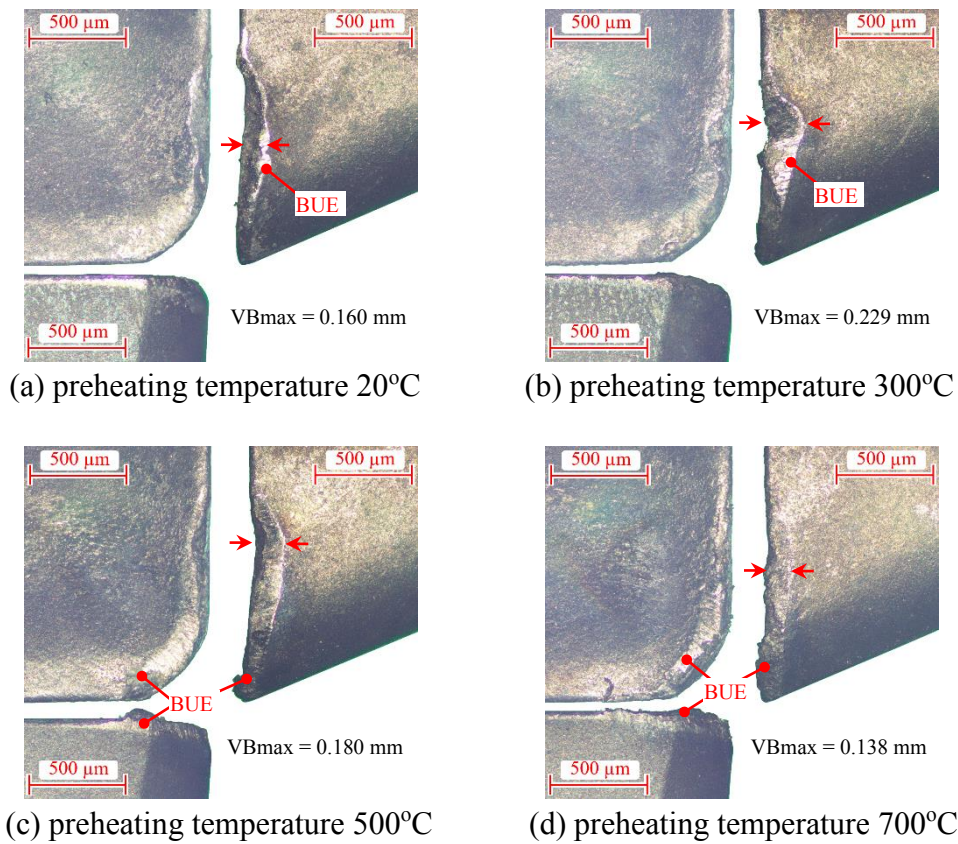
Fig. 4.40 Tool wear after cutting distance of 4.5 m for the cutting speed of 100 m/min

4.3.6 Integrity of machined surface

Figure 4.41 shows the influence of cutting speed and preheating temperature on the quality (physical and mechanical properties changed) of machined surface (roughness and hardness).

(a) Arithmetic mean roughness

(b) Hardness of machined surface

(c) Measuring position of surface roughness

(d) Measuring position of micro-hardness
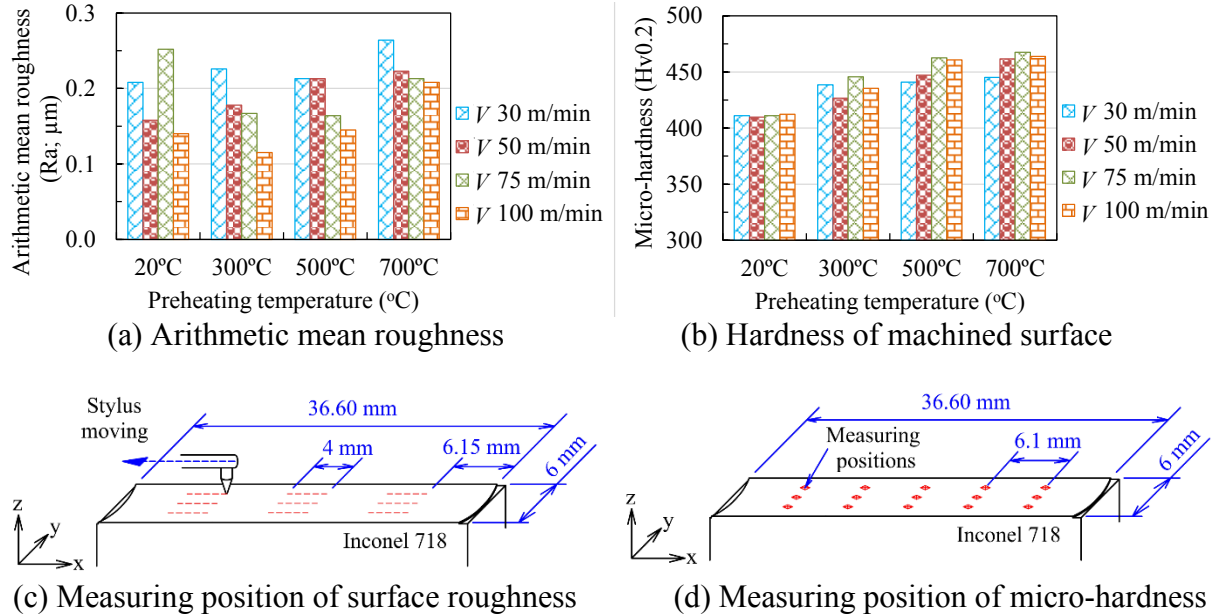
Fig. 4.41 Influence of preheating temperature (T_w) on the quality of machined surface

Figure 4.41 (a) shows the result of surface roughness (arithmetic mean roughness, Ra). This result presents the average values of roughness on the machined surface of 9 positions (3x3 measured positions in x and y-direction) for the machining length of 36.60 mm (cutting distance is 4.5 m) as shown in Fig. 4.41 (c), the surface roughness was measured along the direction of tool feeding, and the measuring length for each positions was 4 mm (0.8 mm of sample length and 5 times of cut off). It can be observed that the surface roughness had a trend to decrease when the cutting speed increased, this is believed that the low requirement of cutting force leading to low vibration of cutting tool and workpiece [28]. In addition, the increase of tool wear (refer Fig. 4.8) also affected to the roughness of machined surface increased due to the high friction of worn tool interface with the workpiece. Moreover, the work material adhered on the bottom edge of cutting tool (BUE) affected to the smeared or scratched on the machined surface (refer Figs. 4.9, 4.10 and 4.11). This is because the height of cutting edge was changed due to the formation of BUE, and during the edge of cutting tool rotated to the position of opposite side with the cutting area, the higher edge of cutting tool was scratched (rubbed) with the finish machined surface (dragging on finish machined surface).

Figure 4.41 (b) shows the result of Vicker micro-hardness measurement that was taken on the machined surface using a square-base pyramidal diamond indenter with a force load of 200g (1.96 N) on the machined surface as shown the measured positions in Fig. 4.41 (d). It can be observed that the micro-hardness of machined surface fluctuated in a very small range when the cutting speed changed. However, the micro-hardness of machined surface slightly increased with the increase of preheating temperature. The maximum increase of

micro-hardness was approximately $12 \pm 2\%$ for the highest preheating temperature by laser assisted machining (700ºC) when compared to the conventional machining. This results indicates that the higher heat input caused the thermal influence on the work materials.

4.4 Conclusions

In this work, the influence of cutting conditions on the preheating temperature was investigated in order to calibrate and control laser power to the particularly preheating temperature at primary shear zone. Then, the experimental cutting was performed to investigate effect of cutting conditions and preheating temperature on the machinability of Inconel 718. The experimental results can be summarized as follows.

1) The minimum distance in feed direction from starting point of laser irradiated to position of a k-type thermocouple could be higher than 15 mm. The unstable of experimental set-up such as position of laser irradiated, polishing surface of workpiece and so on leaded to temperature error in the range $\pm 4\%$ of preheating temperature in this study.

2) The heating temperature has a trend to increase as a linear function of the laser power for any table speed (30, 50, 75 and 100 mm/min). The relationship between laser power and heating temperature can be used to estimate the requirement of laser to retain the particularly preheating temperature of 300, 500 and 700ºC (higher table speed required higher laser power).

3) Increased cutting speed at 50 and 75 m/min for conventional machining had negligible effect on the component of cutting force. When the laser assisted machining was used for preheating work materials, the thrust force (F_x) was decreased lower than conventional machining approximately 22, 23, 23 and 32%, and the tangential force (F_y) was also decreased lower than conventional machining approximated 28, 25, 27 and 27% for the cutting speed of 30, 50, 75 and 100 m/min, respectively.

4) Cutting temperature was increased with the cutting speed for both conventional and laser assisted machining. Although the cutting temperature measured (T_m) was increased with the higher preheating temperature (T_w), the incremental increase of cutting temperature rise (ΔT_p) from the initial temperature of workpiece was decreased with the increase in preheating temperature.

5) The temperature rise (ΔT_p) increased with the cutting speed due to more heat (energy) generated at the high cutting speed. On the other hand, the temperature rise in primary zone decreased with the increase of preheating temperature (T_w) because the reduced strength of work materials lead to low energy consumed for shearing work materials.

6) The increase in cutting speed under the conventional machining leaded to increase in shear angle but chip thickness and tool-chip contact were decreased, which was caused to reduce cutting force and friction coefficient.

7) The highest temperature in primary shear zone with the highest preheating temperature could maximally reduce the shear stress of approximately 20, 30, 35 and 34% to compare with conventional machining at the same cutting speed of 30, 50, 75 and 100 m/min, respectively.

8) The tool wear in laser assisted machining was higher than conventional machining at the low cutting of 30 and 50 m/min, but the wear could be improved at relatively high cutting speed of 75. However, at the high cutting speed of 100 m/min, the tool wear under conventional machining insignificantly changed to compare with the preheating temperature of approximately 700°C.

9) The surface roughness of machined surface had a trend to decrease when the cutting speed increased, but it slightly increased with the preheating temperature increased for almost all cutting speed.

10) The hardness of machined surface with laser assisted machining had a trend to increase as a function of cutting speed, and it was slightly higher than conventional machining approximately 12%.

Chapter 5

Influence of Atmosphere on the Performance of Laser Assisted Milling for Inconel 718 with Carbide Tool

5.1 Introduction

Nickel based superalloys are typically used in high temperature applications such as parts for engines in the aerospace industry due to their high strength and ability to retain strength at high temperature [24, 72]. However, the high mechanical properties require high cutting forces to shear the work material and to generate chips. In addition, the low thermal properties (low thermal conductivity and low thermal diffusivity), high tendency to adhesion and work-hardening were resulted in poor machinability [72-74]. Therefore, laser assisted machining (LAM) has been prospected in various machining processes such as turning and milling to reduce the refractory of these alloys prior the material removal by cutting tool.

Based on the researches, Venkatesan et al. reported that the cutting speed and laser power has influence on the cutting force component and the surface temperature in the range of 750 – 880°C leaded to the maximum force reduction [25]. Kong et al. [63] suggested that the strength of micro-grain tungsten carbide (WC-Co) starts to decrease at temperatures above 500°C and cutting tool is softened when cutting temperature is higher than 1100 °C [57]. In addition, Lima et al. recommended that oxygen in the air may have a lubricating effect due to the oxides formed, oxide on rake face reduce friction and tool wear [4]. Ding et al. reported that the less oxidation on the surface of work materials (Inconel 718) leaded to low optical absorptivity for laser [5]. From these researches, it seems certain that the laser assisted machining process is affected by the atmosphere surrounding the machining area.

However, previous studies have not considered a precaution against the influences of atmosphere on the laser assisted machining. Therefore, the present work focuses on the effect of atmosphere on the requirement of laser power and the machinability in end-milling of Inconel 718 with uncoated carbide tool. The experimental details, methodology and results are discussed in following sections.

5.2 Experimental procedures

Experimental procedure consisted of two stages of tests in this study. First, a chamber system was designed to control atmosphere surrounding the machining area in tests, and the calibration was conducted to decide the required laser power to particular preheating temperatures at primary shear zone within the work material. Secondly, Ni-based alloys (Inconel 718) were heated to the prescribed temperature by laser, and then machined with uncoated carbide end-mills to investigate the influence of atmosphere on the machinability.

5.2.1 Chamber design and calibrating laser power

Figure 5.1 shows the experimental setup for controlled environment in laser assisted milling for Inconel 718 and Fig 5.2 illustrates schematic diagram of chamber systems for

controlled environment surrounding of cutting area. The design of chamber was covered workpiece and fixture that was fixed on the strain gauge dynamometer. The top plate of chamber has a slot for the tool holder moving and laser beam irradiated on the work surface. In order to controlled environment around the machining area the moving plate against chamber was used. The big hole which a small clearance to compare with the diameter of tool holder and laser beam were made in the moving plate. The moving plate against chamber can be together moved with the same feeding speed of cutting tool by using insulation plate fixed on the moving plate to against tool holder.

(a) Work materials was fixed on dynamometer by fixture

(b) Chamber was fixed on dynamometer

(c) Positions of equipment were fixed on milling machine
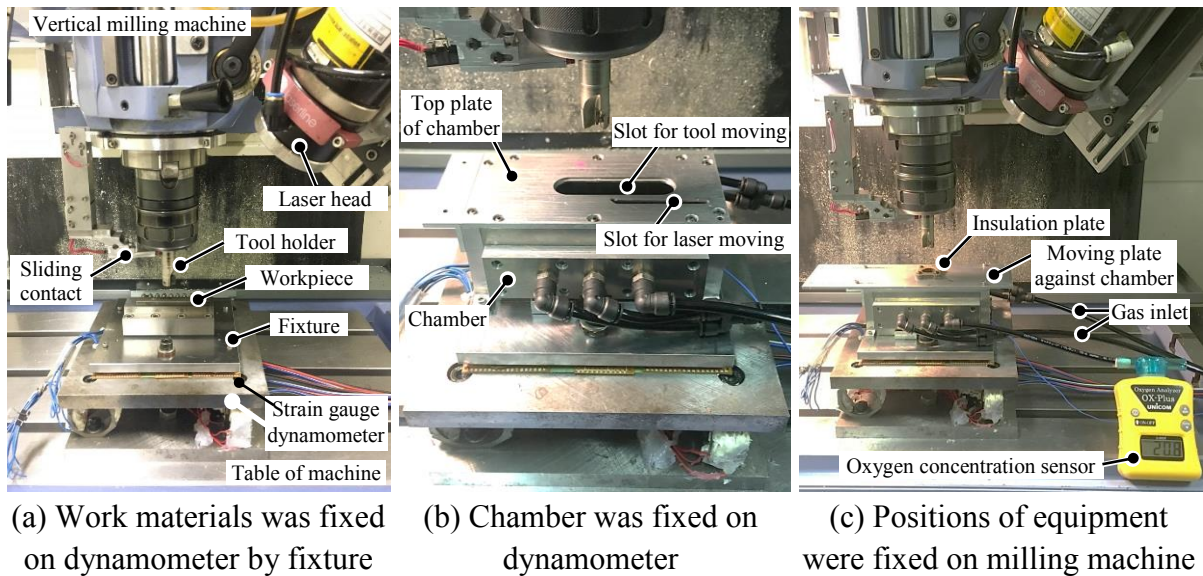
Fig. 5.1 Images of experimental setup for laser assisted milling with controlled atmosphere
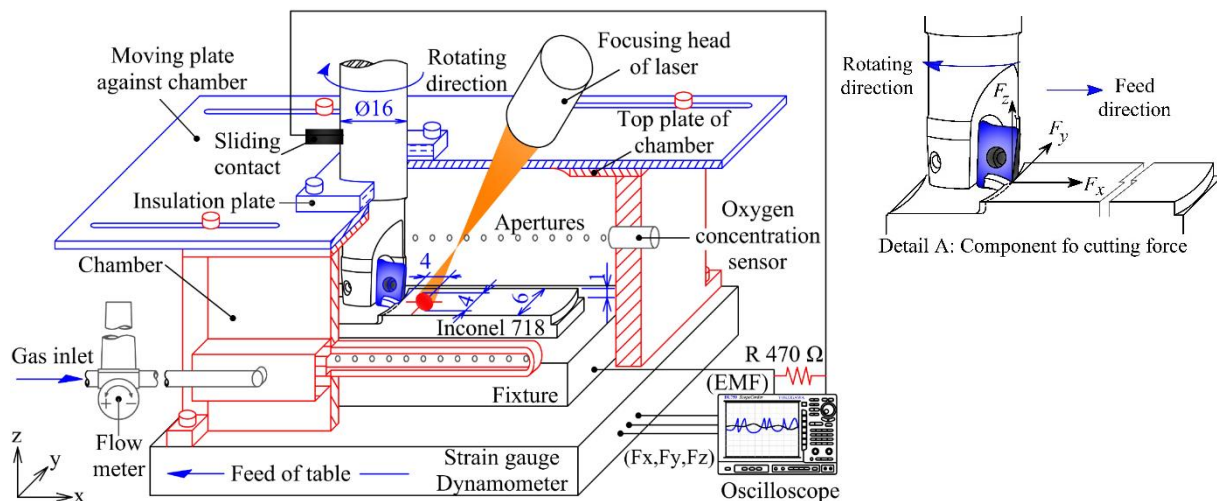

Fig. 5.2 Illustration of chamber system for controlled atmosphere surrounding of cutting area

Compressed air and argon gas can be delivered to the machining area by the hose connected to an inlet-valve which regulates the gas-flow rate and be supplied to around the cutting area through the aligned apertures made on both side surfaces of the chamber. The flow

rate and the pressure of air or argon gas were controlled at constant during the tests; 0.03 m^3/min and 0.15 MPa, respectively. In addition, the oxygen concentration sensor was used to check the oxygen concentration before beginning tests.

A diode laser system with the maximum power of 6 kW (Laserline LDF 6000-40) was used for heating the work material prior to the cutting by the endmill. The focusing unit of laser was mounted on the vertical spindle head of milling machine (Shizuoka ST-NR CNC), and the laser beam axis was set at 50° to x-y plane and 45° to y-z plane as show in Figs. 5.2 and 5.3. The figure also shows that the center of beam spot was positioned 4 mm ahead of the cutting point on the work surface, and diameter of the spot was approximately 4 mm.
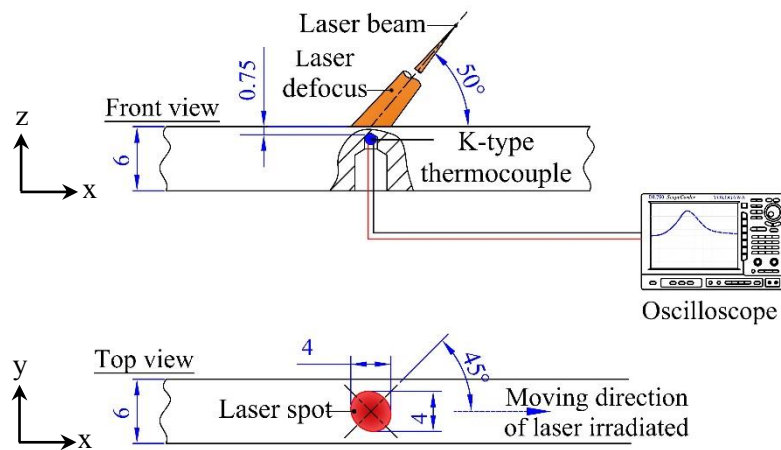
Fig. 5.3 Calibrating test of laser power for preheating temperature (T_w)

In the laser assisted milling, the work material was preheated and reached the maximum temperature just below the laser spot, and then was gradually cooled until the material was fed to the cutting point. Prior the milling test, temperature of the laser heated material was measured to calibrate the laser power required for particular preheating temperatures. A K-type thermocouple (chromel–alumel) with a diameter of approximately 1.0 mm was embedded into the drilled hole (Ø ≈ 1.2 mm). The hot junction of thermocouple contacted with the hole bottom whose depth from the work surface was 0.75 mm (corresponding to the axial depth of cut in milling test). The thermal electromotive force (EMF) was detected and recorded by a digital oscilloscope as shown in Fig. 5.3. Table 5.1 and Table 5.2 show the conditions for calibrating experiments performed to investigate the relationship between laser power and preheating temperature.

Table 5.1 Cutting conditions in experiment

V (m/ min)	Feed (mm/ tooth)	Tool dia- meter (mm)	Axial depth of cut (mm)	Spindle speed (rpm)	Feeding speed (mm/min)
100	0.05	16	0.75	1990	100

Table 5.2 Laser power used for calibrating temperature

Environments	Laser power, L_p (W)				
	Level 1	Level 2	Level 3	Level 4	Level 5
Dry (atmosphere)	150	190	250	270	310
Compressed air blow	220	225	250	290	330
Argon gas	150	300	400	500	690

5.2.2 Laser assisted milling experiment

The symmetrical face milling was performed to evaluate the influence of atmosphere on the performance of laser assisted milling. The preheating temperature was approximately varied as 20, 300, 500 and 700°C for any atmosphere with a constant cutting speed of 100 m/min and a constant feeding speed of table 100 mm/min. An indexable endmill (HM90A-D16-2-C16, ISCAR) was used and single carbide insert (APKR1003PDR-H IC28, ISCAR) was mounted for avoiding the influence of difference in cutting-edge height between inserts. And it also should be noted that new carbide inserts were used to avoid the influence of tool wear. The workpiece was a plate of Inconel 718, which was mounted on the dynamometer as shown in Fig. 5.2.

The cutting temperature at the tool-chip interface area was measured by tool-work thermocouple. The electromotive force (EMF) was converted to the measured temperature by means of a calibration curve approximated by following cubic equation, which had been derived from the calibration tests previously conducted in vacuum furnace [18] (refer chapter 3 section 3.2.3) as following equation (3.3).

$$T_m = 0.0358x^2 - 1.3681x^2 + 66.876x + T_R \qquad (3.3)$$

where, T_m (°C) is measured cutting temperature, x (mV) is electromotive force, T_R is the room temperature (≈20°C)

After the cutting distance of 4.5 m, the maximum width of flank wear was measured with a toolmaker's microscope (Mitutoyo). In addition, the roughness of machined surface was also measured by a roughness tester (Surfcorder SE-30D, Kosaka Lab, Ltd). Furthermore, the hardness of machined surface was examined by Vickers hardness tester (MMT-X7-LCD, MATSUZAWA) with testing load of 200g (1.96N), and evaluated by the average hardness among fifteen measuring points.

It should be note that prior to the cutting tests, a skin cut of 0.2 mm thickness was done in order to remove any deformities on the work surface, and it was polished with abrasive paper to keep same surface absorption as used in the process of laser power calibration.

5.3 Results and discussion

This section consists of three parts; the first part focuses on the requirement of laser power

for retaining preheating temperature with various atmosphere, the second part emphasizes the evaluation of cutting temperature and the cutting force sufficient to shear the work material and to generate chips, and the third part examines the tool wear and integrity of machined surface. These obtained results are discussed and investigate the influence of the atmosphere.

5.3.1 Laser power to the preheating temperature

Figure 5.4 shows temperature signals measured by the K-type thermocouple embedded in the workpiece fed at of 100 mm/min for different laser powers and three kinds of atmosphere (Fig. 5.4 (a) Dry air, (b) Compressed air blow, and (c) Argon gas). It can be seen that the temperature rapidly rose as the thermocouple approached the laser spot, and took the maximum T_p just under the laser spot for any conditions. Then, the measured value gradually decreased because of heat dispersion to the environment. The figure also shows that the peak temperature increased with the laser power L_p. The peak temperature decreased when the argon gas was supplied into the chamber. This is due to the reduction of oxidation by inert gas.

Besides, for discussion on thermal effect at the cutting region which is 4 mm behind the laser spot center, we have to consider not the peak temperature but the temperature at the region. As can be seen in Fig. 5.4, temperature can be easily read from the signals, because the measured signal varied smoothly. Here, authors defined that the temperature measured 2.4s (= 4mm ÷ 100mm/min) after the peak corresponds to the preheating temperature of work material at cutting region T_w. The preheating temperatures T_w were slightly lower than the peak temperature T_p for each laser power, because of the cooling in short time. In addition, environmental atmosphere also affected to the peak and the preheating temperature. For example, in Fig. 5.4, the laser power of 310 W, 330 W and 690 W yielded the peak temperature T_p of 823 ºC, 885ºC and 843 ºC followed by the preheating temperature T_w of 683 ºC, 700 ºC and 691ºC for the atmosphere of (a) Dry air, (b) Compressed air blow and (c) Argon gas, respectively.

Figure 5.5 indicates the relationship between laser power and measured temperatures (T_p & T_w) for different atmospheres. Measured temperatures increased almost linearly with laser power under the conditions employed in this study. The temperature measured in argon atmosphere was obviously lower than ones in the atmosphere containing oxygen. This is due to prevention of the exothermic oxidation and the consequently induced increase of optical absorptivity for laser beam [5]. On the other hand, the difference between dry air and compressed air was slight, because the air flow didn't have much effect on cooling under the conditions employed in this study.

These experimental results indicate that argon gas atmosphere requires higher laser power to retain the temperature high enough to soften the work material in cutting region. The heating temperature proportionally increased as an increase of the laser power for any atmosphere as shown in Fig. 5.5, therefore this relationship can be used to estimate the laser power for particular preheating temperatures. In following laser assisted milling tests, the preheating temperatures were set as approximately 200, 300, 500 and 700ºC for each

atmosphere, because peak heating temperature must be lower than 950ºC to avoid the change of microstructure of Inconel 718 [1].

(a) Dry

(b) Compressed air blow

(c) Argon gas
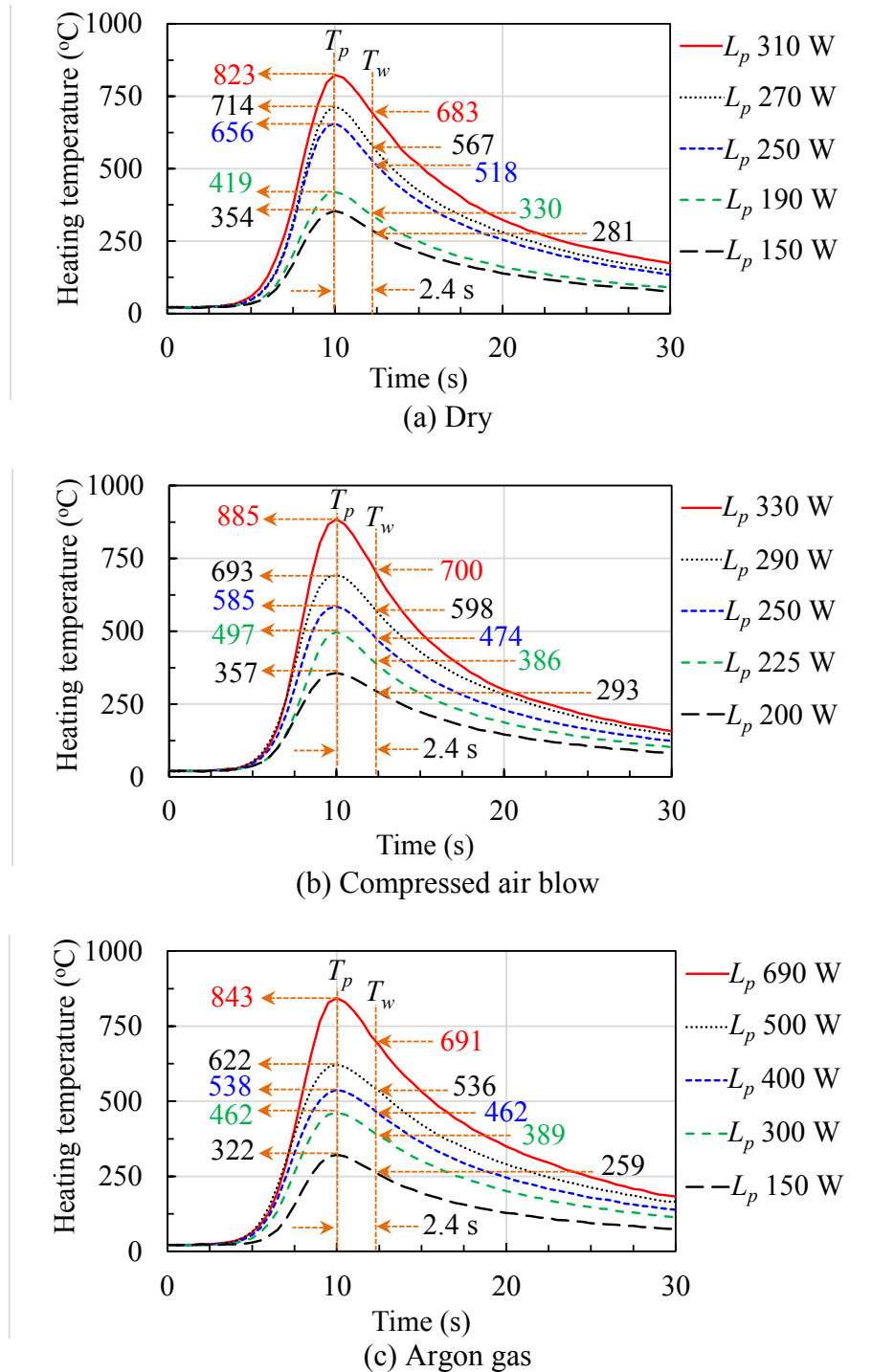
Fig. 5.4 Temperature at depth of 0.75 from irradiated surface in different atmospheres

Above tendency of workpiece temperature can be clearly observed as the color change of irradiated surface due to oxidized/burned layer on the work surface shown in Fig 5.6, photographs captured just after suspending the laser assisted milling process by quick downward withdrawing of the work material. The workpiece was fed leftward in the figure and

64

it can be seen that colored oxidized/burned area was generated in front of the cutting region. Higher laser power caused larger area of oxidized surface, and dry air atmosphere caused the most intense thermal effect. And it can also be seen that excessive preheating left the oxidation on the machined surface (for L_p =316 W in dry air). Whereas, the irradiated surface of work piece under the environment of argon gas almost same as the color of the original work material (silver-white color), even the surface of workpiece was melted.

Fig. 5.5 Relationship between laser power (L_p) and heating temperatures (T_p and T_w) in three different atmospheres

Fig. 5.6 Oxidized/burned areas on surface of Inconel 718 workpiece irradiated with laser power (L_p) for preheating temperature (T_w) of 300, 500 and 700ºC in three different atmospheres

65

It should be noted that the laser irradiated direction was indented from the alignment of workpiece when cutting part was finish, this is because the position of laser irradiated c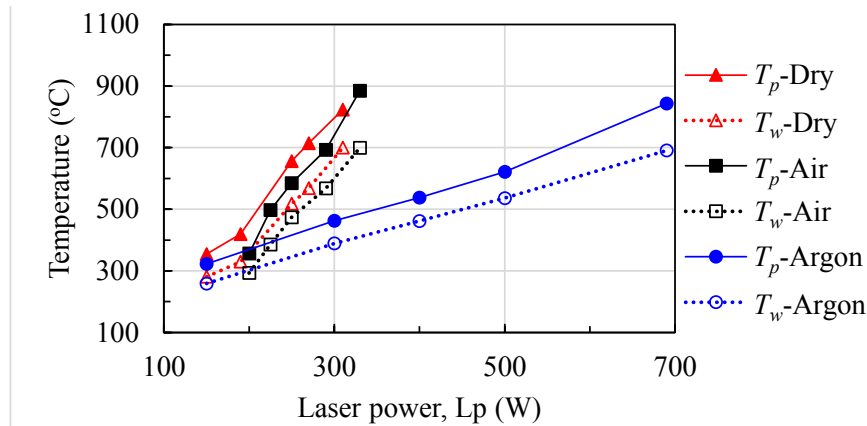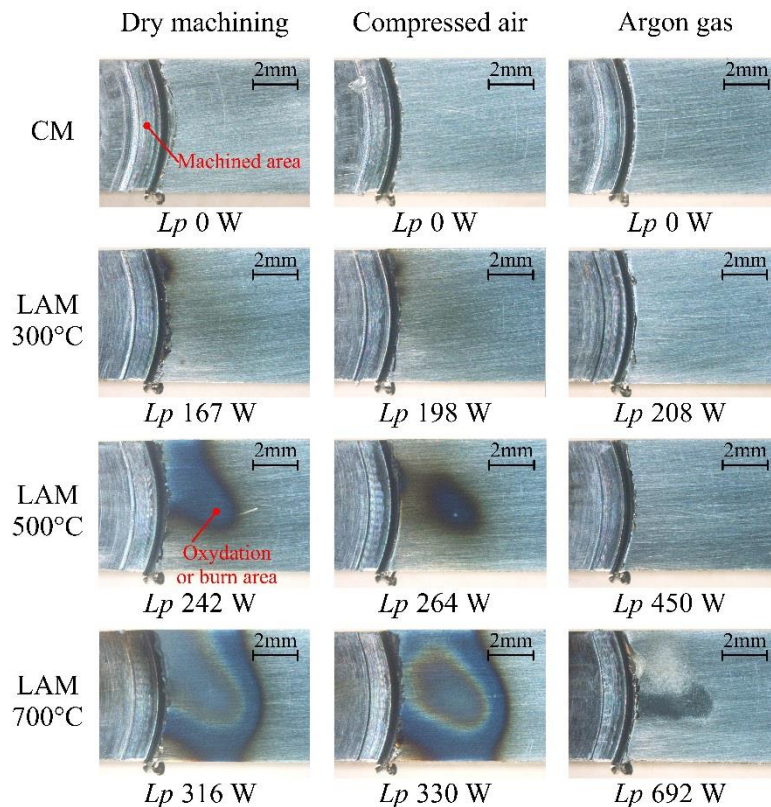hanged during the cutting tool and laser moving out from the cutting area by CNC (the alignment of laser changed when the height of tool position changed).

5.3.2 Cutting temperature

Almost all of the energy consumed in metal cutting is converted into heat, which raises the cutting temperature and often causes the problems on accuracy and cost in machining. In laser assisted machining, preheated materials are plastically deformed and sheared in chip generation process by cutting edges of the endmill, and then the machined materials slide over the rake face of tool. Therefore, machinability of the material highly depends on the temperature at preheating temperature (T_w), while thermal damages of the tool are influenced by the cutting temperature (T_m).
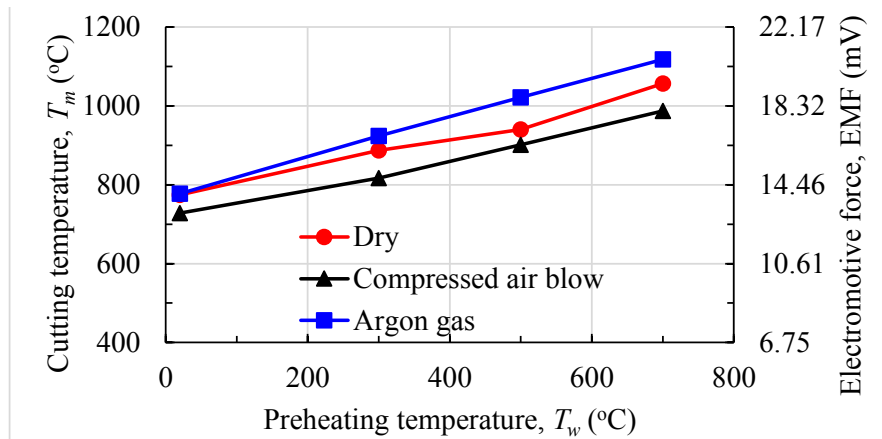
Fig. 5.7 Cutting temperature in regions of tool-work materials interface (T_m) was measured by tool-work thermocouple method

Figure 5.7 shows relationship between the preheating temperature of work material (T_w) and the cutting temperatures measured by tool-work thermocouple method (T_m) in different atmospheres. It can be seen from the figure that the cutting temperature increased linearly with the preheating temperature for any atmosphere. Slopes of increase in cutting temperatures were less than unity. This is because that the increase in the preheating temperature reduced the strength of material and the heat generated in the cutting region both.

Comparing three atmospheres in the figure, argon gas yielded the highest cutting temperature among three atmospheres, while compressed air blow caused the lowest temperature. The lowest temperature in the compressed air blow could be explained by the forced convection with high heat transfer coefficient due to the higher velocity of air [75].

Besides, the highest cutting temperature in the argon gas can be explained the low heat transfer coefficient of argon [76]. And, this is also attributed to low specific heat and thermal conductivity of argon, which are approximately half of ones in air [37, 77]. In addition,

oxygen contained in the air can generate oxides film on tool face and provide lubrication in tool-chip interface which indirectly leads to the decrease in cutting temperature [78, 79].

5.3.3 Cutting forces

Figure 5.8 shows cutting forces measured for the preheating temperatures for which the required laser power was previously examined in three different atmospheres. As already shown in Fig. 5.2, the thrust force F_x is a component of cutting force in direction of the radial depth of cut. Besides, the tangential force F_y is the other one in direction of the motion of cutting edge, so this is also called a principal force. In end-milling, cutting edges on the rotating tool engage the workpiece one after another and they remove the material as chips. Therefore, the direction of motion of each edge changes during the generation of a single chip, even if the workpiece width is small such as the experiments in this study. In order to avoid the influence of this and to discuss the effects of preheating and atmosphere, the measured force of each cutting edge was averaged over the cutting duration. In addition, mean force is calculated and shown in Fig. 5.6 in order to avoid the influence of variation in cutting ability of each edge.
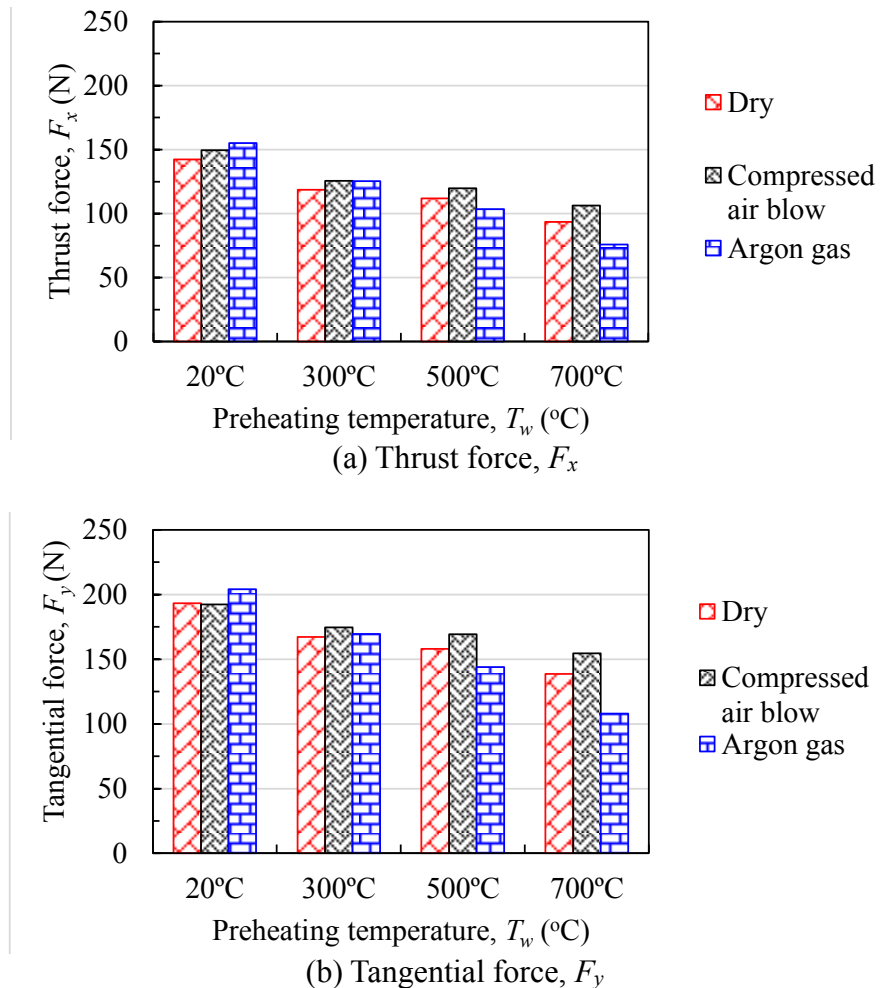

(a) Thrust force, F_x

(b) Tangential force, F_y

Fig. 5.8 Influence of preheating temperature (T_w) and atmosphere on the components of cutting force (F_x and F_y)

As can be seen in Fig. 5.8, the thrust force F_x and the tangential force F_y decreased with the preheating temperature of workpiece T_w. The highest workpiece temperature (T_w=700ºC) with argon gas could reduce the cutting forces to 50% of ones in conventional milling (20ºC). This thermal effect on cutting force contributes the decrease in heat generating in cutting region as mentioned in previous section.

Influence of the atmosphere on the cutting forces (F_x and F_y) can also be seen in the figure, but the relative superiority among atmospheres was not constant but changed by the preheating temperature. For example, the highest cutting force among three atmospheres was argon gas for the conventional milling without preheating, while the force in same atmosphere became the smallest with the highest preheating temperature (T_w=700ºC).

According to Lima et al. [4] and Fan et al. [78], the oxygen in the air may have a lubricating effect due to the oxides formed on the surface of cutting tool. And the strength of materials changes due to the increase in the temperature of workpiece. Therefore, a friction coefficient and a specific cutting force were used to indicate influence of atmosphere in laser assisted milling for Inconel 718. Following equation provides the friction coefficient μ, which can be geometrically calculated from the experimentally measured forces F_x and F_y.

$$\mu = F_x + F_y \tan\alpha / F_y - F_x \tan\alpha \qquad (5.1)$$

where, μ is the coefficient of friction, F_x (N) is thrust force, F_y is tangential force, and α (deg.) is the rake angle (in this test is approximately 4 deg.).

And the specific cutting force, K_s is a required cutting force per unit area of cut, which also can be calculated as following equation.

$$K_s = \sqrt{F_x^2 + F_y^2} \qquad (5.2)$$

where, K_S (N/mm^2) is the specific of cutting force, t is uncut chip thickness (0.05 mm), and b is the depth of cut (0.75 mm).

Figure 5.9 shows the friction coefficient (μ) between the tool face and the chips with the cutting temperatures (T_m) measured in three different atmospheres. The friction coefficient decreased with the cutting temperature in any atmospheres due to the decrease in strength of heated work material. This is because that the friction force was determined by the shear strength of the weaker of the two sliding materials in adhesive sliding contact such as the tool-chip interface [80]. Furthermore, oxygen in the air generated the oxide film on the tool face, which acts as lubricant [4, 78, 79]. Therefore, as shown in Fig. 5.7, argon gas atmosphere resulted in slightly higher friction although the cutting temperature was higher than other atmospheres containing oxygen.
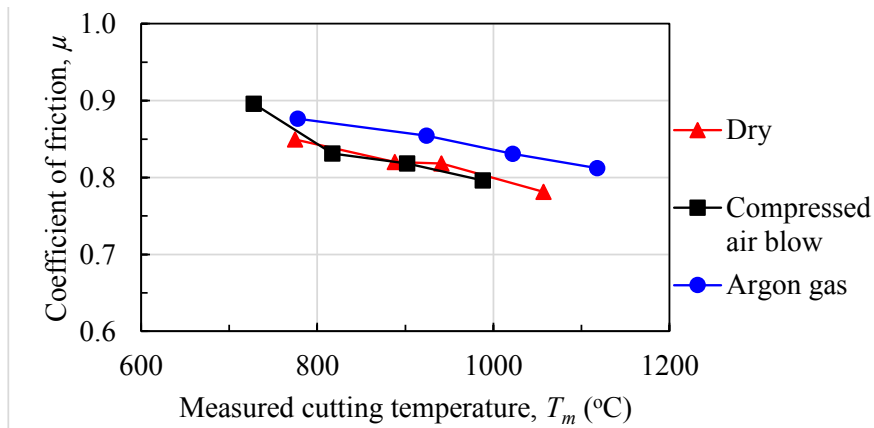
Fig. 5.9 Relationship between friction coefficient (μ) and cutting temperature (T_w) measured in different cutting atmosphere

Meanwhile, The specific cutting force indicated similar tendency as the cutting temperature increased as shown in Fig. 5.10. The higher cutting temperature resulted in lower requirement of cutting force for shearing work material to generate the chips for any atmospheres. For example, the highest cutting temperature of approximately 1120, 1060 and 990°C presented the lowest specific cutting force of approximately 3520, 4460 and 5000 (N/mm^2) for the atmosphere of argon gas, dry and compressed air blow, respectively.
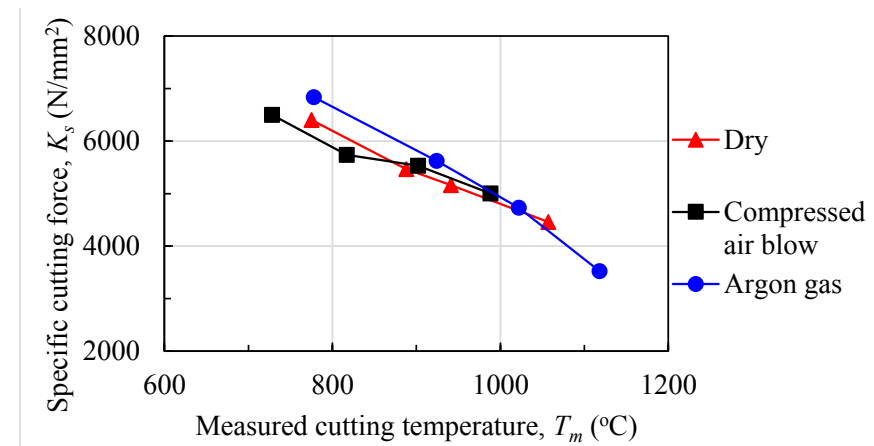
Fig. 5.10 Relationship between specific cutting force (K_s) and measured cutting temperature (T_w) in different atmospheres

5.3.4 Tool wear

Figure 5.11 shows relationship between the measured cutting temperature (T_m) and the maximum of flank wear land of tool (VB_{max}) for cutting distance of 4.5 m (corresponding to machining length of 36.60 mm) in different atmospheres (Dry, Compressed air blow and argon gas) and with various preheating temperatures (T_w = 20, 300, 500 and 700°C). And, Figs. 5.12 − 5.14 present appearance of the cutting edge of tools just after machining test, which were observed with an optical microscope.
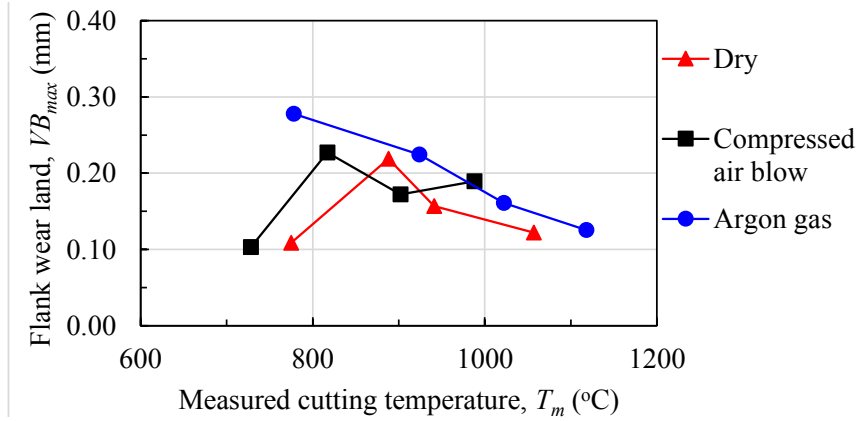
Fig. 5.11 Results of tool wear (Flank wear land, VB_{max}) with various atmospheres

It can be seen from Fig. 5.11 that the tool wear decreased with the cutting temperature, except results for conventional cutting in the air and the air blow. This result indicate that thermal wear of tool was not dominant under the experimental conditions in this study, although the laser irradiation was employed to heat the work material.

And, it is worthy of notice in Fig. 5.11 that atmosphere of dry and compressed air blow restricted the wear in the conventional machining ($T_w = 20^oC$). A comparison of photos in Figs. 5.12-5.14 found that high chemical affinity between tool and work caused thick adhesion layer on the tool face, but oxygen-containing and low-temperature conditions reduced the adhesion of work material on the tool edge. The adhered work materials are highly work-hardened and generally not stable but frequently broken and dragged by the chip flowing along tool surface. Thus, tool surface is scratched by very hard particles resulting in accelerated tool materials loss [24]. Decrease in tool wear with high temperature may be attributed to that the higher temperature decreased cutting forces (refer Fig. 5.8), the friction (refer Fig. 5.9), improved the machinability (refer Fig. 5.10), although the adhesion of material was not reduced as shown in Figs. 5.12-5.14.
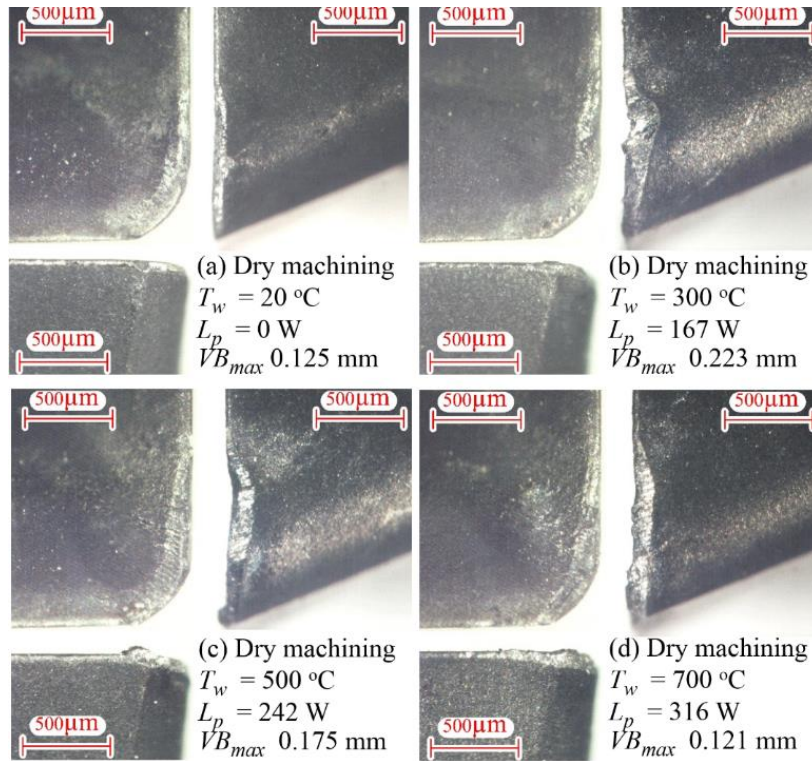
(a) Tool wear after removed work materials from the rake face of cutting tool
(Test no.1)
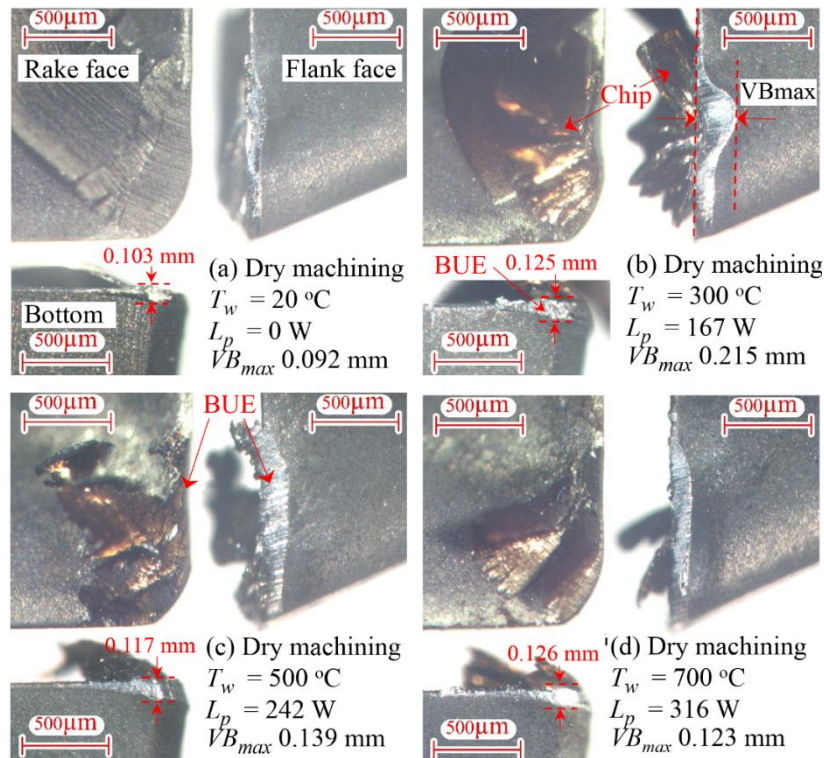
(b) Tool wear and work materials adheres on the tool face
(Test no.2)

Fig. 5.12 Photograph of tool wear in the atmosphere of dry machining with various preheating temperature

(a) Air blow
$T_w = 20$ °C
$L_p = 0$ W
VB_{max} 0.131 mm

(b) Air blow
$T_w = 300$ °C
$L_p = 198$ W
VB_{max} 0.252 mm

(c) Air blow
$T_w = 500$ °C
$L_p = 264$ W
VB_{max} 0.197 mm

(c) Air blow
$T_w = 500$ °C
$L_p = 330$ W
VB_{max} 0.208 mm

(a) Tool wear after removed work materials from the rake face of cutting tool
(Test no.1)

(a) Air blow
$T_w = 20$ °C
$L_p = 0$ W
VB_{max} 0.075 mm

(b) Air blow
$T_w = 300$ °C
$L_p = 198$ W
VB_{max} 0.202 mm

(c) Air blow
$T_w = 500$ °C
$L_p = 264$ W
VB_{max} 0.147 mm

(c) Air blow
$T_w = 500$ °C
$L_p = 330$ W
VB_{max} 0.171 mm

(b) Tool wear and work materials adheres on the tool face
(Test no.2)

Fig. 5.13 Photograph of tool wear in the atmosphere of compressed air blow with various preheating temperature
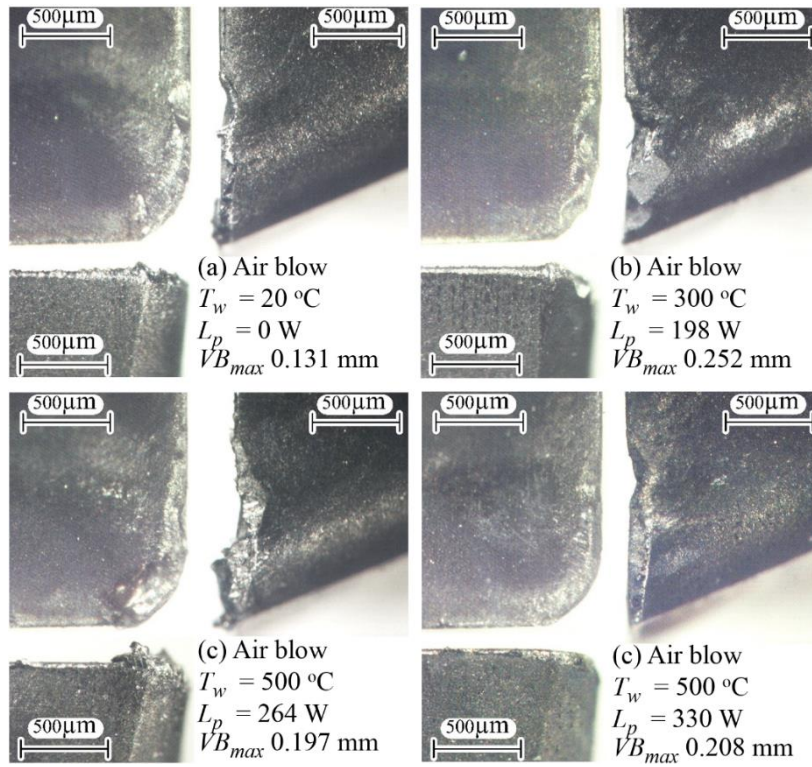
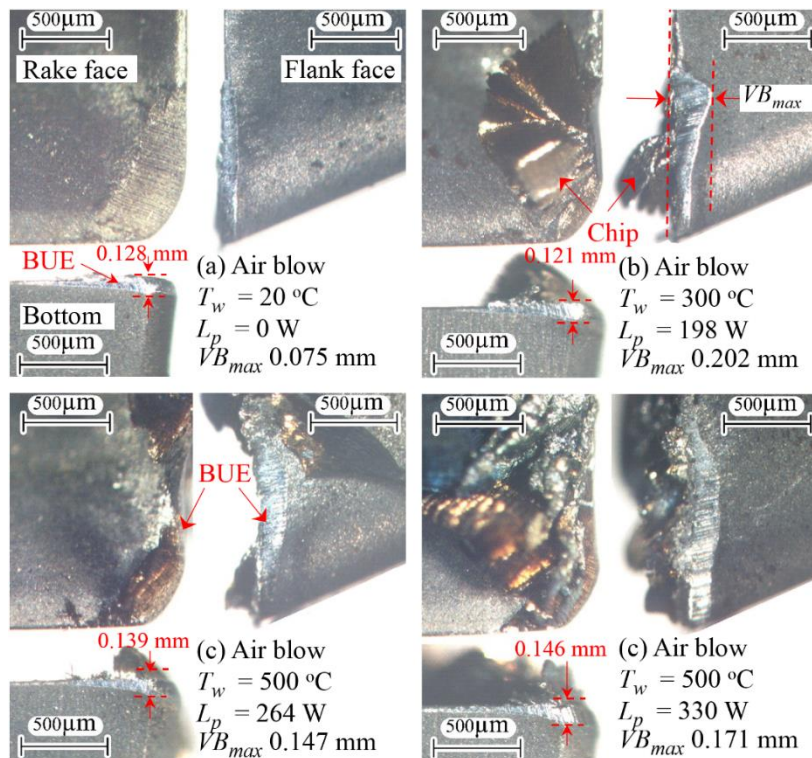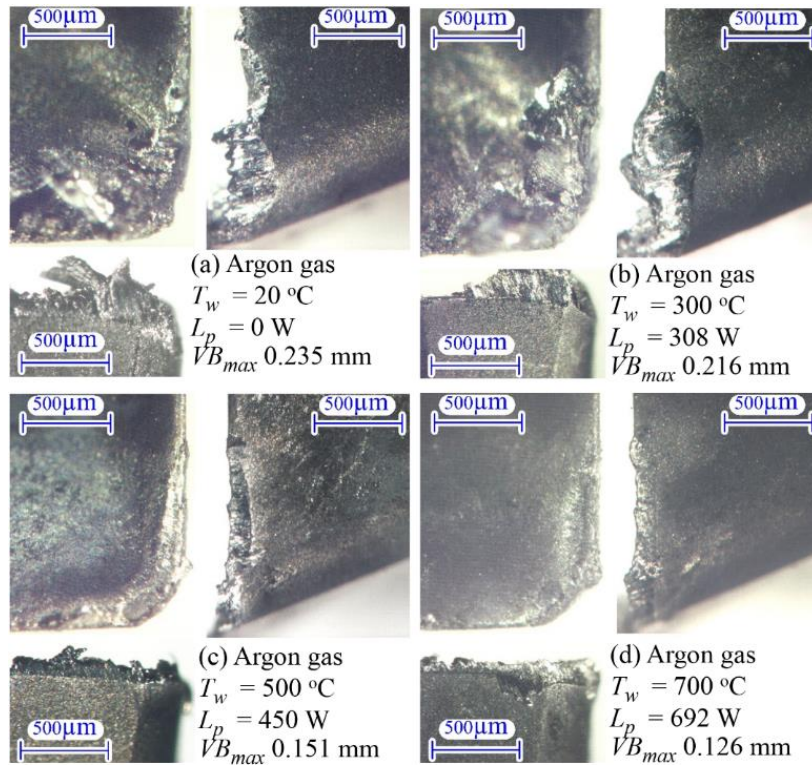(a) Tool wear after removed work materials from the rake face of cutting tool
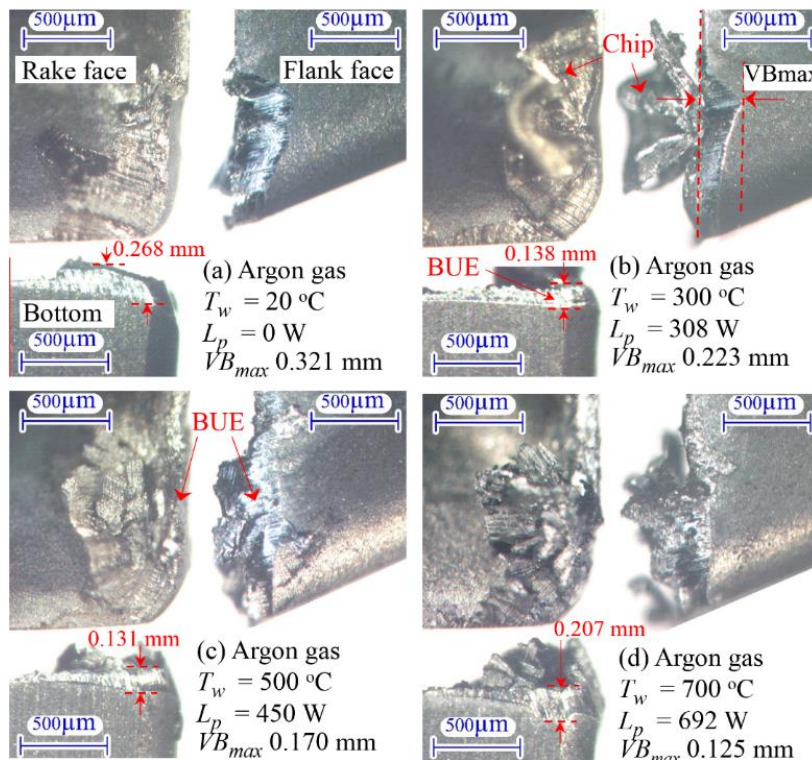
(Test no.1)

(b) Tool wear and work materials adheres on the tool face

(Test no.2)

Fig. 5.14 Photo of tool wear in the atmosphere of argon gas with various preheating temperature

5.3.5 Integrity of machined surface

Figure 5.15 summarizes the influence of atmospheres and preheating temperature on the integrity of machined surface such as arithmetical mean roughness (Ra) and Vickers hardness (HV0.2).

(a) Surface roughness, Ra

(b) Micro-hardness, HV0.2
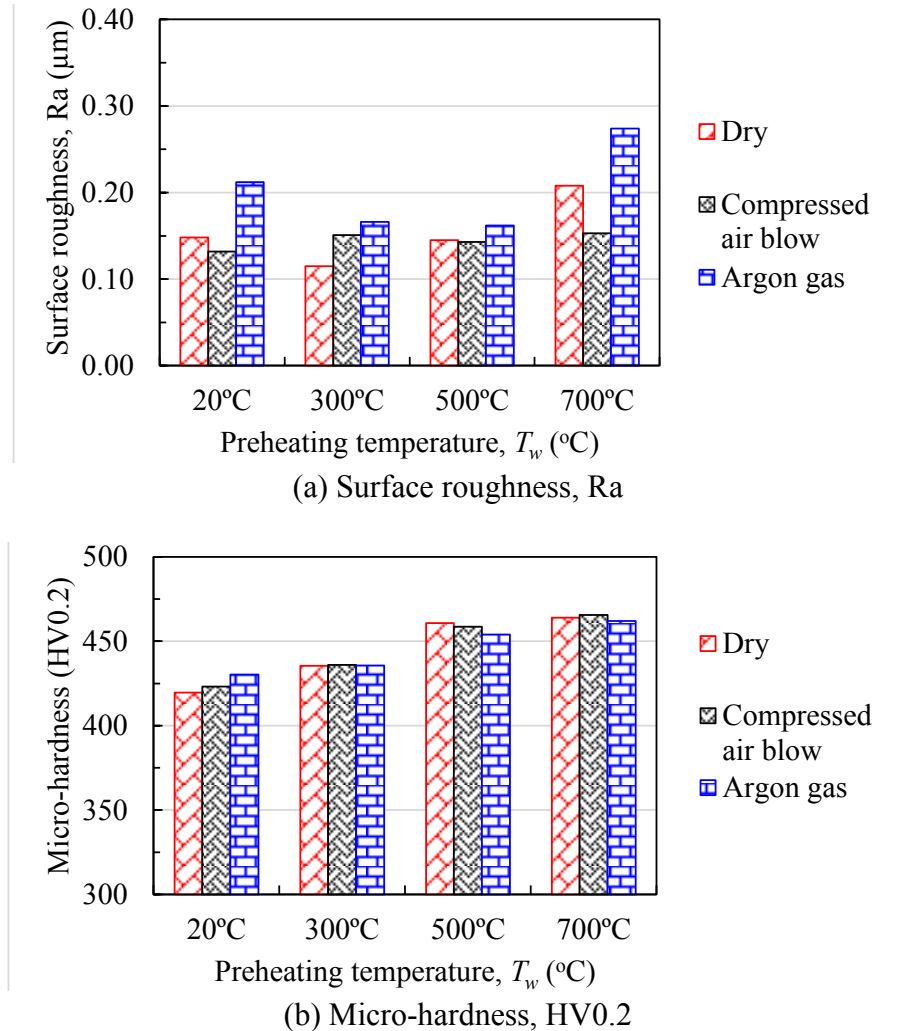
Fig. 5.15 Integrity of machined surface

Surface roughness in Fig. 5.15 (a) was measured for the length of 36.60 mm on the machined surface. As can observed in the figure, argon gas yielded the highest surface roughness among three atmospheres, while compressed air blow caused the lowest roughness. The highest roughness in the argon gas could be explained by the high cutting temperature, which leads to thick adhesion layer on the cutting edge of tool as illustrated in Figs. 5.12-5.14. Consequently, the adherent material would scratch the machined surface and cause scratch marks which increase the roughness.

Figure 5.15 (b) shows the hardness (HV0.2) on machined surface, which slightly increased with the preheating temperature of workpiece (T_w). For example, the hardness was approximately 425±10 HV0.2 in the conventional machining (T_w 20ºC), but the highest

preheating temperature (T_w=700ºC) caused the highest hardness of approximately 460±10 in any atmospheres. This result indicated that the atmosphere does not have a great influence on the hardness of machined surface.

5.4 Conclusions

This chapter concerned the influence of preheating temperature and atmosphere on the performance of laser assisted end-milling for Inconel 718 using uncoated carbide inserts. The obtained results are concluded as follows.

1. Laser could raise the temperature of work material to improve the machinability, while the dry and compressed air blow decreased the laser power required to retain particular preheating temperatures compared with the atmosphere of argon gas. This is because the oxygen in air accelerated the oxidation and burning on irradiated surface which increase the optical absorptivity. On the other hand, argon gas prevents such influences, therefore the required laser power was higher.

2. The specific cutting force of Inconel 718 decreased with the preheating temperature in any atmospheres, and the lowest specific cutting force was obtained in the argon atmosphere due to the increase in friction coefficient. Measured temperature in end-milling tests presented that the atmosphere of argon also increased the cutting temperature.

3. Tool adhesion layer was built on tool face and it played a major role for the wear of tool material in the conducted experiments. This would be attributed to high affinity of work material against the tool material used here. Therefore, hard coating would be prospective for the tool life extending.

4. Comparing three atmospheres, compressed air blow yielded the lowest roughness of machined surface, while argon gas caused the highest roughness among three atmospheres. The lowest roughness of machined surface was achieved at the preheating temperature of 300ºC for any atmosphere.

5. The hardness of machined surface had a trend to increase with the preheating temperature in any atmospheres. The hardness was slightly higher than conventional machining and was 460 HV at most for the temperature of 700ºC in this study.

Chapter 6

Improved Machinability of High Hardened Die Steel by Using Pulsed Laser Surface Treatment

6.1 Introduction

Tool steel is widely used to make molds and dies for the mass production, because of its mechanical properties and wear resistance which can be improved by the thermal and thermo-chemical treatment [81]. According to Lee et al., nitriding process produces the surface layer whose hardness is approximately 1100 HV and the diffusion layer of 150 μm thick for hot work tool steel (SKD61) [82]. And hardness of the nitride surface layer was two times higher than that of the base material [82]. However, in spite of the improved life of dies [83], wear and damage on the die surface cannot be completely avoid [84,85]. These failures significantly affect the quality and costs of the product, so that the dies are regularly replaced with new ones or are reused after reforming process to correct the surface shape and the dimensions.

Due to its high consistency with CAD/CAM systems and its high suitability for machining of curved surface of dies, the milling process is expected to remove the worn surface layer for retaining the complex shape and to correct dimensions of forging dies [86]. However, high cutting force is caused to machine the hard surface of dies, which increases the machining error due to the deflection of cutting tool [8,9]. Therefore, material remove rate must be low with no regard to increase in the machining time and the costs [10] and the solution has been studied. For example, Qian et al. investigated the cutting forces in turning of hardened steels with HRC 44 to 58, and presented high machining forces required for the high hardness work materials [11]. De Lacalle et al. reported that deflection of tool increased the dimensional error in endmilling of hardened steels [12]. Biermann et al. proposed modification of NC-path as a common approach to minimize the cutting force and reduce the tool deflection [10]. From these researches, improvement of machinability in the nitrided layer is expected to contribute to decrease in machining error and reduction of the cost in reforming process of dies.

In order to decrease the hardness and improve the machinability in nitride layer, thermal processes are prospective methods. Laser has been used as a controllable heat source in different surface treatment of work materials [13,14] such as surface hardening [42,87], ablation [44,88] polishing [43] and cleaning [89,90]. On the other hand, the excessive heat could damage the work surface due to melting of the materials [91]. These melting and recasting process has the potentially expected to reduce amount of nitrogen and reduce the hardness of nitrided layer [92], which could improve the machinability in the reforming operation for forging dies.

Therefore, this paper aims to apply the laser surface treatment to reduce the hardness of nitride layer on the die steel. After the treatment process, simulating the die walls with a draft,

the inclined workpieces are machined with ball end-mills. The machinability of irradiated surface is investigated from the tool deflection, actual depth of cut, specific cutting force and uncut chip thickness, and those results are compared with ones for non-treated workpiece.

6.2 Experimental procedures

Two stages of testing were conducted in this study. For the first stage, the pulsed laser was irradiated on the high hardness layer of the nitrided die steel in order to evaluate the influence of pulsed laser conditions. In the second stage, the irradiated workpiece was machined to determine the improvement of machinability.

6.2.1 Experimental materials

The hot work die steel (Diado steel Co., Ltd., DH31S) with a substrate hardness of approximately 500 HV and the surface layer with ion nitride hardness of approximately 1100 HV was prepared as a workpiece. A 30W pulsed fiber laser (Sun Instruments Inc., YS-P30) was used to irradiate the surface of workpiece in order to improve the machinability of work materials. Then, the milling operation was performed by a 3-axis vertical milling machine (Shizuoka Machine Co., Ltd., CNC, ST-NR). Two flutes of ball end-mills with a diameter of 6 mm (Create tool Co., Ltd., CT2-R3-CSI) was used for inclined surface milling experiments. Two stages of testing were conducted in this study. For the first stage, the pulsed laser was irradiated on the high hardness layer of nitrided die steel in order to evaluate the influence of pulsed laser conditions. In the second stage, the irradiated workpiece was machined to determine the improvement of machinability.

6.2.2 Pulsed laser irradiated experiments

Figure 6.1 shows the illustration of pulsed laser irradiation on the surface of workpiece. The laser irradiated conditions are summarized in Table 6.1 These tests were conducted to investigate the influence of the pulse energy and energy density on the surface profile and hardness in the region with the laser irradiated. The energy of a single pulse laser e, and the irradiated energy density Q_s, in these experiments can be defined by following equations (6.1) and (6.2), respectively.

$$e = \frac{Q}{f_p} \tag{6.1}$$

where, e is pulse energy (mJ/pulse), Q is average laser power (W) and f_p is laser pulse frequency (kHz)

$$Q_S = \frac{10^3 Q}{S_p \, S_L \, f_p} \tag{6.2}$$

where, Q_S is energy density (J/mm^2), S_p is pulse spacing (μm) and S_L is scan line spacing (μm)

(a) Directions of laser scanning

(b) Details of pulsed laser
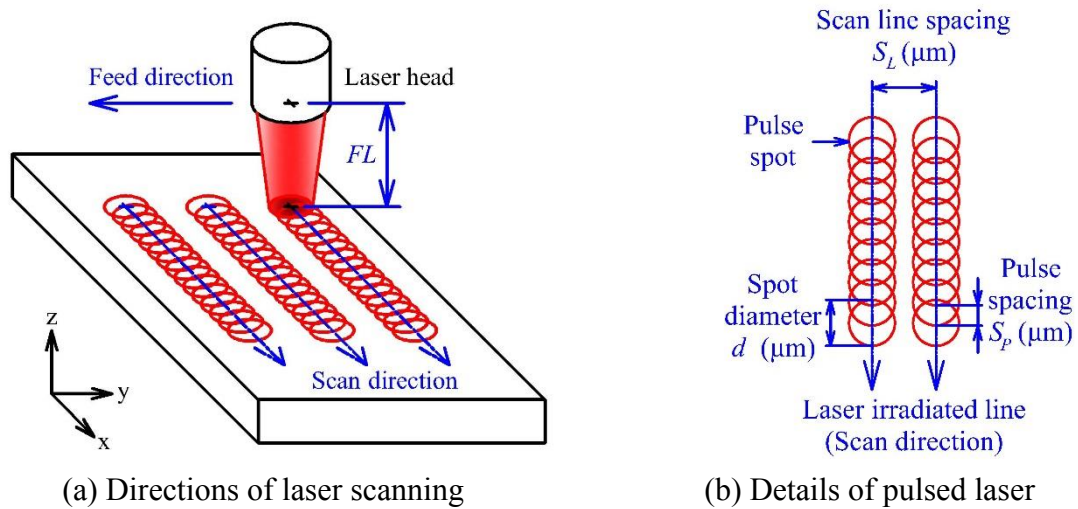
Fig. 6.1 Illustration of pulsed laser treatment on the surface of workpiece

Table 6.1 Laser irradiated conditions

Parameter, (unit)	Descriptions	
Wave length, (nm)	1064	
Focal length FL, (mm)	160	
Spot diameter D_s, (μm)	50	
Average laser power Q, (W)	5.1 – 26.9	
Scan feed rate V_S, (mm/s)	150	
Testing conditions	Test A	Test B
Laser pulse frequency f_p, (kHz)	30, 50, 100	50
Pulse spacing S_P, (μm)	5	3
Scan line spacing S_L, (μm)	100	10
Max. energy density Q_s, (J/mm^2)	1.8	17.9

Table 6.2 Machining conditions

Parameter, (unit)	Details	
Cutting conditions	Test A	Test B
Axial depth of cut Ad, (μm)	500	1800
Theoretical depth of cut Dc, (μm)	43.58	156.88
Feed per tooth f_z, (μm/tooth)	100	
Tool diameter Ø, (mm)	6	
Corner radius, (mm)	3	
Tool overhang S_T, (mm)	45	
Spindle speed S, (rpm)	125	
Inclined angle of workpiece ξ, (deg.)	85	
Cutting operation	Down cut milling	

The pulsed laser conditions in the experiment were designed for low energy density (refer Table 6.1, Test A, maximum Q_s is 1.8 J/mm^2) and high energy density (refer Table 6.1, Test B, maximum of Q_s is 17.9 J/mm^2). The surface roughness tester (Kosaka Laboratory Ltd.,

SE-30D), which was equipped with a diamond stylus with a tip radius of 2 μm was used to detect the profile of irradiated surface. The peak and valley of the surface profile were used to explain the effect of the pulsed laser conditions, while the micro-hardness testing was used to indicate the change in the mechanical property of the irradiated area.

6.2.3 Inclined surface milling experiments

Assuming the side wall of grooves on the die surface, ball end-milling tests were performed with plates inclined against the tool axis of 3-axis vertical milling machine as shown in Fig. 6.2. The irradiated workpiece was fixed on the angle plate at a setup angle of 85 degrees which was determined similarly to an actual forging die. The down cut milling was operated with feeding tool in the x-direction as shown in Fig. 6.2 (a) and is perpendicular to the laser scanning lines, which is shown in Fig. 6.1. The cutting conditions are summarized in Table 6.2.

(a) Illustration of experimental setup   (b) Detail of acting forces and tool deflection
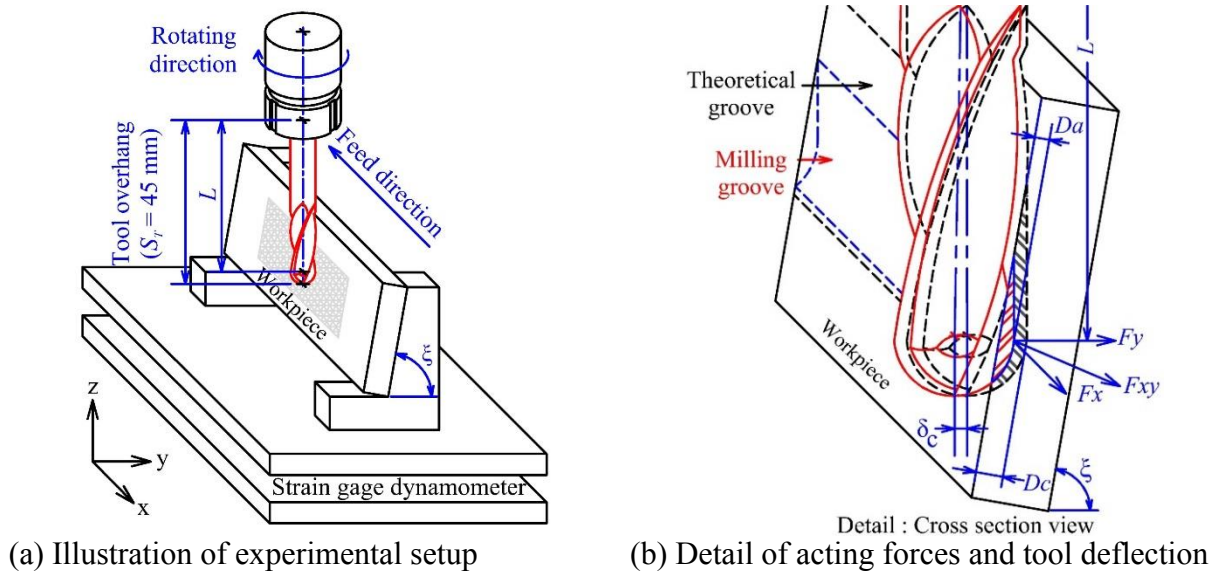
Fig. 6.2 Schematic diagram of inclined milling surface experiment

In this work, the component of cutting force was measured by a dynamometer. The cutting force F_y was used to estimate the tool deflection δ_c (refer Fig. 6.2 (b)), which can be obtained by following equations (6.3) and (6.4).

$$\delta_C = \frac{F_y L^3}{3EI} \tag{6.3}$$

$$I = \frac{\pi \varnothing^4}{64} \tag{6.4}$$

where, δ_c is tool deflection (μm), F_y is tangential force (N), L is the tool length contact (≈ 42 mm in this testing), E is the Young's modulus of cutting tool (520 GPa), I is the geometrical moment of inertia (mm^4), and $\varnothing$ is the tool diameter (mm).

In addition, the specific cutting force K_S was derived by resultant cutting force F_{xy} and cutting area A, as following equations (6.5) and (6.6).

$$K_S = \frac{F_{xy}}{A} \tag{6.5}$$

$$F_{xy} = \sqrt{F_x^2 + F_y^2} \tag{6.6}$$

where, K_S is specific cutting force (GPa), F_{xy} is resultant cutting force (N), A is the cross-sectional area (mm^2) to be cut which is related to the actual depth of cut, D_a as shown in Fig. 6.3 (a). This represents the area of geometrical interference between the cutting tool and the workpiece as shown in Fig. 6.3 (b), and can be derived by following equations (6.7) and (6.8).

(a) Geometrical interference of cutting and tool with work material

(b) Relationship between radius of tool (r) and actual depth of cut (D_a).
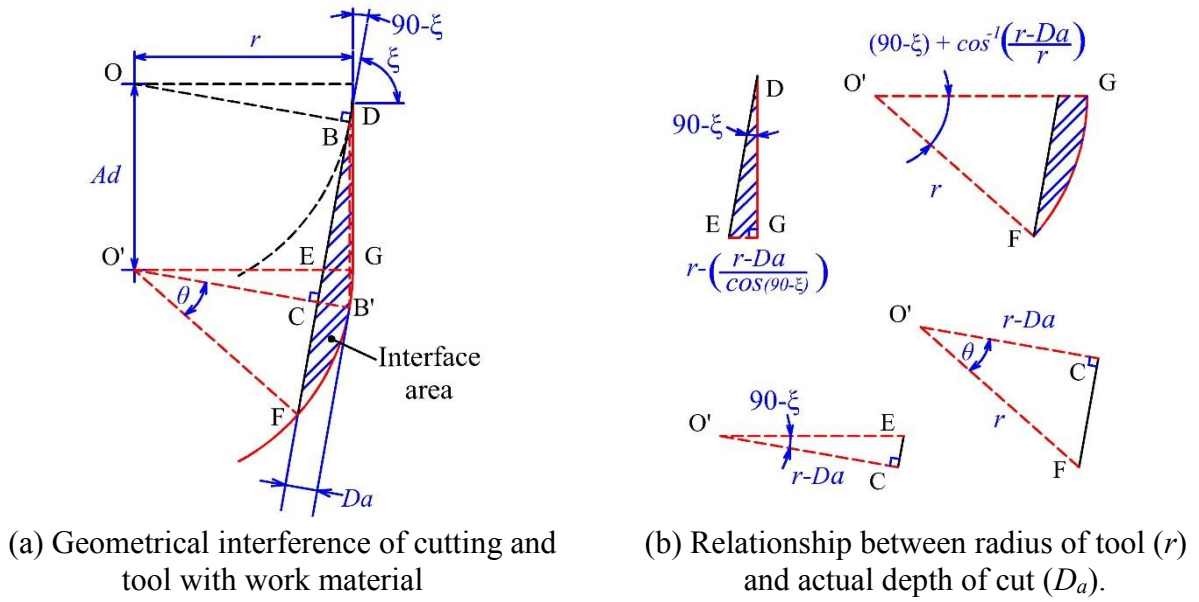
Fig. 6.3 Schematic diagram of cutting areas by ball end-mills

$$A = DEG + FO'G - CO'E - CO'F$$

$$= \frac{\tan \xi}{2}\left(r - \frac{r \cos \theta}{\sin \xi}\right)^2 + \frac{\pi r^2}{360}(90 - \xi + \theta) - \frac{(r \cos \theta)^2}{2} - \frac{r^2 \sin \theta \cos \theta}{2} \tag{6.7}$$

$$\cos \theta = (r - D_a)/r \tag{6.8}$$

where, ξ is inclined angle of workpiece (deg.), r is radius of ball endmills (mm) and θ is cos^{-1} $((r-Da)/r)$. It should be noted that the actual depth of cut D_a can be experimentally obtained from the profile of a machined surface using a surface roughness tester.

In addition, the maximum uncut chip thickness h_{max} is derived from the actual depth of cut Da and the feed per tooth f_z as following equation (6.9).

$$h_{max} = 2 f_z \sqrt{\frac{D_a}{\emptyset}\left(1 - \frac{D_a}{\emptyset}\right)} \tag{6.9}$$

where, h_{max} is maximum uncut chip thickness (µm), f_z is feed per tooth (100 µm/tooth) and $\emptyset$ is tool diameter (6 mm)

Furthermore, the theoretical depth of cut D_c in this work can be derived from the axial depth of cut A_d and the inclined angle of workpiece ξ as following equation (6.10).

$$D_C = A_d Sin\,(90 - \xi) \tag{6.10}$$

where, D_c theoretical depth of cut (µm) and A_d axial depth of cut (µm)

6.3 Results and discussion

6.3.1 Surface profiles of laser irradiated under several pulse frequencies

Figure 6.4 shows the surface profiles on the cross-sectional perpendicular to laser scanning lines (refer Fig. 6.1), which were obtained under relatively low energy density conditions (Test A).
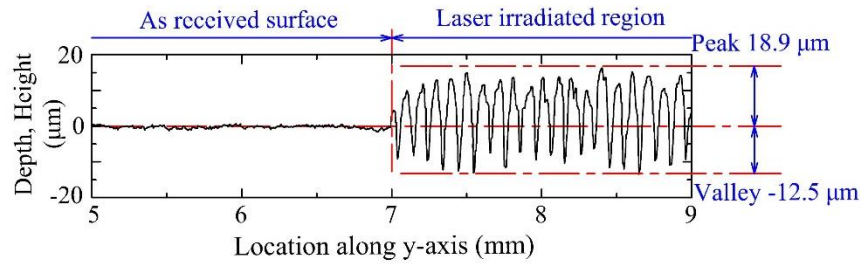
(a) Boundary between original and irradiated surface with f_p=100 kHz and Q_s=0.54 J/mm^2
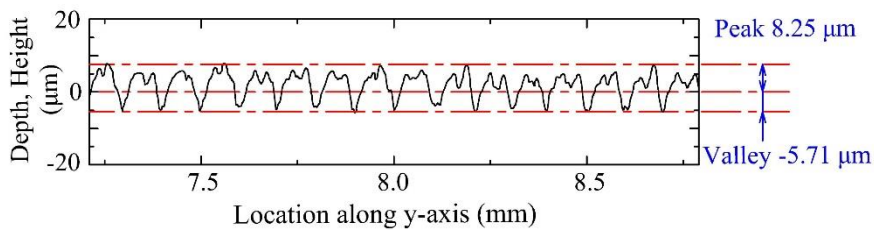
(b) Irradiated surface with f_p=50 kHz and Q_s=0.22 J/mm^2
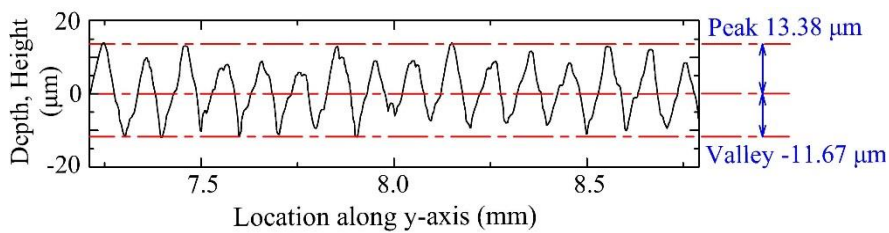
(c) Irradiated surface with f_p=50 kHz and Q_s=1.08 J/mm^2

Fig. 6.4 Surface profiles of work materials obtained by the laser irradiation
(Test A, low energy density)

It can be seen that valleys were engraved on the areas where the pulsed laser was irradiated, which are indicative of material removal due to the ablation [88] and liquid expulsion [44]. These profiles also contain peaks with even pitch corresponding to the scan line spacing, which were the recast layers formed due to the deposit of material erupted from the laser regions.

As can be seen in Fig. 6.4 (a), the height of the original surface is within the value of the peaks and valleys. This is because the ablation and liquid expulsion were efficiently formed at the area where energy was concentrated (center of pulsed spot along the direction of laser irradiated), and then the melting layer was combined with ablated particle to generate the recast layer beside the regions of laser irradiated. In Fig. 6.4, comparing of the 3 profiles under different conditions show that the energy density Q_s had a dominant effect on the maximum height of formed peak and valley pattern, while the laser pulse frequency f_p has a little effect on it.

The relationship between the energy of a single pulse laser e with the peak height and valley depth of profiles for different pulse frequencies f_p under Test A conditions is shown in Fig. 6.5. It can be seen that both the peak height and the valley depth increased with increasing pulse energy e, while the used pulse frequency f_p had a small effect. At the pulse energy of $e = 0.90$ mJ/pulse and the pulse frequency of $f_p = 30$ kHz, the height of recast layer reached approximately 35 μm while the depth of valley reached approximately -15.5 μm. Based on these results, the undulation of irradiated surface seems to increase with the pulse energy e.
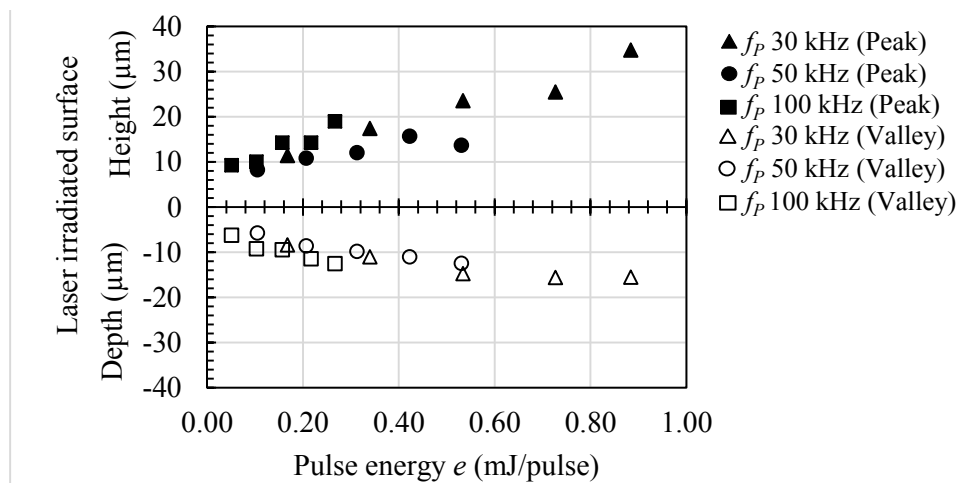
Fig. 6.5 Relationship between pulse energy (e) with peak and valley of laser irradiated region (Test A, low energy density)

6.3.2 Surface structure formed by high energy density of laser

In the next series of tests, the high energy density condition was employed to the work surface (Test B) with decreasing the scan line spacing S_L and the pulse spacing S_P. Figure 6.6 shows the surface profiles obtained by laser irradiation. As can be seen in Fig. 6.6 (a), the height level of the laser irradiated region was lower than that the height of original surface of

the workpiece when the energy density was Q_s = 3.6 J/mm^2. This suggests that the energy density of 3.6 J/mm^2 was sufficient to remove material though the evaporation and melt expulsion [16].

(a) *Qs* is 3.6 J/mm^2

(b) *Qs* is 10.8 J/mm^2

(c) *Qs* is 17.9 J/mm^2
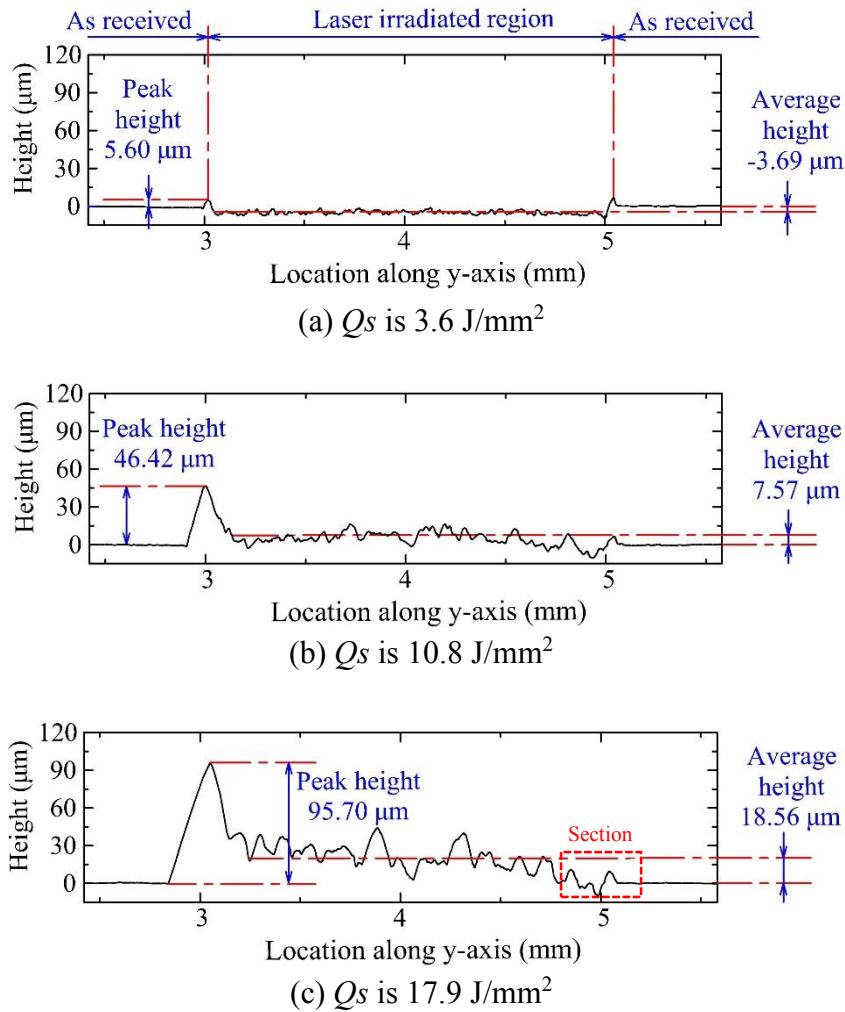
Fig. 6.6 Surface profile of work materials at laser irradiated region
(Test B, high energy density)

Besides, the higher energy density elevated the profile in the laser irradiated region as shown in Fig. 6.6 (b) and 6.6 (c). This is believed that the excessive energy melts the work material in a large area, and then the particle from removal materials could be combined in recast layer. In addition, the released nitrogen gas generated pores [92], and thereby decreased density and swelled the surface over the irradiated region.

It also can be seen that the formed profiles were slanted and had the high deposits piled up at the edge of starting scan of irradiated region. According to the irradiating conditions shown in Table 6.1, the scanning line spacing S_L was smaller than the spot diameter D_s (the overlapping ratio was up to 80% = 100(D_s - S_L) / D_s). This means that under Test B conditions, the surface of workpiece was irradiated repeatedly, which very much different from the conditions in Test A. This could mean that the higher swelled surface was due to the lower

overlap of scanning lines and the slant surface was due to the accumulative thermal effect. In the other words, the low swelled surface was formed because overlapping laser spots reproduce a melting process in the prior recast layer leading to a decreased height of irradiated surface as represented in average height.

Figure 6.7 shows the relationship between the energy density Q_s and the height of the irradiated surface. It can be seen that the peak height strongly increased and the average height slightly increased as a function of the energy density. This suggests that the depth of recast layer is also increased with the energy density of irradiation.
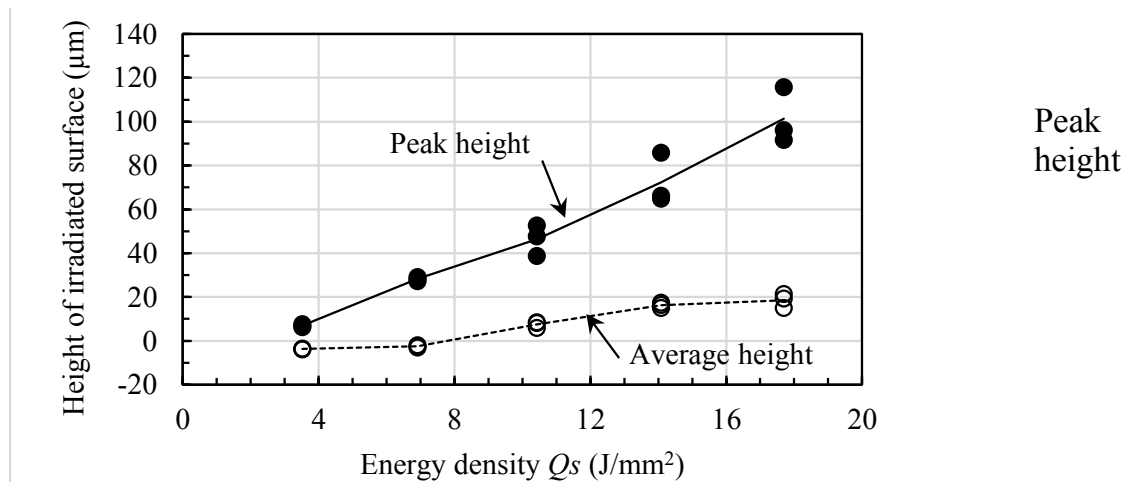

Fig. 6.7 Peak height and average peak of laser irradiated region
(Test B, high energy density)
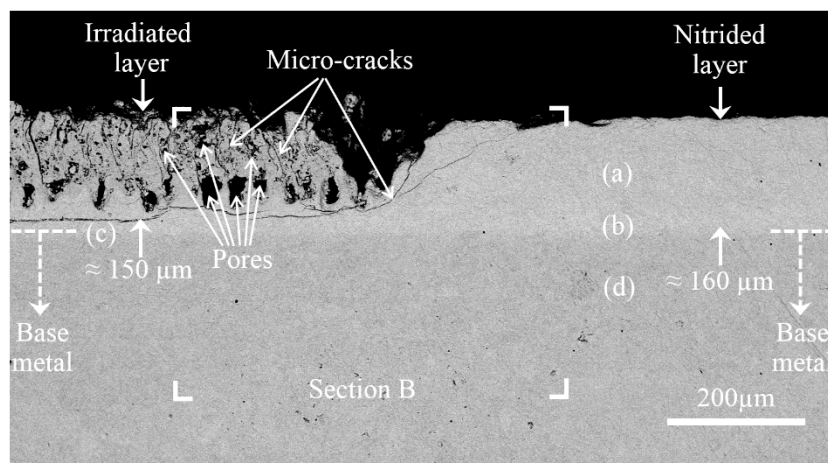

Fig. 6.8 Section views of laser irradiated area in depth of workpiece
(Test B, Q_s 17.9 J/mm^2)

Figure 6.8 shows microscopic photograph for the cross section of work material irradiated with a high energy density of Q_s =17.9 J/mm^2. The observed area corresponds to the

section A shown in Fig. 6.6 (c), which includes both irradiated region and non-irradiated region. From the figure, it can be seen that the thickness of nitrided layer was approximately 160 μm. Many pores and cracks were also observed in the irradiated region, and size of these pores became large near the bottom of recast zone, whose depth reached approximately 150 μm. In the non-irradiated region, the boundary is observed between the nitrided layer and the base metal, which is approximately 160 μm below the surface. Fang et al. [93] explained that the micro-crack originates from the residual stresses which are inducted by the thermal expansion and contraction. Tan et al. [94] reported that the porosity can be generated due to the reduction of material density as the result of high laser energy and chemical interactions, too. The observed pores contribute to reduce the material strength and to improve machinability, while damages were not observed in base metal from the figure.
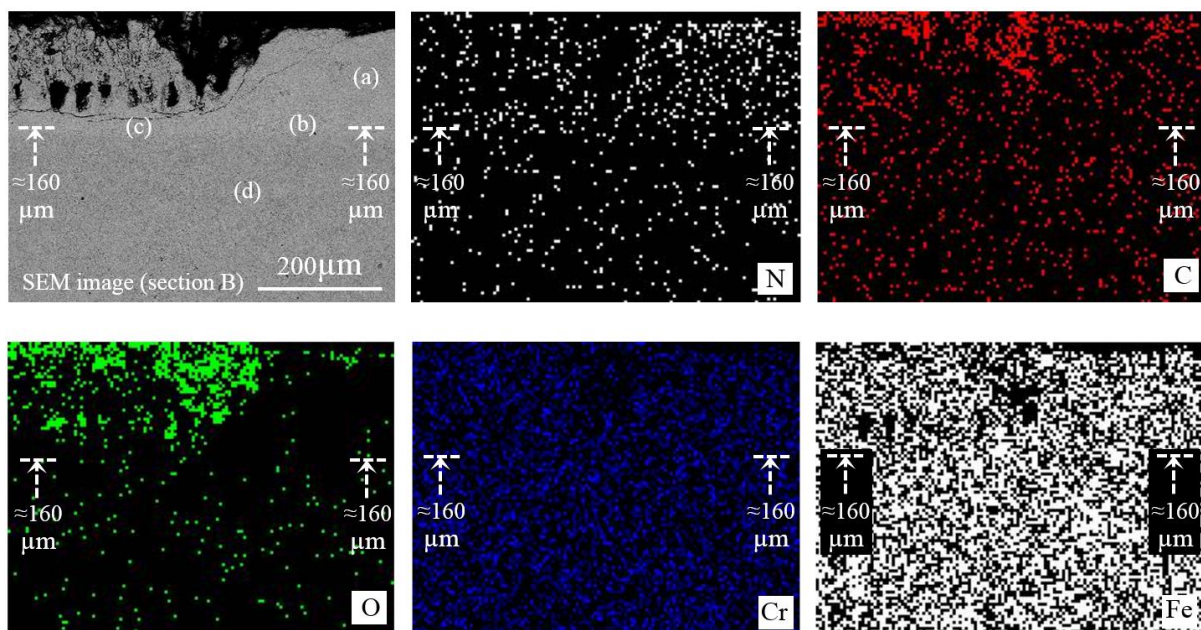
Fig. 6.9 SEM images and elemental mapping by EPMA in the laser irradiated region and nitrided layer

Figure 6.9 is an element mapping on the cross section of the work material to examine the thermal effects by laser irradiation. The distribution of ferrous (Fe) and chromium (Cr) in any area was insignificantly changed, but the intensity of nitrogen (N) was slightly high in the nitrided layer. In addition, influence of oxidation can be found in the laser irradiated region as high intensity of oxygen (O), but the influence is not found in the base metal. Therefore, it could be confirmed that the element of base metal under the laser irradiated with a high energy density of Qs =17.9 J/mm^2 was insignificantly changed.

6.3.3 Hardness in the region of laser irradiated

The hardness test was also carried out on the cross-section of the irradiated work material shown in Fig. 6.8. Figure 6.10 shows the measured hardness as a function of depth from the irradiated surface of work materials. In this figure, it should be noted that negative values of depth represent positions within the recast layer swelled higher than the original

surface of material and that the hardness of nitrided layer is indicated with a black dashed line. It can be seen that the hardness of varied in the range of 200 to 600HV0.05 for the depth of -25 to 125 μm under the irradiated surface, but it was clearly lower than the original nitrided layer. This is believed to be caused by the release of nitrogen to the recast layer and heat affected zone resulting in a reduced density and mechanical properties of nitrided layer. However, at a depth of more than 160 μm, the difference of hardness was negligible for the irradiated layer and the nitrided layer.
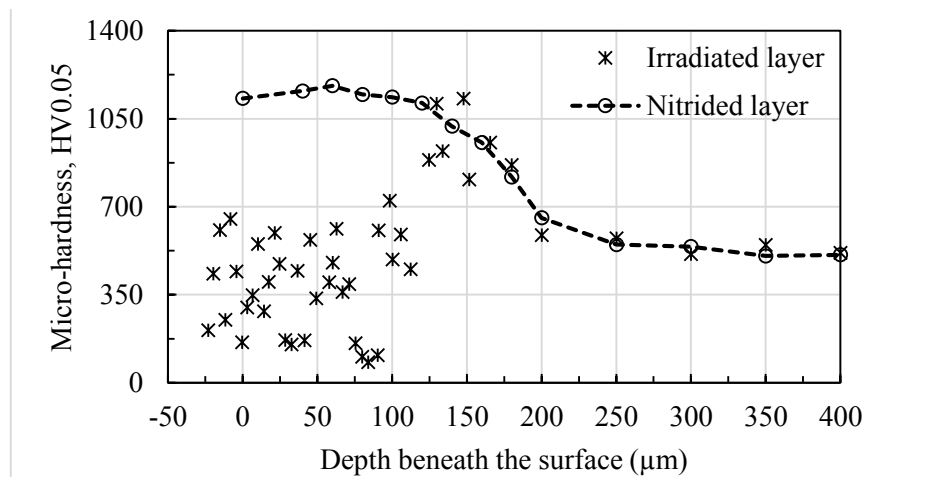
Fig. 6.10 Micro hardness as a function of depth from surface of laser irradiated
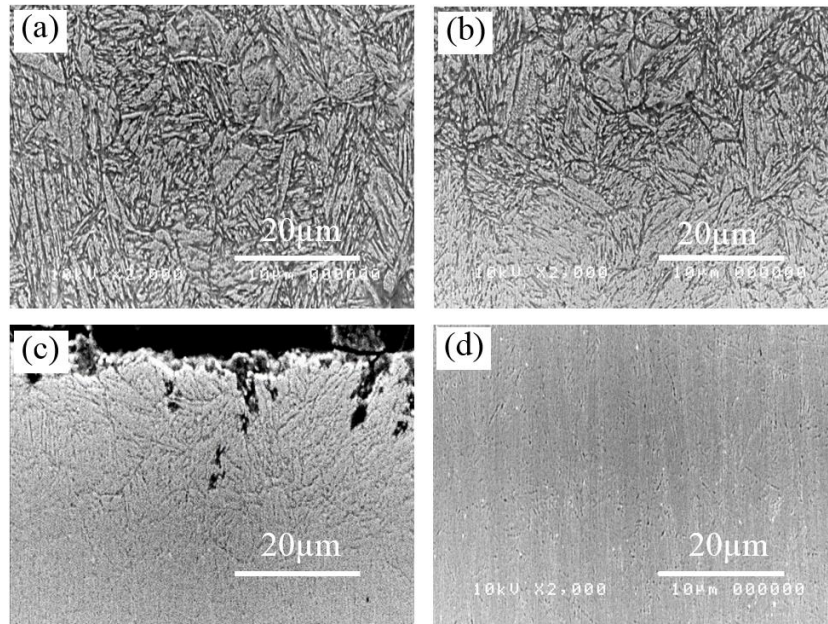

Fig. 6.11 SEM, microstructure of work materials, (a) nitride layer, (b) interface zone of nitride layer and base metal, (c) interface zone of irradiated layer and base metal, and (d) base metal

The hardness of nitrided layer is due to that dislocation motion is impeded by the interstitial solid solution and the nitride precipitates dispersed. Lee et al. reported that the main

nitride precipitates in the diffusion zone were identified to be ε-$Fe_{2-3}N$ and γ'-$Fe4N_2$. Figure 6.11 gives SEM images for the section of work material before and after the laser irradiation. Figure 6.11 (a) and (b) show microstructure within the nitrided layer and one at boundary of the nitrided layer, respectively. As can be seen, nitride precipitates are distributed in nitrided layer, while the base metal did not include the precipitates as shown in Fig. 6.11 (d). This difference in the distribution of diffused nitrogen caused hardness distribution shown in Fig. 10. On the other hand, Figure 6.11 (c) indicates that the precipitates decreased after the laser irradiation. This effect and the damages (pores and cracks) would lead to the decrease in hardness within the irradiated region shown in Fig. 6.10.

6.3.4 Tool deflection and actual depth of cut

In machining of high strength materials, high cutting force is needed to shear the work materials and generate the chips in the vicinity of the cutting edges. Because of the linearity of the elastic deformation of cutting tool δ_c with respect to the cutting force, the machinability of material can be directly estimated.

Figure 6.12 shows the tool deflection calculated from the cutting force F_y and the actual depth of cut D_a measured from the depth of the groove on the machined surface under Test A conditions. Represented as filled symbols in Fig. 6.12, the tool deflection δ_c decreased when the pulse energy of laser e became high. This behavior can be recognized as improved machinability of the nitrided steel due to modification using the laser, even when the irradiation with low energy density formed a small recast layer. In contrast, the actual depth of cut D_a (no fill symbols in Fig. 6.12) increased as a function of pulse energy e. These results suggest that the cutting edges of the tool penetrated the nitrided steels shallowly, but it became better with laser irradiation.
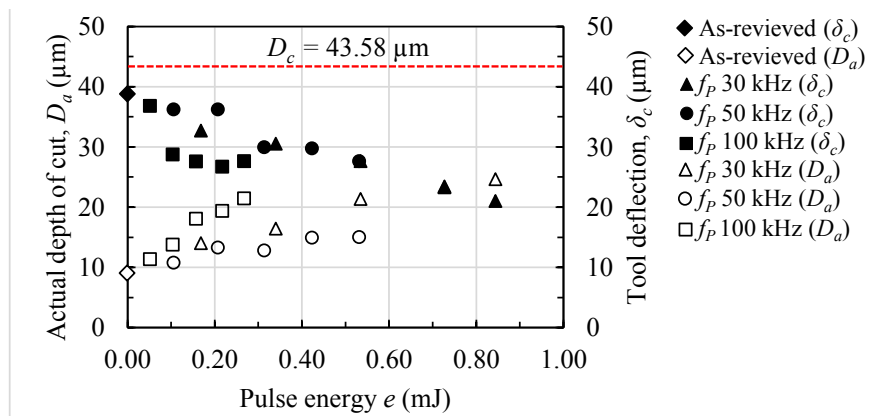
Fig. 6.12 Relationship between pulse energy (e) with actual depth of cut (D_a) and tool deflection (δ_c)

As the pulse energy increased (refer Fig. 6.12), the tool deflection reduced, but the actual depth of cut increased, the total of them was almost constant and close to the value of theoretical depth of cut. This mean that the amount of machining error considered from the profile of machined surface is equal to the amount of tool deflection. Although the laser surface

modification improves the machinability of the materials, the actual depth of cut D_a still does not reach the theoretical depth of cut D_c indicated with a broken line in Fig. 6.12. This can be construed that a certain tool deflection is caused by the cutting force used to machine materials.
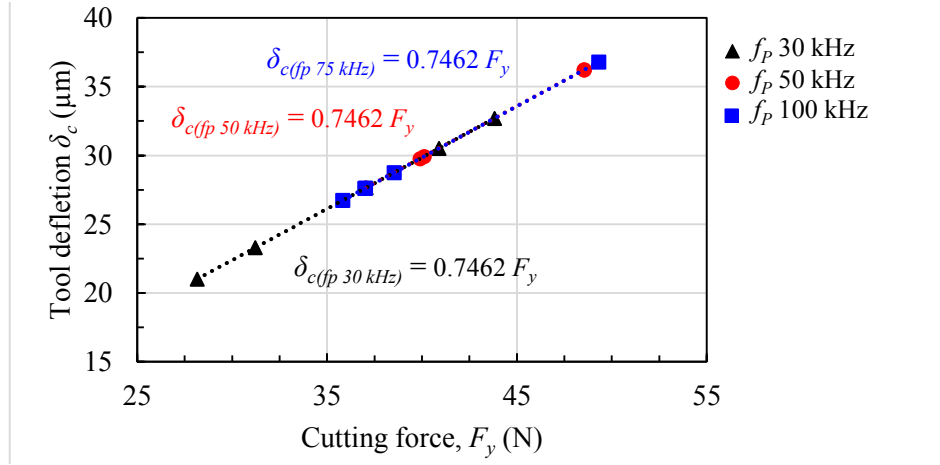
Fig. 6.13 Relationship between cutting force (F_y) and tool deflection (δ_c)

Figure 6.13 indicates the relationship of cutting force F_y and tool deflection δ_c at various pulse frequencies f_p with the regression line obtained for data as equation (6.11). As can be seen, the tool deflection increases with the cutting force in regardless of the pulse frequency.

$$\delta_c = 0.7462\ F_y \tag{6.11}$$

where, δ_c is tool deflection (µm) and F_y is tangential force (N)
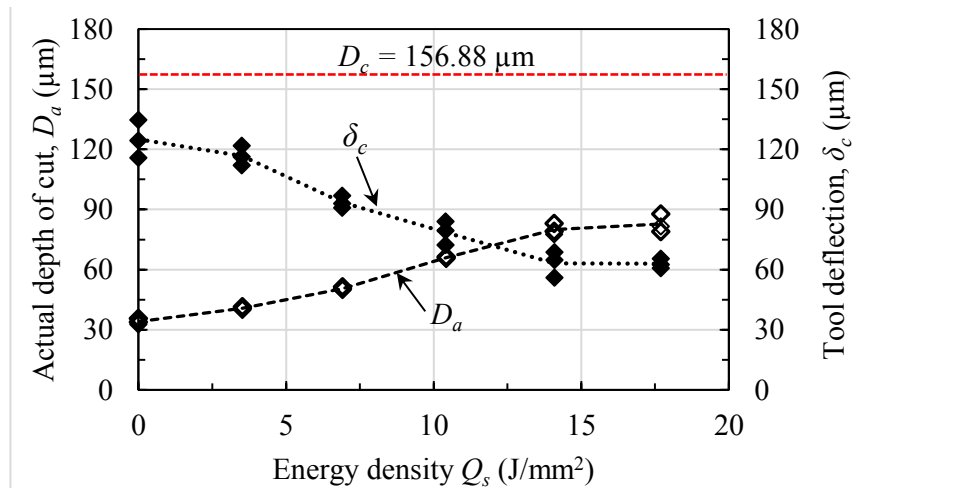
Fig. 6.14 Relationship between energy density (Q_s) with actual depth of cut (Da) and tool deflection (δ_c)

Figure 6.14 shows the influence of relative high energy density (Test B) on the tool deflection δc and actual depth of cut Da. It can be seen that the tool deflection decreased as the

energy density increased, while the actual depth of cut increased. With the energy density of 17.9 J/mm^2, the highest improved actual depth of cut reached 84 μm and the lowest tool deflection was reduced to 64 μm. Therefore, in the next series of test, the irradiated workpiece with the energy density of 17.9 J/mm^2 was used for inclined milling in order to investigate the influence of theoretical depth of cut on the machinability.
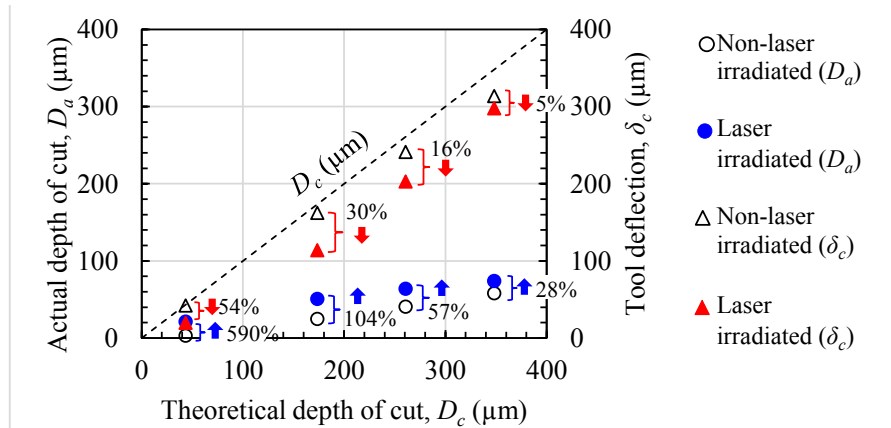
Fig. 6.15 Relationship between theoretical depth of cut (D_c) with actual depth of cut and tool deflection (δ_c)

Figure 6.15 shows the tool deflection and actual depth of cut for several theoretical depth of cut (D_c = 44, 174, 261 and 350 μm), and the effect of the laser irradiation. It can be seen that the tool deflection and actual depth of cut both increased as a function of the theoretical depth of cut. However, the clearly improved tool deflection and actual depth of cut were obtained with the lowest theoretical depth of cut. This finding could be explained by the low mechanical properties of irradiated workpiece leading to a reduced requirement of cutting force. When the theoretical depth of cut is increased, the mechanical properties of the irradiated workpiece become close to the non-irradiated workpiece leading to a diminished benefit of pulsed laser surface treatment.

6.3.5 Specific cutting force and uncut chip thickness

Figure 6.16 shows the results of specific cutting force K_s with uncut chip thickness h_{max}, which was calculated from the actual depth of cut D_a in the inclined milling for the different surfaces of die steel (non-nitride, nitrided, and pulsed laser irradiated on the nitrided surface). The specific cutting force generally decreases as the uncut chip thickness increased or mechanical properties of material decreased. Comparing the results for non-nitride and nitrided workpiece presented by two interpolating lines, the specific cutting force clearly reduced with the decrease in hardness of workpiece.

In the milling for workpieces with different irradiating conditions (f_p = 30, 50, 100 kHz, Q = 5.1 – 26.9 W), the tool deflection varied as shown in Fig. 6.13, so that the specific cutting force also varied as a function of the uncut chip thickness as shown in Fig. 16. In the series test with varied theoretical depth of cut (D_c = 44, 174, 261 and 350 μm) for the workpiece

irradiated with a high energy density of 17.9 J/mm^2, the specific cutting force decreased as the uncut chip thickness increased.
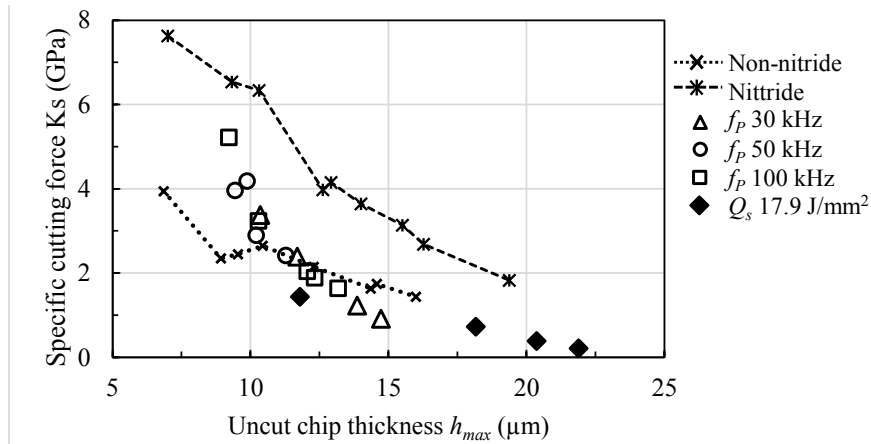
Fig. 6.16 Relationship between uncut chip thickness (h_{max}) and specific cutting force (K_s) when the conditions of surface workpiece were varied

Consequently, data of specific cutting force are aligned on a same curve as shown in Fig. 6.16, instead of the variations of irradiating and cutting conditions. Results have shown that the mechanical properties of irradiated surface decreased with high pulse energy and energy density. This, in turn, reduced the cutting force and tool deflection in machining process, thereby increasing the depth of milling groove and the uncut chip thickness. These results prove that the pulsed laser treatment on the high hardness layer can reduce mechanical properties of materials resulting in an improved machinability of high hardness layer such as nitrided die steel.

6.4 Conclusions

In this study, the pulsed laser surface treatment was carried out on the high hardness of nitrided die steels in order to investigate the effects on the irradiated surface and improvement of machinability. The obtained results are summarized as follows.

1. Destroying the high hardness of nitride layer is a key to the improvement of machinability. The measurement of hardness showed that the nitride layer can be efficiently reduced by pulsed laser surface treatment. In addition, the profile irradiated surface becomes remarkable as pulsed energy and energy density increase.

2. The high pulse energy and energy density increased the actual depth of cut and uncut chip thickness but decreased the tool deflection and specific cutting force. These results indicate that the pulsed laser surface treatment can improve machining accuracy and material removal rate compared to non-treated surface.

Chapter 7

General Conclusions

In this dissertation, experimental results on the effect of laser assisting for milling difficult-to-cut materials were presented. The conclusions are summarized as follows;

1. Carbon brush can be used to connect signal of electromotive force (EMF) in the milling test from rotating part (end-mill) to the date acquisition (oscilloscope). However, the EMF generated in the measuring circuit must be investigated because the heat was generated at the contact area of rotating part and the measuring circuit cannot be perfectly insulated from the structure of machine. The EMF in the measuring circuit increased approximately 0.14, 0.30, 0.52 and 0.57 mV for the spindle speed of 600, 1000, 1500 and 2000 rpm, respectively. This value used to compensate EFM in the cutting test before convert to the cutting temperature. For the conventional machining, the cutting temperature increased with the cutting speed due to more heat generated at the high cutting velocity.

2. Calibrating laser power to heating temperature by embedded K-type thermocouple into the Inconel 718 at the same depth of cut in the cutting test was founded that the heating temperature proportionally increased with the laser power. However, the peak heating temperature was far from the primary shear zone to avoid influence of laser irradiated on the cutting tool. Therefore, the preheating temperature in the primary zone must be estimated with included cooling time. The cooling time decreased with the increased table speed, but the requirement of laser power increased to retain the particular preheating temperature.

3. In cutting tests for end-milling Inconel 718, the natural frequency of strain gauge dynamometer included in the signal of cutting force. Therefore, the component of cutting force in cutting test represented by averaged force from the peak and valley of signal. The cutting results founded that the highest force occurred in the direction of cutting velocity (Fy; tangential force) and force in the direction of tool feeding (Fx; thrust force) was slightly lower than tangential force. Both tangential and thrust force decreased when the cutting speed and preheating temperature increased. Whereas, the measured cutting temperature proportionally increased with cutting speed due to more heat generated at high cutting velocity and slightly increased with the preheating temperature due to high temperature of workpiece. Although, the temperature rise in the primary shear zone was increased with the cutting speed, it was decreased when the initial temperature of workpiece increased due to lower requirement of energy for shearing softened material.

4. The conventional end-milling of Inconel 718 was found that the thickness of chip decreased when cutting speed increased. This can be explained by the increased cutting speed leaded to increase shear angle resulted to low friction coefficient. However, in the laser assisted

milling, the highest chip thickness at low cutting speed of 30 and 50 m/min was occurred when the preheating temperature of 300ºC was employed, for further increase in preheating temperature leaded to decreased chip thickness due to more work material adhered on the tool. This was leading to changed geometry of tool shape and accelerated adhesion wear. The increase in preheating temperature at the high cutting speed of 75 and 100 m/min resulted in an increased chip thickness. Although, the tool wear in laser assisted machining was higher than conventional machining, the wear could be improved at relatively high cutting speed of 75 and 100 m/min.

5. The influence of atmosphere on the performance of laser assisted milling for Inconel 718 was found that the requirement of laser power to retain the particular heating temperature was highest under the atmosphere of argon gas to compare with dry and compressed air blow. This is because the oxygen in the air have benefit to accelerate the oxidation on the irradiated surface which increased the optical absorptivity. The less oxidation in cutting test for argon atmosphere leaded to high friction coefficient resulted in high cutting temperature to compare with other atmosphere. This is leading to the highest decrease specific cutting force and tool wear decreased when the preheating temperature increased to compare with dry and compressed air. However, the surface roughness of machined surface under the atmosphere of dry and compressed air are slightly lower than argon gas. The influence of atmosphere on the hardness of machined surface can be neglected.

6. The experimental results of pulsed laser surface treatment for improved machinability of high hardened die steel was found that the hardness of nitride layer can be destroyed by using pulsed laser surface treatment without damage in the based metal. The high pulse energy and energy density increased the damage of irradiated area which leading to increased actual depth of cut and uncut chip thickness but decreased tool deflection and specific cutting force. This experimental results indicate that the pulsed laser surface treatment can improve machining accuracy and material removal rate compared to non-treated surface.

Acknowledgements

I would like to express my sincere gratitude to Professor YAMADA Keiji for his kindness and guidance throughout this study. He give me full support not only with my research, but also with my life and career, and has played an important role in both my academic and personal development. I appreciate all the time that Professor SUGATA Atsushi and Professor SASAKI Gen dedicated in reviewing this dissertation.

I would like to express my heartfelt thanks to Associate Professor TANAKA Ryotaro and Assistant Professor SEKIYA Katsuhiko for helping my study. I would like to thank the past and present members of the Machining and Machining Systems Laboratory, in the Department of Mechanical Systems Engineering, Hiroshima University, for their enthusiastic help to both my life and study.

I would like to thank to the staff of international student support and engineering student support office for their kindness and support since I arrive to Hiroshima University until the last period of my stay in Hiroshima.

I would like to thank my parents for their support and encouragement from my youth to my time as a doctoral student. Their teaching is gratefully appreciated and has been invaluable in my life. Thanks to my family, all my friends and all my colleagues.

Reference

[1] W.-S. Woo and C.-M. Lee, "A study of the machining characteristics of AISI 1045 steel and Inconel 718 with a cylindrical shape in laser-assisted milling," *Applied Thermal Engineering,* vol. 91, pp. 33-42, 2015.

[2] R. Erween, W. Norazlan, and M. Zazuli, "Thermal-Assisted Machining of Nickel-based Alloy," *In Superalloys. IntechOpen,* pp. 1-29, 2015.

[3] C.-M. Lee, D.-H. Kim, J.-T. Baek, and E.-J. Kim, "Laser assisted milling device: A review," *International Journal of Precision Engineering and Manufacturing-Green Technology,* vol. 3, pp. 199-208, 2016.

[4] F. F. Lima, W. F. Sales, E. S. Costa, F. J. da Silva, and Á. R. Machado, "Wear of ceramic tools when machining Inconel 751 using argon and oxygen as lubri-cooling atmospheres," *Ceramics International,* vol. 43, pp. 677-685, 2017.

[5] H. Ding, N. Shen, and Y. C. Shin, "Thermal and mechanical modeling analysis of laser-assisted micro-milling of difficult-to-machine alloys," *Journal of Materials Processing Technology,* vol. 212, pp. 601-613, 2012.

[6] E. O. Ezugwu, R. B. Da Silva, J. Bonney, and Machado A. R., "The effect of argon-enriched environment in high-speed machining of titanium alloy," *Tribology Transactions*, vol. 48, pp. 18-23. 2005.

[7] Y. Fan, Z. Hao, J. Lin, and Z. Yu, "New observations on tool wear mechanism in machining Inconel 718 under water vapor+ air cooling lubrication cutting conditions," *Journal of Cleaner Production*, vol. *90*, pp. 381-387, 2015.

[8] B. Denkena, D. Dahlmann, and H. Boujnah, "Tool Deflection Control by a Sensory Spindle Slide for Milling Machine Tools," *Procedia CIRP,* vol. 62, pp. 329-334, 2017.

[9] S. Heo, M. Lee, S. H. Kim, W. Lee, and B.-K. Min, "Compensation of tool deflection in micromilling using workpiece holder control device," *International Journal of Precision Engineering and Manufacturing,* vol. 16, pp. 1205-1208, 2015.

[10] D. Biermann, E. Krebs, A. Sacharow, and P. Kersting, "Using NC-path Deformation for Compensating Tool Deflections in Micromilling of Hardened Steel," *Procedia CIRP,* vol. 1, pp. 132-137, 2012.

[11] L. Qian and M. R. Hossan, "Effect on cutting force in turning hardened tool steels with cubic boron nitride inserts," *Journal of Materials Processing Technology,* vol. 191, pp. 274-278, 2007.

[12] L. N. López de Lacalle, A. Lamikiz, J. A. Sánchez, and M. A. Salgado, "Effects of tool deflection in the high-speed milling of inclined surfaces," *The International Journal of Advanced Manufacturing Technology,* vol. 24, pp. 621-631, 2004.

[13] Y. Jeon, H. W. Park, and C. M. Lee, "Current research trends in external energy assisted machining," *International Journal of Precision Engineering and Manufacturing*, vol. 14, pp. 337-342, 2013.

[14] C.-M. Lee, W.-S. Woo, D.-H. Kim, W.-J. Oh, and N.-S. Oh, "Laser-assisted hybrid processes: A review," *International Journal of Precision Engineering and Manufacturing*, vol. 17, pp. 257-267.

[15] Serope Kalpakjian and Steven R. Schmid, "Manufacturing Engineering and Technology," 4th Ed., Prentice-Hall, Inc., Upper Saddle New Jersey, 2001, pp. 530-568.

[16] M. C. Shaw: "Metal Cutting Principles -2nd ed." (Oxford University Press, New York, 2005), pp. 15-38.

[17] E. O. Ezugwu, J. Bonney, and Y. Yamane, "An overview of the machinability of aeroengine alloys," *Journal of Materials Processing Technology*, vol. 134, pp. 233-253, 2003.

[18] I. Martinez, R. Tanaka, Y. Yamane, K. Sekiya, K. Yamada, T. Ishihara, et al., "Wear mechanism of coated tools in the turning of ductile cast iron having wide range of tensile strength," *Precision Engineering*, vol. 47, pp. 46-53, 2017.

[19] A. Shokrani, V. Dhokia, and S. T. Newman, "Environmentally conscious machining of difficult-to-machine materials with regard to cutting fluids," *International Journal of Machine Tools and Manufacture*, vol. 57, pp. 83-101, 2012.

[20] M. Anderson, R. Patwa, and Y. C. Shin, "Laser-assisted machining of Inconel 718 with an economic analysis," *International Journal of Machine Tools and Manufacture*, vol. 46, pp. 1879-1891, 2006.

[21] G. Le Coz and D. Dudzinski, "Temperature variation in the workpiece and in the cutting tool when dry milling Inconel 718," *The International Journal of Advanced Manufacturing Technology*, vol. 74, pp. 1133-1139, 2014.

[22] A. Sharman, R. C. Dewes, and D. K. Aspinwall, "Tool life when high speed ball nose end milling Inconel 718™," *Journal of Materials Processing Technology*, vol. 118, pp. 29-35, 2001.

[23] M. Alauddin, M. A. Mazid, M. A. El Baradi, and M. S. J. Hashmi, "Cutting forces in the end milling of Inconel 718," *Journal of Materials Processing Technology*, vol. 77, pp. 153-159, 1998.

[24] N. H. Razak, Z. W. Chen, and T. Pasang, "Modes of tool deterioration during milling of 718Plus superalloy using cemented tungsten carbide tools," *Wear*, vol. 316, pp. 92-100, 2014.

[25] K. Venkatesan, R. Ramanujam, and P. Kuppan, "Analysis of Cutting Forces and Temperature in Laser Assisted Machining of Inconel 718 Using Taguchi Method," *Procedia Engineering*, vol. 97, pp. 1637-1646, 2014.

[26] K. Yamamoto, M. Kuroda, H. Omokawa, and K. Itakura, "High-Efficiency Cutting of Super-Heat-Resistant Alloy". *Mitsubishi Heavy Industries Technical Review*, Vol *38* (1), (2001).

[27] C. Brecher, C. J. Rosen, and M. Emonts, "Laser-assisted milling of advanced materials, " *Physics Procedia*, vol. *5*, pp. 259-272, 2010.

[28] K. Venkatesan, R. Ramanujam and P. Kuppan, "Laser assisted machining of difficult to cut materials: research opportunities and future directions - A comprehensive review, " *Procedia Engineering*, vol. 97, pp. 1626-1636, 2014.

[29] M. J. Bermingham, P. Schaffarzyk, S. Palanisamy and M. S. Dargusch, "Laser-assisted milling strategies with different cutting tool paths, " *Int J Adv Manuf Technol*, vol. 74, pp. 1487-1494, 2014.

[30] M. J. Bermingham, W. M. Sim, D. Kent, S. Gardiner, and M. S. Dargusch, "Tool life and wear mechanisms in laser assisted milling Ti–6Al–4V," *Wear*, vol. 322-323, pp. 151-163, 2015.

[31] M. Kumar, S. N. Melkote, and R. M'Saoubi, "Wear behavior of coated tools in laser assisted micro-milling of hardened steel, " *Wear*, vol. 296, pp. 510–518, 2012.

[32] Y.Yamane, N. Narutaki, and K. Hayashi, "Suppression of tool wear by using an inert gas in face milling, " *Journal of materials processing technology*, vol. *62*(4), pp. 380-383, 1996.

[33] S, Xavierarockiaraj. and P. Kuppan, "Investigation of cutting forces, surface roughness and tool wear during Laser assisted machining of SKD11Tool steel," *Procedia Engineering*, vol. 97, pp. 1657-1666, 2014.

[34] S. Debnath, M. M. Reddy, and Q. S. Yi, "Environmental friendly cutting fluids and cooling techniques in machining: a review, " *Journal of cleaner production*, *83*, 33-47, 2014.

[35] E. O. Ezugwu, "Key improvements in the machining of difficult-to-cut aerospace superalloys," *International Journal of Machine Tools and Manufacture*, vol. *45*(12-13), pp. 1353-1367, 2005.

[36] M.J. Bermingham, D. Kent and M.S. Dargusch, "A new understanding of the wear processes during laser assisted milling 17-4 precipitation hardened stainless steel," *Wear* vol. 328, pp. 518–530, 2015.

[37] Y. Kamata and T. Obikawa, "High speed MQL finish-turning of Inconel 718 with different coated tools," *Journal of Materials Processing Technology*, vol. 192-193, pp. 281-286, 2007.

[38] I. Lee, and I. Park, "Microstructures and mechanical properties of surface-hardened layer produced on SKD 61 steel by plasma radical nitriding," *Materials Science and Engineering: A*, vol. *449*, pp. 890-893, 2007.

[39] M.Vedani, B. Previtali, G. M. Vimercati, A. Sanvito, and G. Somaschini, "Problems in laser repair-welding a surface-treated tool steel," *Surface and Coatings Technology*, vol. *201*(8), pp. 4518-4525, 2007.

[40] M. Hawryluk, "Review of selected methods of increasing the life of forging tools in hot die forging processes," *Archives of civil and mechanical engineering*, vol. *16*(4), pp. 845-866, 2016.

[41] B. Buchmayr, "Damage, lifetime, and repair of forging dies," *BHM Berg-und Hüttenmännische Monatshefte*, vol *162*(3), pp. 88-93, 2017.

[42] K.-A. Chiang and Y.-C. Chen, "Laser surface hardening of H13 steel in the melt case," *Materials Letters*, vol. 59, pp. 1919-1923, 2005.

[43] A. M. K. Hafiz, E. V. Bordatchev, and R. O. Tutunea-Fatan, "Influence of overlap between the laser beam tracks on surface quality in laser polishing of AISI H13 tool steel," *Journal of Manufacturing Processes*, vol. 14, pp. 425-434, 2012.

[44] B. Jaeggi, B. Neuenschwander, M. Schmid, M. Muralt, J. Zuercher, and U. Hunziker, "Influence of the Pulse Duration in the ps-Regime on the Ablation Efficiency of Metals," *Physics Procedia*, vol. 12, pp. 164-171, 2011.

[45] N. A. Abukhshim, P. T. Mativenga, and M. A. Sheikh, "Heat generation and temperature prediction in metal cutting: A review and implications for high speed machining," *International Journal of Machine Tools and Manufacture*, vol. 46, pp. 782-800, 2006.

[46] R. Komanduri and Z. B. Hou, "A review of the experimental techniques for the measurement of heat and temperatures generated in some manufacturing processes and tribology," *Tribology International*, vol. 34, pp. 653-682, 2001.

[47] T. Kitagawa, A. Kubo, and K. Maekawa, "Temperature and wear of cutting tools in high-speed machining of Inconel 718 and Ti-6Al-6V-2Sn," *Wear*, vol. 202, pp. 142-148, 1997.

[48] T. Yashiro, T. Ogawa, and H. Sasahara, "Temperature measurement of cutting tool and machined surface layer in milling of CFRP," *International Journal of Machine Tools and Manufacture*, vol. 70, pp. 63-69, 2013.

[49] Childs, T., Maekawa, K., Obikawa, T. and Yamane, Y., "Metal machining: theory and applications," Butterworth-Heinemann., (2000) pp. 147-152

[50] Y. Yamane, "Calibration System of Tool-Work Thermocouple with Infrared Heating," *Bulletin of the JSPE*, vol. 23, pp. 5-9, 1989.

[51] Mosaic-industries. Mosaic documentation web [Online]. Available: http://www. mosaic-industries.com/embedded-systems/microcontroller-projects/temperature-measurement/thermocouple/type-k-calibration-table. (August 2017).

[52] O. Abdulghani, M. Sobih, A. Youssef, and A. M. El-Batahgy, Modeling and simulation of laser assisted turning of hard steels. *Modeling and Numerical Simulation of Material Science*, vol. *3*(4) pp, 106-113, 2013.

[53] Dipl.-Ing. Robert Wiedenmann. Laser-assisted milling of titanium alloys [Online]. Available: https://www.industrial-lasers.com/articles/print/volume-26/issue-5/departments/update.html [June 2018]

[54] B. Azarhoushang, B. Soltani, and A. Zahedi, "Laser-assisted grinding of silicon nitride by picosecond laser*," The International Journal of Advanced Manufacturing Technology*, vol. 93, pp. 2517-2529, 2017.

[55] H. R. Krain, A. R. C. Sharman, and K. Ridgway, "Optimisation of tool life and productivity when end milling Inconel 718TM," *Journal of Materials Processing Technology*, vol. 189, pp. 153-161, 2007.

[56] Takuya INOUE: Effects of Laser Surface Treatment on Endmilling for Die Steels, (2019) Master thesis Hiroshima University.

[57] Y. S. Liao, H. M. Lin, and J. H. Wang, "Behaviors of end milling Inconel 718 superalloy by cemented carbide tools," *Journal of Materials Processing Technology*, vol. 201, pp. 460-465, 2008.

[58] D. G. Thakur, B. Ramamoorthy, and L. Vijayaraghavan, "Machinability investigation of Inconel 718 in high-speed turning," *The International Journal of Advanced Manufacturing Technology*, vol. *45*(5-6), pp. 421-429, 2009.

[59] E.-G. Ng and D. K. Aspinwall, "The Effect of Workpiece Hardness and Cutting Speed on the Machinability of AISI H13 Hot Work Die Steel When Using PCBN Tooling," J. *Manuf. Sci. Eng*, vol. 124, pp. 588-594, 2002.

[60] S. Sulaiman, A. Roshan, and S. Borazjani, "Effect of Cutting Parameters on Tool-Chip Interface Temperature in an Orthogonal Turning Process," *Advanced Materials Research*, vol. 903, pp. 21-26, 2014.

[61] D. Dudzinski, A. Devillez, A. Moufki, D. Larrouquère, V. Zerrouki, and J. Vigneau, "A review of developments towards dry and high speed machining of Inconel 718 alloy," *International Journal of Machine Tools and Manufacture*, vol. 44, pp. 439-456, 2004.

[62] C. E. Leshock, J.-N. Kim, and Y. C. Shin, "Plasma enhanced machining of Inconel 718: modeling of workpiece temperature with plasma heating and experimental results," *International Journal of Machine Tools and Manufacture*, vol. 41, pp. 877-897, 2001.

[63] X. Kong, L. Yang, H. Zhang, K. Zhou, and Y. Wang, "Cutting performance and coated tool wear mechanisms in laser-assisted milling K24 nickel-based superalloy," The *International Journal of Advanced Manufacturing Technology*, vol. 77, pp. 2151-2163, 2015.

[64] K. Venkatesan, R. Ramanujam, and P. Kuppan, "Investigation of machinability characteristics and chip morphology study in laser-assisted machining of Inconel 718," *The International Journal of Advanced Manufacturing Technology*, vol. 91, pp. 3807-3821, 2017.

[65] L. T. Ginta, M. A. Lajis, and A. N. Amin, "The performance of uncoated tungsten carbide insert in end milling titanium alloy Ti-6Al 4V through work piece preheating," *Am. J. Engg. & Applied Sci*, vol 2 (1), pp. 147-153, 2009.

[66] X. Q. Song, Y. Takahashi, W. M. He, and T. Ihara, "On the Formation Mechanisms of Adhering Layer during Machining Metal Material," *Key Engineering Materials*, vol. 749, pp. 39-45, 2017.

[67] X. SONG, Y. TAKAHASHI, and T. IHARA, "Influence of Built-up layer on the wear of uncoated cemented carbide tool during cutting of Inconel 718." In *Proceedings of International Conference on Leading Edge Manufacturing in 21st century: LEM21 2017.9*. The Japan Society of Mechanical Engineers, pp. 056, 2017.

[68] N. Razak, Z. Chen and T. Pasang, "Effects of increasing feed rate on tool deterioration and cutting force during end milling of 718plus superalloy using cemented tungsten carbide tool" *Metals*, vol. *7*(10), pp. 441, 2017.

[69] X. Ren, and Z. Liu, "Influence of cutting parameters on work hardening behavior of surface layer during turning superalloy Inconel 718," *The International Journal of Advanced Manufacturing Technology*, vol. *86*(5-8), pp. 2319-2327, 2016.

[70] B. H. Kear, J. M. Oblak, and A. F. Giamei, "Stacking faults in gamma prime Ni3(Al,Ti) precipitation hardened nickel-base alloys," *Metallurgical Transactions*, vol. 1, p. 2477, 1970.

[71] G. Venkatesh and D. Chakradhar, "Influence of Thermally Assisted Machining Parameters on the Machinability of Inconel 718 Superalloy," *Silicon*, vol. 9, pp. 867-877, 2017.

[72] W. Akhtar, J. Sun, P. Sun, W. Chen, and Z. Saleem, "Tool wear mechanisms in the machining of Nickel based super-alloys: A review". *Frontiers of Mechanical Engineering*, vol. *9*(2), pp. 106-119, 2014.

[73] H. Z. Li and J. Wang, "A Study of Cutting Forces in High-Speed Dry Milling of Inconel 718," *Advanced Materials Research*, vol. 500, pp. 105-110, 2012.

[74] H. Ding and Y. C. Shin, "Improvement of machinability of Waspaloy via laser-assisted machining," *The International Journal of Advanced Manufacturing Technology*, vol. 64, pp. 475-486, 2013.

[75] E. Sartori, "Convection coefficient equations for forced air flow over flat surfaces," *Solar Energy*, vol. *80*(9), pp. 1063-1071, 2006.

[76] J. Li, Y. Tian, S. Sun, J. Li, L. Zhang, and K. Chen, "Effect of Argon Filling Ratio on Heat Transfer Coefficient of Double-Glazing," In *Chinese Materials Conference,* Springer, Singapore, pp. 327-336, 2017.

[77] E. O. Ezugwu, R. B. Da Silva, J. Bonney, and A. R. Machado, "The effect of argon-enriched environment in high-speed machining of titanium alloy," *Tribology Transactions*, vol. *48*(1), pp. 18-23, 2005.

[78] Y. Fan, Z. Hao, J. Lin, and Z. Yu, "New observations on tool wear mechanism in machining Inconel 718 under water vapor+ air cooling lubrication cutting conditions," *Journal of Cleaner Production*, vol. *90*, pp. 381-387, 2015.

[79] E. M. Trent and P. K. Wright: "Metal Cutting -4th ed." (Butterworth Heinemenn, Woburn MA,2000) p.324.

[80] M. C. Shaw: "Metal Cutting Principles -2nd ed." (Oxford University Press, New York, 2005), pp. 157.

[81] M. Hawryluk, "Review of selected methods of increasing the life of forging tools in hot die forging processes," *Archives of Civil and Mechanical Engineering*, vol. 16, pp. 845-866, 2016.

[82] I. Lee and I. Park, "Microstructures and mechanical properties of surface-hardened layer produced on SKD 61 steel by plasma radical nitriding," *Materials Science and Engineering: A*, vol. 449-451, pp. 890-893, 2007.

[83] R. Ebara and K. Kubota, "Failure analysis of hot forging dies for automotive components," *Engineering Failure Analysis*, vol. 15, pp. 881-893, 2008.

[84] Z. Gronostajski, M. Kaszuba, S. Polak, M. Zwierzchowski, A. Niechajowicz, and M. Hawryluk, "The failure mechanisms of hot forging dies," *Materials Science and Engineering: A*, vol. 657, pp. 147-160, 2016.

[85] D.-G. Ahn, "Hardfacing technologies for improvement of wear characteristics of hot working tools: A Review," *International Journal of Precision Engineering and Manufacturing*, vol. 14, pp. 1271-1283, 2013.

[86] B. Buchmayr, "Damage, Lifetime, and Repair of Forging Dies," BHM Berg- und Hüttenmännische Monatshefte, vol. 162, pp. 88-93, 2017.

[87] N.-R. Park and D.-G. Ahn, "Wear characteristics of Stellite6 and NOREM02 hardfaced SKD61 hot working tool steel at the elevated temperature," *International Journal of Precision Engineering and Manufacturing*, vol. 15, pp. 2549-2558, 2014.

[88] K.-H. Leitz, B. Redlingshöfer, Y. Reg, A. Otto, and M. Schmidt, "*Metal Ablation with Short and Ultrashort Laser Pulses*," Physics Procedia, vol. 12, pp. 230-238, 2011.

[89] Y. F. Lu, M. Takai, S. Komuro, T. Shiokawa, and Y. Aoyagi, "Surface cleaning of metals by pulsed-laser irradiation in air," *Applied Physics* A, vol. 59, pp. 281-288, 1994.

[90]   G. X. Chen, T. J. Kwee, K. P. Tan, Y. S. Choo, and M. H. Hong, "Laser cleaning of steel for paint removal," *Applied Physics A*, vol. 101, pp. 249-253, 2010.

[91]   J.-H. Moon, P.-K. Seo, and C.-G. Kang, "A study on mechanical properties of laser-welded blank of a boron sheet steel by laser ablation variable of Al-Si coating layer," *International Journal of Precision Engineering and Manufacturing*, vol. 14, pp. 283-288, 2013.

[92]   M. Vedani, B. Previtali, G. M. Vimercati, A. Sanvito, and G. Somaschini, "Problems in laser repair-welding a surface-treated tool steel," *Surface and Coatings Technology*, vol. 201, pp. 4518-4525, 2007.

[93]   S. Fang, R. Lima, D. Sandoval, D. Bähre, and L. Llanes, "Ablation Investigation of Cemented Carbides Using Short-Pulse Laser Beams," *Procedia CIRP*, vol. 68, pp. 172-177, 2018.

[94]   J. L. Tan, D. L. Butler, L. M. Sim, and A. E. W. Jarfors, "Effects of laser ablation on cemented tungsten carbide surface quality," *Applied Physics A*, vol. 101, pp. 265-269, 2010.